Low-Frequency Acoustic Noise Mitigation Characteristics of Metamaterials-Inspired Vibro-Impact Structures

By

Anuj Rekhy

Bachelor of Technology

Jawaharlal Nehru Technological University

Hyderabad, Telengana, India

2012

Submitted to the Faculty of the
Graduate College of the
Oklahoma State University
in partial fulfillment of
the requirements for
the Degree of
MASTER OF SCIENCE
Dec, 2016

Low-Frequency Acoustic Noise Mitigation Characteristics of Metamaterials-Inspired Vibro-Impact Structures

Thesis Approved:

Dr. James M. Manimala

Thesis Adviser

Dr. Rick Gaeta

Dr. Xiaoliang Jin

ACKNOWLEDGEMENTS

This work was carried out under the watchful guidance of my adviser Dr. James M. Manimala. His patience and readiness to help me have been invaluable for all I have achieved. I am incredibly grateful for the faith he endowed upon my fewer capabilities for his greater ideas. I feel fortunate to have an opportunity to learn and develop my working capabilities directly from him. This experience has taught me to be disciplined and well organized. To do the right thing when no one is watching is what I have learned.

I would like to thank Dr. Gaeta for his inputs on our testing problems and teaching me the basics of engineering acoustics. Also, I would like to thank Dr. Jin for his contribution in making me understand the concepts in vibrations and being a part of my defense committee. I would like to thank Dr. Jeffrey Callicoat for his immense help in making me develop an understanding of the working of Transmission Loss tube and his adviser Dr. Jamey Jacob.

During my time at the graduate school in Oklahoma state university, I had the privilege of collaborating with outstanding researchers with the help of Dr. Manimala. I would like to thank Dr. Randolph Cabell and Dr. Noah Schiller of the Structural Acoustics Branch, NASA Langley for their guidance with the testing methods. This research was enabled by support from Concepts 2 Systems Inc. (C2Si) through a NASA SBIR Phase-I grant. Dr. Shiv Joshi was the C2Si technical consultant and a great organizer of professional meetings. I was very fortunate to be helped by Robert Snyder at NextGen Aeronautics on the construction of the spacers and composite materials used in this research. I was very lucky to complete an internship at MaxQ Research LLC on "Manufacturing of Honeycomb Composite Structures" under the guidance of Dr. Arif Rahman and Dr. Saravan Kumar. In collaboration with Textron Aviation, I was able to learn transmission loss testing using the reverb-anechoic chamber facility using ASTM and SAE standards.

I would also express sincere thanks to my colleagues at the "Solid and Structural Dynamics Lab." Thanks to Ryan Aiken for always being there for help with experiments and later on becoming a great friend. I appreciate the technical aptitude of Prateek Kulkarni and Andrew Chambers, and also their presentations skills have helped me learn immensely, and I have enjoyed whenever we collaborated on projects.

My gratitude for the support and encouragement from my parents, Anoop and Varsha, and loved ones without which none of this would have been possible.

Anuj Rekhy
Stillwater, OK

Name: Anuj Rekhy

Date of Degree: DECEMBER, 2016

Title: Low-Frequency Acoustic Noise Mitigation Characteristics of Metamaterials-Inspired Vibro-Impact Structures

Major Field: MECHANICAL & AEROSPACE ENGINEERING

Acoustic absorbers like foams, fiberglass or liners have been used commonly in structures for infrastructural, industrial, automotive and aerospace applications to mitigate noise. However, these conventional materials have limited effectiveness to mitigate low-frequency (LF) acoustic waves with frequency less than ∼400 Hz owing to the need for impractically large mass or volume. LF acoustic waves contribute significantly towards environmental noise pollution as well as unwanted structural responses. Therefore, there is a need to develop lightweight, compact, structurally-integrated solutions to mitigate LF noise in several applications. Inspired by metamaterials, which are manmade structural materials that derive their unique dynamic behavior not just from material constituents but more so from engineered configurations, tuned mass-loaded membranes as vibro-impact attachments on a baseline structure are investigated to determine their performance as a LF acoustic barrier. The hypothesis is that the LF incident waves are up-converted via impact to higher modes in the baseline structure which are far more evanescent and may then be effectively mitigated using conventional means. Such Metamaterials-Inspired Vibro-Impact Structures (MIVIS) could be tuned to match the dominant frequency content of LF acoustic sources in specific applications. Prototype MIVIS unit cells were designed and tested to study the energy transfer mechanism via impact-induced frequency up-conversion, and the consequent sound transmission loss. Structural acoustic simulations were done to predict responses using models based on normal incidence transmission loss tests. Experimental proof-of-concept was achieved and further correlations to simulations were utilized to optimize the energy up-conversion mechanism using parametric studies. Up to 36 dB of sound transmission loss increase is obtained at the anti-resonance frequency (326 Hz) within a tunable LF bandwidth of about 200 Hz while impact-induced up-conversion could enable further broadband transmission loss via subsequent dissipation in conventional absorbers. Moreover, this approach while minimizing parasitic mass addition retains or could conceivably augment primary functionalities of the baseline structure. Successful transition to applications could enable new mission capabilities for aerospace and military vehicles and help create quieter built environments.

TABLE OF CONTENTS

LIST OF FIGURES

LIST OF TABLES

SYMBOLS AND ABBREVIATIONS

A	Incident Wave Amplitude
B	Reflected Wave Amplitude
C	Transmitted Wave Amplitude
c	Speed of Sound
d	Diffusion Coefficient
ds	Structural Damping
dB	Decibel
E	Young's Modulus
f	Operating Frequency
f_l	Lower Operating Frequency of Impedance Tube
f_u	Upper Operating Frequency of Impedance Tube
G	Gap
g	grams
K	Bulk Modulus of Air
k	Wave Number

k	Effective Stiffness of Entrapped Air
P_1	Pressure at Mic Location 1
P_2	Pressure at Mic Location 2
P_3	Pressure at Mic Location 3
P_4	Pressure at Mic Location 4
p	Sound Pressure
R	Reflection Coefficient
S	Scattering Coefficient
t	Transmission Coefficient
U	Mean Steady Flow Velocity
x_1	Distance of the First Mic from the Surface of the Specimen
x_2	Distance of the Second Mic from the Surface of the Specimen
x_3	Distance of the Third Mic from the Surface of the Specimen
x_4	Distance of the Fourth Mic from the Surface of the Specimen
Y	Admittance
Z	Acoustic Impedance
Z_c	Characteristic Impedance
α	Absorption Coefficient
v	Particle Velocity
ρ_0	Fluid Density

σ	Air Flow Resistivity
ρ	Mass Density
ν	Poisson's Ratio
ABS	Acrylonitrile Butadiene Styrene
AM	Acoustic Metamaterials
ASTM	American Society for Testing and Materials
MIVIS	Metamaterial Inspired Vibro-impact Structures
MLM	Mass Loaded Membrane
VI	Vibro-Impact
LF	Low Frequency
TL	Transmission Loss
SOA	State of the Art
HF	High Frequency

CHAPTER 1

Introduction

1.1. Motivation

Eliminating unwanted noise has always been an area of interest for engineers and scientists alike. Characterization of the unwanted noise source becomes necessary in such situations. Greeks were the first to experiment with sound waves. The excitation from a source causes vibrations in the medium, and if this medium is air, then the waves created are termed as sound. These waves do not travel in the vacuum. Acoustic waves are the scientific word for the sound waves. The Human ear is a sensor that can detect these vibrations and the 20 Hz to 20 KHz frequency bandwidth is defined as the audible range in acoustics.

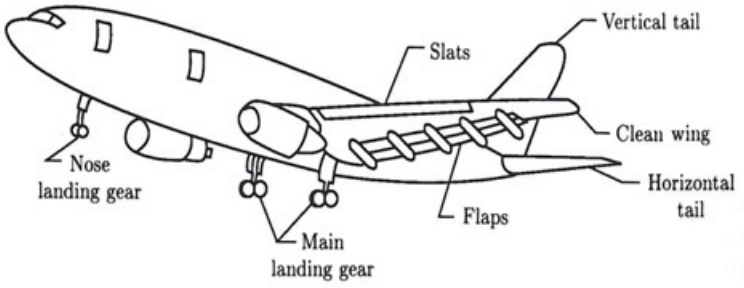

Figure 1: Sources of airframe noise [1]

Low-frequency (LF) airborne noises have several undesirable consequences as well as detrimental effects. These can range from structural damage due to excitation of mode shapes, contribution to noise pollution and mission restrictions enforced by the

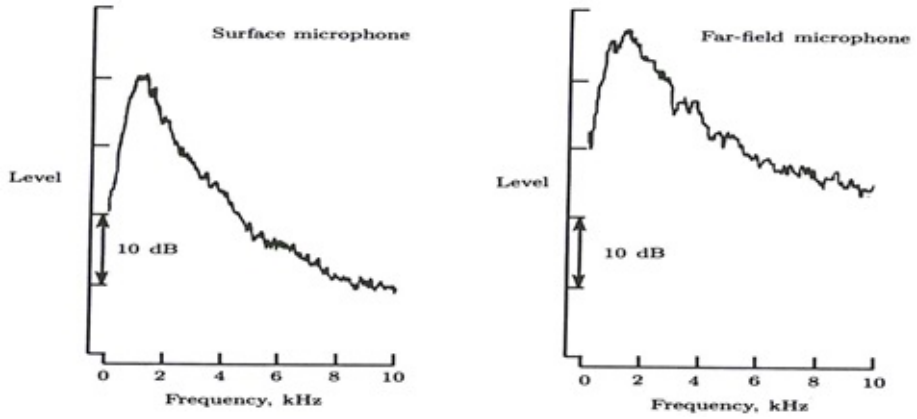

Figure 2: Pressure Spectra: Surface and far-field microphones [1]

acoustic emissions. Fig. 1 and 2. shows the sources of airframe noise and frequency spectrum of the surface and far-field microphones having high energy content localized in the low-frequency region.

The mass law acoustically limits lightweight structures and materials currently used in aerospace applications. These materials exhibit poor sound insulation properties to mitigate LF noise. Conventional acoustic absorbers − foam, fiberglass and liners are ineffective and impractical at lower frequencies ($\leq$400 Hz). LF acoustic signature below 400 Hz is a significant contributor to noise output. Possible sources of the low-frequency acoustic signature are industrial machines, such as boilers, pumps, cooling towers and electrical installations and aerospace vehicles such as helicopters, aircraft and spacecraft. Ineffectiveness of the foams, when applied to mitigate LF noise, can be understood by looking at the testing result from NASA Glenn Research Center is as shown in Fig. 3(a). In this test various types of foams have been included over a base panel and from the transmission loss curves it is clear that the effectiveness of the foam addition on LF sound transmission is insignificant. These foams typically are part of the fairing acoustic protection for spacecraft and therefore their ineffectiveness at lower frequencies create a demand for other effective alternatives.

Acoustic liners are porous resonating chambers working on the principle of Helmholtz resonance as shown in Fig. 3(b). One challenge with acoustic liners is that as the

frequency becomes lower the volume of unit cell increases and this makes the dimensions required to attenuate LF sound waves larger as given by equation 1. These methods while demonstrating an excellent transmission loss performance for different types of high frequency (HF) noise signatures are impractical to use for sound signatures that generate frequencies below 400 Hz. Therefore, it becomes necessary that alternative lightweight, compact techniques are developed to improve the LF sound transmission loss through structures to be used primarily in the aerospace, but also in industrial, military and civil infrastructural applications.

$$f = \frac{c}{2\pi}\sqrt{\frac{S}{tV}} \tag{1}$$

Where:

f = resonance frequency, Hz

c = speed of the sound, m/s

S = area of the holes in perforated sheet, m^2

t = thickness of perforated sheet, m

V = volume of each unit cell, m^3

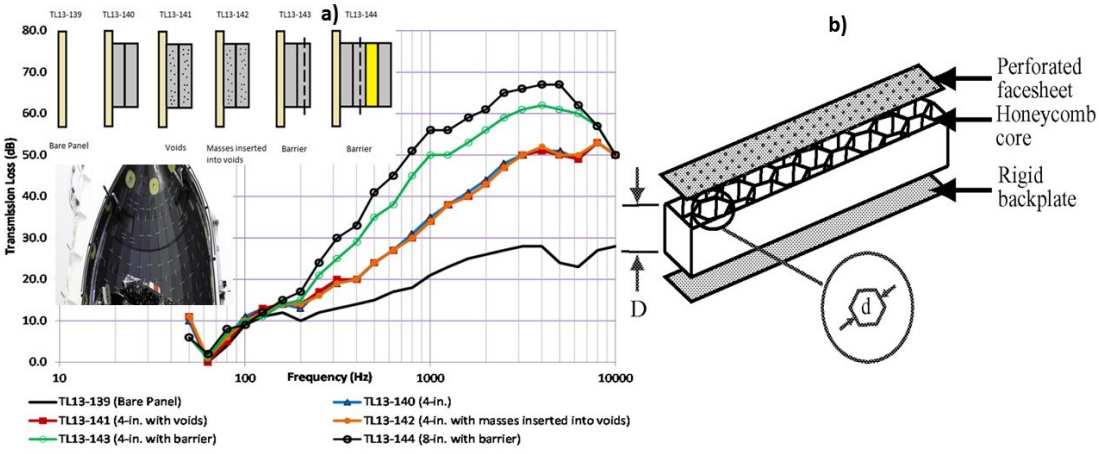

Figure 3: (a) Transmission loss curves for a base panel with foam additions and acoustic fairing protection in inset [2] and (b) Schematic of acoustic liner [3].

In the recent years, improved LF performance of various equipment, fired and rotary-wing aircraft and mainly space launch vehicles is becoming increasingly mission critical. These machines are known to generate the significant dominant low-frequency acoustic signals. Reducing the LF acoustic signature for these applications have become a critical design objective. Therefore understanding and developing various approaches to mitigate low-frequency acoustic signature becomes an important aspect of contemporary acoustic research.

Open source noise signals were used to confirm the LF acoustic signature characteristics for rotor-wing aircraft. FFT's were taken to obtain spectrum of these transmitted acoustic responses. The acoustic noise signals of two US Army helicopters Apache and Chinook are evaluated. In the Fig. 4(b) and (d) the FFT's of both the helicopters are shown from which it is clear that the dominant content of the spectrum is below 500 Hz for both the attack and transport helicopters respectively.

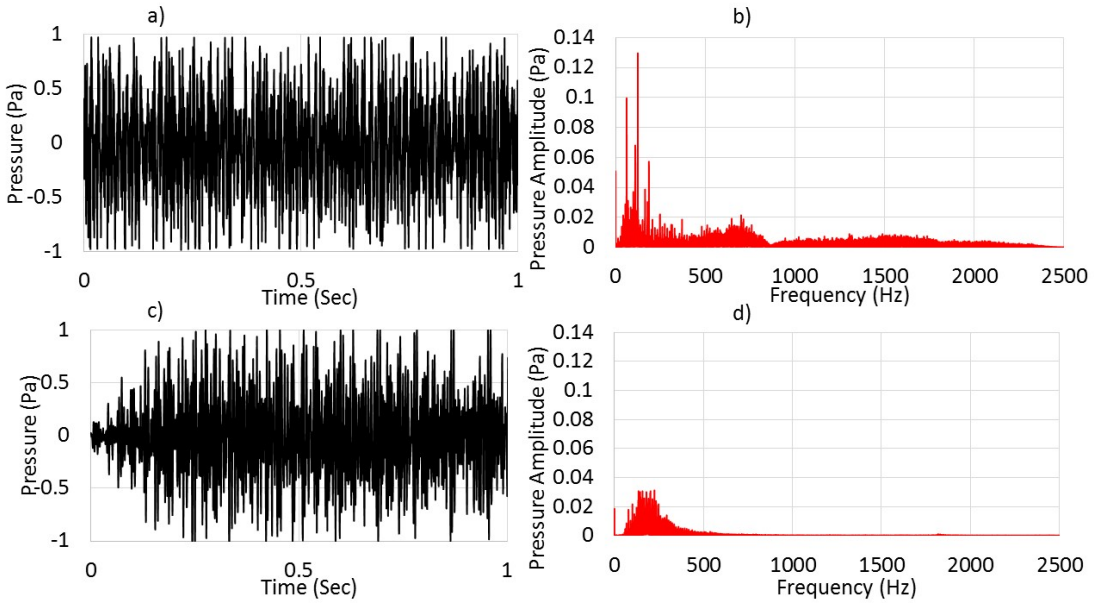

Figure 4: (a) Pressure signal and (b) its FFT for Apache helicopter, (Ref: goo.gl/834abA) (c) Pressure signal and (d) its FFT for Chinook helicopter (Ref: goo.gl/tJTPe2). (The values indicated are not absolute but are just for demonstration)

1.2. Acoustic Metamaterials

Acoustic Metamaterials (AM) are man-made structural materials that derive their unique dynamic behaviour not just from material constituents but more so from engineered configurations [16]. They can exhibit properties that are not generally available in naturally available materials but can be induced by effectively designing engineered configurations. These materials can exhibit frequency-dependent negative and complex effective-mass density and modulus. AM are man-made materials that display unusual elastic wave phenomena beyond those achievable in natural materials. These properties are derived from engineered microstructural configurations. Potential applications exist in protective structures, acoustic devices for noise control and imaging, energy harvesting and transducers.

Development of new AM to improve LF acoustic performance has been attaining prominence amongst researchers. A structural engineering problem that has recently been of interest is: can we construct acoustic barriers that have increased acoustic performance over a broadband frequency range and at the same time keep the structure lightweight? Along with this application, can AM be applied other fields of engineering to solve problems such as, if it is possible to create a lens with negative diffraction and go past the diffraction limit to be able to make more powerful optical devices. To prevent the scattering of the sound fields caused by the microphones or sensors and to be able to record very high frequencies without distortion. In this section, a brief discussion is carried out on the various applications and recent research trends in AM.

Microstructures can be designed within the materials that could be made to respond out of phase with the external excitation, these type of materials can be part of metamaterials [17]. Metamaterials are called left-handed materials, and they have attracted a lot of research interest. Veselago [18] in 1968 proposed the idea that some materials might have negative electric permittivity (ε) and magnetic permeability (μ). Split ring resonators is a technology based on electromagnetic metamaterials [19]. There are similarities in the analogy between electromagnetic and acoustic waves; it implies that if negative properties exist in electromagnetic metamaterials, then properties like negative

mass density and negative modulus must also exist in AM [20, 21, 22, 23, 24].

Some of the optical applications of AM are as follows: By allowing the evanescent waves to be completely imaginary, it is possible to achieve enhanced images having high resolution. Hence a slab of negative refractive index material was created because the wavelength of the light limits the sharpness of the image [25]. A lens consisting of sub-wavelength Helmholtz resonators was used as an acoustic metamaterial to demonstrate the phenomena of negative refraction [26]. Evanescent waves were amplified making use of acoustic metamaterial slabs that had negative effective density; 17 times amplification of these waves at a remote distance by overcoming dissipation [27]. Based on the similar technique supper resolution focusing was achieved [28]. Important engineering concepts such as super-resolution imaging [29, 30] as well as cloaking [31, 32] have been studied. Some other studies are based on super lens [33], the addition of electromagnetic sub-wavelength structures [34] and hyperlens [35].

AM which are acoustic counterparts of EMM have found its applications in the manipulation of elastic waves. Such AM are divided into two categories, and they are; intrinsic AM and inertial AM. The intrinsic AM exhibits local resonances in tunable bandgaps and will be used in our study, whereas the inertial AM are mass-damper-spring oscillators that absorb the energy and keeps the structure holding these stationary. Periodic composite materials have been studied to understand the propagation of elastic waves, and these are also known as phononic crystals. These create acoustic band gaps either due to Bragg scattering or local resonance. Metallic stubs have been set up on the surface of thin homogeneous plates, the changing dimensions of the stubs are correlated with the low-frequency bandgaps [36]. Experimental evidence of locally resonant two-dimensional plates consisting of an arrangement of silicone rubber stubs on the aluminum plate has demonstrated the creation of bandgaps for the out of plane lamb waves [37]. Few other works relating to the elastic wave manipulations discuss effective experimental and numerical techniques conducted [38, 39]. Cloaking in thin plates was first proposed by Farhat et al. [40]; this was used to cloak bending waves in heterogeneous thin plates and produced no phase shift for forward and backward scattering waves. Following this theoretical proposal, a design of 1 mm thin polymer plate consisting of 20 concentric rings

and 16 different metamaterials; this design shows good cloaking behavior in the range of 200 to 400 Hz [41]. An attempt at increasing the bandgap was carried out by placing ten concentric resonating cylindrical beams over a thin plate [42]. Investigation for negative refraction of elastic waves was carried out in AM [43]. Lastly, sub-diffraction focusing was demonstrated in thin plates [44]. Hybrid elastic solids have shown super anisotropy, in which the waves can travel only in the different directions except for longitudinal direction [45]. Negative mass density and shear modulus were shown to exist over a broad frequency band are demonstrated that cannot occur in naturally available solids [46]. Based on the small scale(micro, nano) of photonics and phononics, for studying the attenuation of seismic waves testing was carried out on bigger(meter) civil engineering designs [47].

These materials derive their atypical dynamic behavior not just from material constituents but more so from engineered local configurations. New trends and advances in this field have led to the development of structures demonstrating negative effective mass and negative modulus [48, 49]. Theoretical and experimental methods have been used to demonstrate negative-mass phenomena below the cut-off frequency. About the decaying nature of the lattice waves a drop in the transmitted waves is demonstrated using this mechanism using both experimental and theoretical approach [50]. After using elastic continuum model to study dispersive wave propagation in the lattice system, it is compared with another model in which multi-displacement microstructure continuum model is used to represent mass-in-mass lattice system [4] as shown in Fig. 5. To model the dynamic behavior of an AM in the form of composite material embedded with internal resonators a homogeneous classical continuum model was used along with a continuum model described by two variable LF band gaps are also be generated [51]. By designing locally resonant artificial resonators; unidirectional split rings, as well as bidirectional chiral split rings, were studied for determining wave propagation characteristics [52].

The spring-mass system can be used to study the concept of negative mass density. The possibility of objects having a negative momentum on being excited by a positive momentum has been studied by Milton and Willis [53] within the framework of newtons laws. Later on, some extension to the theoretical model was carried out by Yao et al.

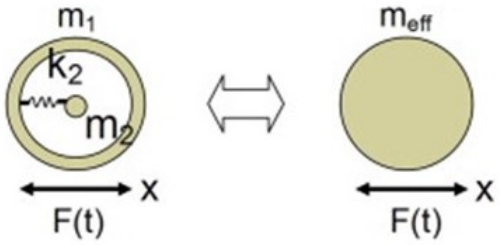

Figure 5: a) Single spring-mass system and its effective mass [4]

[54] making use of the experiments.

Foams having a negative value of Poisson's ratio are created. Compressing a material along longitudinal direction leads to an expansion in the other two orthogonal directions. This phenomenon is not the same in the case of the materials with negative Poisson's ratio, in turn, these tend to contract [55]. Dip-in direct-laser-writing optical lithography is used to make a tailored 3D mechanical metamaterial. Production of lattice structures made out of any material will maintain the same stiffness, even at low densities has been made possible by projection micro stereolithography [56]. Pentamode materials enable the 3D transformation to the field of elastodynamics this concept is similar to acoustic or optical transformation. Milton discussed pentamode mechanical metamaterials [57], by developing a cylindrical body covered with a lattice structure made out of lithography for the purpose of elastically hiding objects and hence, development of elastomechanical cloak was successful [58]. The division of bulk modulus to shear modulus was made significant to about 1000; this was possible due to the fabrication made available by using lithography on 3D microstructures [59].

1.3. Literature Review

Generally, in aerospace applications, the sound is attenuated by making use of different types of elastic porous media such as foams and fiber batting, the transmission loss

of these were calculated at random incidence angles [60] and vibroacoustic attenuation devices such as foams were investigated for low-frequency fairing-noise mitigation [61]. Microperforated panels mostly working on the principle of Helmholtz resonator have been studied, but it has been found to be difficult to adjust the acoustic resistance due to geometric constraints [62]. Heterogeneous blankets (poroelastic media with small embedded masses) have been studied for sound transmission through double panels and been found to reduce low-frequency sound radiated through structures significantly in comparison with a poroelastic medium [63]. By the addition of mass inclusions, the mass inclusions act as spring-mass resonant systems and so increases the structures impedance [64], leading to an increase in transmission loss by (10-20 dB) when compared to the acoustic mass law at 100 Hz. As it is of general knowledge that traditional treatments are effective for attenuating higher frequencies, the mass inclusions are provided to attenuate low frequencies.

To achieve a broadband sound insulation, assembling narrow band resonators in the array have been studied. Traditional resonators, such as Helmholtz resonators have been configured both in series and parallel [65]. AM have been gaining popularity amongst researchers as a solution towards efficiently mitigating LF acoustic noise without taking a hit on mass addition. Previously, various types of resonant acoustic metamaterials have been investigated to understand their sound insulation properties under the effect of low-frequency airborne noise [66, 67]. Mass loaded membranes have been engineered and studied for their effect on LF acoustic waves [11, 12]. Locally resonant acoustic metamaterials were analyzed after addition of the ring masses [68]. For locally resonant acoustic metamaterials a study is done on the effects of scaling [69]. Stacking of membranes can improve the effectiveness of the membranes for broadband noise mitigation into panels [70]. Analytical models have been developed based on vibroacoustic coupling to be able to quickly design and predict the behavior of mass loaded membranes under normal incident pressure [71]. Another analytical approach provided a quick estimation of sound transmission loss; in this paper, the first dip and peak frequencies depend mostly on the mass attached to the membrane. The second dip depends on the material properties defined for the membrane; a study is carried out on the effects of position

and tension on the transmission loss [72]. All of these models while studying membranes in different layups do not attempt to examine the structural integrity of such designs. Maintaining the structural load bearing capability and retaining low mass addition is very critical in these applications and are intended to be used as aerospace structures. Hence, we attempt to study the performance of one such mass loaded membrane over a baseline structural component.

Governing equations are employed to carry forward analytical work in the field of plates carrying distributed masses. These are converted into a set of ordinary differential equations using Galerkin method, and these equations were solved numerically. Variations observed in the frequency with respect to the location; an investigation was carried out by changing the weight of distributed mass and density of the plates [73]. Creating an impedance mismatch between the layers of different gasses leads to an inefficient energy transfer and in turn causes a reduction of sound energy transmitted [74]. Cellular structures [13] and thin flexible structures [**?**] with tuned resonances display the negative dynamic mass effect within the frequency range of exploration. The aspects of modeling mass loaded membranes are explained using spring-mass system [75]. A doubly negative metamaterial that has both monopolar and dipolar resonances that can be separately tuned leading to both negative effective bulk modulus and density is shown in Fig. 6(a) [5]. Multiple peaks on the absorption coefficient curves were generated by using semi-circular discs over a membrane and this structure that acts as a low-frequency absorber is shown in Fig. 6(b) [6]. Mass loaded membranes have been used as acoustic filters to exploit the out-of-phase resonance of the membranes to negatively interfere with the in-phase excitation passing through the orifice at a frequency just below the resonance frequency of membranes and such a metamaterial is shown in Fig. 6(c) [7]. About 99.7% acoustic absorption has been observed by using two out of phase resonators that produce a destructive interference as shown in Fig. 6(d) [8]. For an improvement in the acoustic performance at low frequencies, an in-depth analysis is carried out on various bandgap materials [76, 20]. Experiments on mass loaded membranes placed adjacent to each other having variations in the quantity of the mass and explanation for the mechanism responsible for broadband attenuation has been carried out in the process of studying acoustic

transmission characteristics [77]. Many practical applications of acoustic metamaterials are required to serve as load-carrying structures within deflection limits. A minimum weight addition is a critical issue in regards to aerospace structures. A solution is effective if it has a broader range of the effective frequency bandgap.

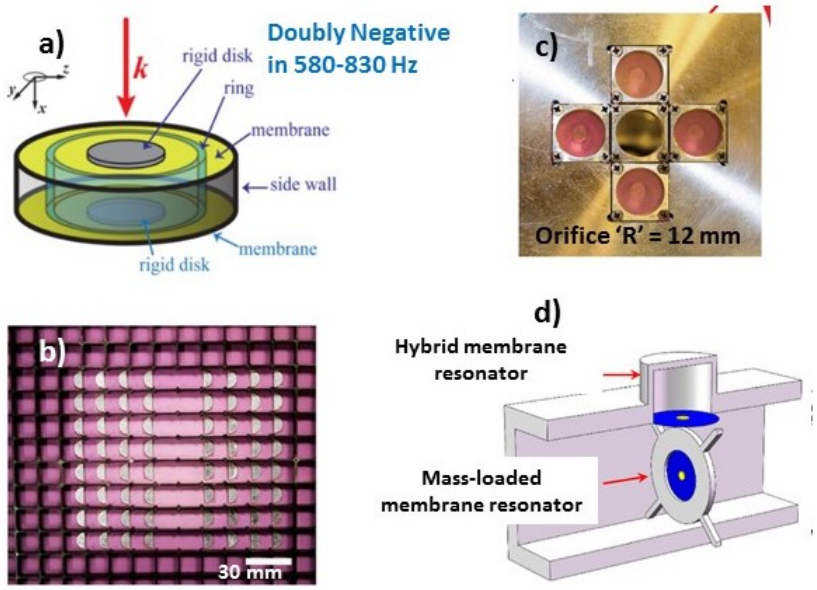

Figure 6: a) Doubly negative metamaterial with coupled membranes [5], b) Acoustic metamaterial as low-frequency absorbers [6], c) Metamaterial based low-frequency filter with orifice [7] and d) Metamaterial based total acoustic absorption [8].

Recently, the low-frequency seismic waves have been attenuated using 3% mass addition [14]. Nucera et al. made use of the tuned vibro-impactors mounted on civil structures, and the reduction in the vibration amplitude was more than 50% over just the master structure without vibro-impactors. These vibro-impact oscillators are nonlinear energy sinks; the study has been carried out to analyze the capacity of impactor to diminish 'as much as possible' and dissipate 'as fast as possible. Incorporating MLM over a BS can create a counterpart for acoustic waves, resulting in a vibro-impact coupling. Bellet et al. studied an almost irreversible transfer of energy from a linear acoustic medium to a nonlinear viscoelastic membrane [78]. It was shown to perform effectively over a broadband frequency range. These studies provide a basis to consider vibro-impact-based energy up-conversion as potential mechanism for LF acoustic noise mitigation.

1.4. Hypothesis and Definition of Objectives

Hypothesis: Vibro-impact coupling between the low-frequency mass-loaded membrane-type resonator and structurally integral high-frequency acoustic absorber can be used to transfer energy via impacts to high frequency modes in the structure. This frequency up-conversion phenomenon can lead to a improved broadband transmission loss against baseline structures.

Definition of Objectives: Metamaterial-inspired vibro-impact structures (MIVIS) consist of tuned mass-loaded membranes as vibro-impact attachments on a baseline structure. MIVIS has a tuned low-frequency membrane resonator attachment placed at an optimum gap from the backing structure. The sequestration and reflection of acoustic waves from the membrane is expected to result in energy from the incident low-frequency acoustic waves being up-converted via impacts on a backing structure to its natural frequencies for subsequent dissipation in conventional materials like foam. In the present study, various prototype MIVIS configurations have been investigated. The following objectives are identified in order to test this hypothesis as part of this study:

1) Demonstrate experimental proof of concept for improvement in overall sound transmission loss (STL) using MIVIS unit cells in comparison to conventional structural acoustic treatments used in aerospace applications. The goal is to obtain at least 20-30 dB improvement in STL in normal incidence transmission loss tests.

2) Investigate and optimize the impact-induced energy up-conversion mechanism using simulations and experiments. Conduct parametric studies to evaluate the effect of parameters including membrane resonator properties, gap between impactor and back plate, and excitation pressure on the up-conversion efficiency.

3) Minimize any degradation to the mechanical properties of the baseline structure, in particular, to limit parasitic mass addition to the baseline structure using optimization of designs as well as retain the stiffness of the baseline structure unaltered or if possible, augment it.

4) Prioritize tunability and modularity in designs in order to tailor MIVIS-based solutions to a wide range of LF acoustic noise mitigation applications.

1.5. Overview of Chapters

This thesis reports the investigation on the mechanism, design and testing of MIVIS. In the first chapter a discussion on recent research and trends in acoustic metamaterials is discussed followed by a review of literature available on acoustic metamaterials with a particular focus on membrane type AM. This survey gives a perspective on the further development of theoretical models, simulations and experimental testing methods for MIVIS and identifies key gaps in the literature.

A survey of acoustic materials is done to understand different types of conventional absorbers and diffusers currently being used in Chapter 2. The characterization of acoustic properties of these materials play a major role in matching their performance in specific applications. Various parameters and standards are discussed briefly to compare and contrast the different approaches.

In Chapter 3, firstly, preliminary studies using 3D-printed test articles are presented. Simulation models are created at length for various designs to optimize the upconversion mechanism using parametric studies. Potential designs for MIVIS unit cells are downselected and detailed.

Chapter 4, deals with experimental testing of MIVIS unit cells. The characterization methods along with the limits and capabilities of the experimental setup are explained followed by the discussion of the experimental testing and results. A comprehensive list of conclusions followed by recommendations for future work related to MIVIS are discussed in Chapter 5.

CHAPTER 2

Acoustic Materials and Characterization Methods

The purpose of this chapter is to discuss, compare and contrast various aspects of currently available conventional acoustic materials and their selection methods for specific applications.

2.1. Introduction

Absorption of the unwanted noise that is in general rendered by using acoustic materials. Determining acoustic properties is known as the characterization of acoustic materials. Depending on the acoustic properties these materials can be used in various applications. Noise is generated because of different activities related to naturally occurring events or by human intervention. In such a situation it becomes crucial to provide public places with the best technology for sound insulation so that people feel comfortable. Two methods of reducing the transmission of sound through objects are available. Various types of general purpose acoustic treatments are widely known, such as fiberglass, foam, acoustic partitions, baffles, soundproofing partitions. Acoustic materials can be generally classified as follows:

- Sound absorbers
- Sound diffusers
- Noise barriers
- Mufflers

Sound absorbing materials are used to prevent the reflection of the sound waves striking their surface. Absorbers work on the principle of penetrating waves dissipating into the porous material through surface pores and then by reflection of these waves continuously till they attenuate or convert wave energy into heat energy. Sound absorbing materials can be used only to absorb sound in a room but cannot be used to reduce the transmission of sound through the walls. Polyurethane foams, melamine foams, fiberglass, wool and fabrics are sound absorbing materials. These can be cut to give many shapes and are abundantly available. Absorbing materials are characterized by making use of absorption coefficient discussed in Section 2.3. Sound absorbing materials in the music recording and radio broadcasting studios, anechoic chambers, wall and ceiling panels in conference rooms, theaters, offices are used in mitigating excessive noise sources and maintaining reverberation time of the room.

Sound diffusers are used to scatter sound waves striking their surface. Rooms with echoes and high reverberation are treated with these type of surfaces to be able to remove the unwanted reflections but keep the total energy same. Sometimes the reflections can change the response of the original signal, and this can create a deterrent sound within the target space. Diffusers are considered to be a product of the invention of number theoretic diffusers by a German physicist named as Manfred Schroeder [79].

Noise barriers are used to reduce the transmission of the airborne sound. Due to the diffraction of low-frequency waves around walls and obstacles the noise barriers can only reduce the noise levels up to 15 dBA [80]. People living near highways and airports construct noise barriers by building walls that could reduce noise considerably. Different types of noise barriers available are concrete walls, metal, wooden, plastic, rubber, composite as well as transparent walls. Noise barriers that surround a sound source are known as enclosures. Enclosures are very effective in reducing noise when compared to the noise barriers. Multi-layered enclosures along with a lining of absorptive material can provide up to 70 dBA of reduction in sound pressure levels [80].

Mufflers are used as attachments along with conduits. By designing conduits to attenuate the frequencies of interest, sound traveling through these are mitigated. The most general application is use in the silencers fitted along with internal combustion en-

gines. These mufflers while minimizing the noise from the engine also help in developing the back pressure on the engine which in turn improves an engine's efficiency.

2.2. Survey of Acoustic Materials and Noise Mitigation Techniques

The low-frequency sound has always been an area of concern as it transfers through structures and also travels unattenuated to very long distances in a medium (air). Walls, solid metal structures can attenuate mid frequencies as well as high frequencies ($\sim$>400 Hz) but attenuating low frequencies ($\sim$<400 Hz) is very difficult in practical applications. At 100 Hz the brick walls and metallic structures can attenuate only 20 dB of sound energy [81, 82, 60, 83]. However, such a brick wall or metallic structure can be insulated by making use of the widely available acoustic materials. To attenuate low frequency using foams would require a heavy insulation and this makes it an impractical option for aircraft structures. The survey and characterization that becomes a part of this thesis have been carried after studying a vast range of references but mostly based on relevant information from the books by Trevor J. cox [10] and Michel Bruneau [84].

In acoustics, when a sound wave interacts with a new surface or medium it is either absorbed, transmitted or reflected. In most of the audio production, reproduction and control applications a combination of diffusers and absorbers are used to keep a control on the intended sound levels. Hence, it becomes necessary to study both absorbers and diffusers as these materials cover most of the acoustic materials used for sound treatments across various applications.

Absorbers are used to absorb the sound energy and reduce the reverberation in closed spaces. Traditional absorbent materials were made from mineral wool while the modern methods use micro-perforated absorbers not to compromise aesthetics. Two types of absorbers are used in music rooms and they are: porous absorbers and resonant absorbers. Porous absorbers are placed in the corner of rooms and are good at absorbing high frequencies. However, they are ineffective at lower frequencies and can be seen in Fig. 7(a) and (b). Resonant absorbers are analogous to mass-spring systems with

damping absorption at the resonant frequency as shown in Fig. 7(c). Resonant absorbers cannot be used effectively as they have a narrow bandwidth of absorption, so double layer absorbers which are expensive and difficult to manufacture are generally employed. The sound from air conditioning ducts and pipelines can be reduced at the source if the absorbent material can be applied. Sometimes the ducts have an internal lining of foam. Porous absorbers are also used in silencers and mufflers to reduce sound within pipework.

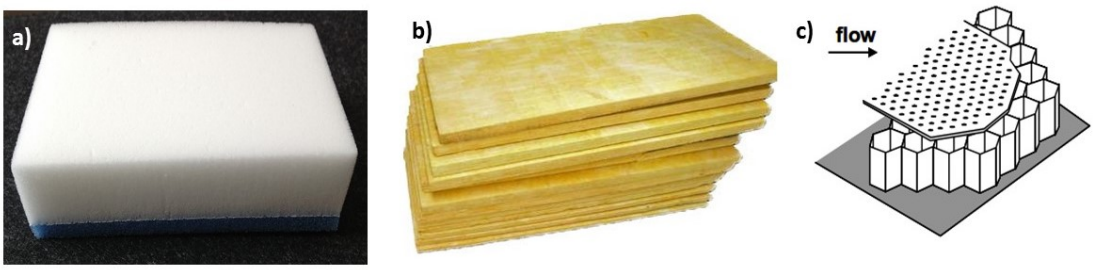

Figure 7: Porous absorber a) Melamine foam, b) Fiberglass and Resonant absorber c) Acoustic liner [9].

Porous absorbers are materials where sound dissipates into a network of interconnected pores. Different materials used as porous absorbers are like mineral wool, foam, sustainable materials, carpets, aerogels, acoustic plasters and activated carbon. Mineral wool from sand, basaltic rock and recycled glass. Sustainable methods like sheep wool are being tried to reduce the use of human-made vitreous fibers. Where aesthetics is a high priority, then employ acoustic fibers. The walls and ceilings are coated with glass-granulates (grain size of 2 to 4 mm) and plastered with a binder allowing the surface to remain open for absorption. The fundamental properties that determine the behavior of sound within porous absorbers are flow resistivity and porosity.

Resonant absorbers use resonance phenomenon to absorb at low-mid frequencies which in porous absorbers is not achievable because of low particle velocity at room boundaries. Whereas, resonant absorbers are efficient when placed at boundaries. However, resonant absorbers are limited by the bandwidth of absorption that is achievable. Helmholtz absorbers are predictable within reasonable accuracy. The design for membrane devices can only be done using trial and error approach. The basic mechanism of

resonant absorber has a mass vibrating against a spring. By changing mass and spring properties, tuning of the resonances is carried out.

Some other interesting absorbers include micro-perforated and clear absorbers. In the micro-perforated, when the sound passes through these micro-holes it has high viscous losses thus reducing sound energy and absorption. This kind of absorbers also eliminates the need for absorbent and damping material along with the necessity of a reflective surface. The mid-low frequency absorption can be promoted using curved panels. In some cases, narrow micro-slits cut into acrylic or Polyethylene terephthalate (PETG) using lasers which are cheap and looks aesthetically appealing [10]. These devices are employed for low-frequency absorption. Masonry concrete blocks with two slotted resonant chambers are designed to provide bass absorption as shown in Fig. 8. Since the flat or split face can create a reflection problem, a phase grating diffuser is used to break the reflected sound waves. Painting these devices decreases the high-frequency absorption capacity, but the low-frequency absorption remains intact [10].

Figure 8: CMU (concrete masonry unit) which uses two slotted Helmholtz absorbers to provide bass absorption [10].

Metal plate absorbers unlike other absorbers that mostly use air in the cavities as spring unlike the porous material. Considering the stiffness of spring, a heavy mass, which is a steel plate >= 1 mm against foam polyester spring. When sound strikes plate, it vibrates against the spring thus absorbing sound energy [85]. A perforated metal frame is utilized to support low-frequency absorption. Polyester foam is also used on the plate to absorb high-frequency waves and increasing overall absorption efficiency

of the system.

Diffusers conserve the sound energy, unlike absorbers where the energy is absorbed. For example, in closed auditoriums, the echo from the back wall disturbs the singers. Hence, a diffused sound is needed. The sound energy drops and the listening experience spoils due to the usage of absorbers. Diffuser uses different shapes to diffuse the sound at the impact. The study and research on diffusers are still in progress, and their application is based on precedence and intuition.

Phase grating or Schroeder diffusers have brought predictability and optimization to the diffusers. These are 1D-diffusers with series of wells having different depths separated by fins. Depths of wells are determined by mathematical number sequence, like a quadratic residue sequence. When a mid-frequency wave hits, the plane waves are reflected from the bottom of the well and radiate back into space [86].

Amongst geometric reflectors and diffusers, almost every geometric shape has diffusing capability from the planar surface to the triangle, pyramids, concave and convex arcs. However, the planar surface is very ineffective. At powerful low frequencies, i.e., when the wavelength is significant compared to panels size, the negligible or null sound is scattered from the plane. When a high-frequency sound hits the plane, a great specular reflection occurs. By using Rindel formulation, cut off frequency above which specular reflection occurs is calculated, and transition frequency between specular reflection and significant diffraction are determined to use the panel for desired diffuser function. In triangles and pyramids, deflection occurs depending on the geometry. From an array of pyramids or triangles, the steepness of slopes along with the varying angle of incidence dictate scattering of sound. It is effectively a redirecting surface generating two clear reflections at two different directions. However, the performance will deteriorate at low and mid frequencies [10].

Concave arcs are often termed as an acoustician's nightmare since a wrong design can result in focusing of sound and uneven energy distribution, echoes and sometimes coloration of timbre across the room. The performance of the arc is largely dependent on its radius, position of source and receiver. The focusing problem is only limited to a set of receivers at certain distances close to the focal point of concavity. It is sometime

possible to take the focus of the audiences away. Having focus above the level of the public can cause paradoxical dispersion and having it below the general level results in a concentration of non-lateral sound which is undesirable acoustically. Conventional absorbers or diffusers surface treatments are used specifically in cases where the focus on the listeners is inevitable [10].

In convex arcs, a single cylinder is efficient in one plane and single sphere in dispensing hemispherically. Though it might appear that a single cylinder is an ideal diffuser, it is not. A single cylinder of the width of at least 1 m is not enough for many applications, but architects would not allow at least 0.5 m in their design, and hence the array of single cylinders is preferred over a single cylinder by a large width. In the array of cylinders, the response dominated by the arrangement of cylinders rather than expecting a perfect response from a single cylinder. Flattened cylinders used as an alternative, but the perfect angular dispersion is lost especially for oblique sources [10].

Many diffusers utilized on the surfaces and walls. Volumetric diffusers are used to scatter the sound in a room, by not limiting the diffusion only at the ceilings and walls. Due to a limited depth, surface diffusers have a limited bass response which can be defeated by volumetric diffusers. They are spread across the space of the room, and hence they influence 360-degree space. The only problem is to make sure that these diffusers do not affect the sight lines of audiences in a room. They are usually hung from ceilings like overhead canopies in halls and auditoriums. Reverberation chambers use volumetric diffusers. However, the effectiveness testing and design methodologies are not developed except in the case of reverberation chambers.

Wood is the most widely used material for diffusing. In most of the cases choice of material is more aesthetic and a wide range of materials like thermoformed plastics, fiber reinforced gypsum, concrete, high-density polyester. In recent years, concern for sustainability also influenced material choice. Wood and plastic materials raise concerns about fire resistance. When indoor air quality is desirable, low emission materials unlike formaldehyde and other carcinogenic materials are preferred.

Hybrid surfaces are capable of producing both absorption and diffusion functions. A binary amplitude diffsorber (planar hybrid surface) provides diffusion at high-mid level

frequencies and absorption at a level below cut-off frequency. A perforated mask used with a porous absorber has random holes and reflective surfaces. Some panels are fabric wrapped for visual appeal. Hybrid surfaces cover a higher range of frequencies without deadening at low-mid frequencies [87]. Their visual appeal also reduces the conflict of interest between aesthetic concerns and acoustic requirements. Curbed hybrid surfaces are used to reduce specular reflection and produce uniform diffuse reflections, unlike the flat hybrid surfaces. Though the absorption performance is the same, the dispersion capacity improves.

Here, we have addressed briefly different types of absorbers and their applications. While there may be several other types of materials that fit into this category, the above list for types of absorbers and diffusers are very common and used in various aerospace as well as other places where there is a need to address the sound waves.

2.3. Characterization Methods

Characterization of acoustic materials is useful for making an engineering judgment on the selection of materials for a required application. Different parameters can be evaluated making use of various techniques widely known. Every parameter evaluated gives a numerical sense for the physical ability of the acoustic material. Based on the acoustic properties of a material it is then finalized for a particular application. Various techniques by different organizations such as ASTM and ISO are generally employed for characterization of acoustic materials. Some techniques covered in these standards includes; standing wave method, transfer function method, multi-microphone free field measurements, Reverberation chamber method and anechoic chamber method. In this section, we will learn briefly about these standards and the parameters along with their brief descriptions.

Transmission coefficient ‘t’ is described as the ratio of the amplitude of the sound radiating from a partition to that of the sound incident on this partition at a particular frequency.

Transmission loss 'TL' is described as the ten time the common logarithm of the ratio of the amplitude of the sound radiating from a partition to that of the sound incident on this partition at a particular frequency.

Reflection coefficient 'R' is described as the ratio of the pressure amplitude of the reflected wave to that of the incident wave.

The absorption coefficient 'α' describes the amount of incident energy absorbed. The ratio of the amplitude of the reflected wave to the incident wave at a particular frequency.

Diffusion coefficient 'd' is used to understand the uniformity in the reflected waves. Such data is interesting to make engineering choices for material and designs considered for treatment over walls.

Scattering coefficient 's' is defined as the ratio of scattered to the reflected sound energy. This kind of a number can be efficiently used in computer simulations as well as to characterize the choices for various surface materials.

Wave number 'k' is described as the number of waves present in a given amount of space. Wave number is a complex entity.

Acoustic impedance 'Z' at a surface is the ratio of the surface averaged sound pressure to particle velocity normal to the surface. The real part of this number is termed resistance and imaginary as reactance. The units for this parameter is the rayl or Pa. s/m. For progressive plane waves, it is a real number as it indicates that both pressure and velocity are in phase.

$$Z = \frac{p}{v} \tag{2}$$

Where:

p = sound pressure, Pa

v = particle velocity, m/s.

Admittance 'Y' is the ratio of the particle velocity to that of the sound pressure. This parameter is the exact reverse of the impedance.

Characteristic impedance 'Z_c' is described as the product of the fluid density and the speed of sound in that fluid. This quantity is used to characterize the medium and

hence the name.

$$Z_c = \rho_0 c \tag{3}$$

Where:

ρ_0 = fluid density, kg/m^3

c = speed of sound, m/s.

Impedance ratio is the ratio of a specific normal acoustic impedance at the surface to the characteristic impedance of the medium. The real part of this ratio is resistance ratio, and the imaginary part is reactance ratio.

Admittance ratio is the reciprocal of the impedance ratio, and the real part of this quantity is termed as conductance ratio, whereas the imaginary part is known as susceptance ratio.

Decay rate is the rate at which a quantity decreases in amplitude with time after the source is turned off. In acoustics, this is applied to sound pressure level to describe the effectiveness of the material in damping the excitation. A related parameter can be used to study various other concepts.

The porosity of acoustic materials is the ratio of void volume in the material to the volume occupied by a substance in the material. High porosity implies good absorbing capacity as long as pores remain interconnected .

Air flow resistivity 'σ' is measured to indicate the amount of pressure that is lost by a fluid during a steady stream around the material. Mostly applicable for porous materials this is an intrinsic property that gives a measure of the porous materials. This parameter gives some information about the low-frequency performance of the materials and hence is paramount. The formula for resistivity is as follows:

$$\sigma = \frac{\Delta P}{Ud} \tag{4}$$

Where:

ΔP = pressure drop, Pa

U = mean steady flow velocity, m/s

d = thickness of material, m.

Tortuosity is a parameter to describe the pores that are twisted as well as have turns and bends. Mainly used to determine the velocity of sound waves at higher frequencies that comes through porous materials because of small wavelengths and absence of any viscous drag forces responsible for the dispersion of low-frequency waves.

ASTM E2611-09 is the "standard test method for measurement of normal incidence sound transmission of acoustic materials based on transfer matrix method." It employees two tubes and at most four microphones along with an analysis system for measurement of parameters like transmission coefficient, transmission loss, reflection coefficient, absorption coefficient, propagation wave number and characteristic impedance. An in-depth explanation of this standard has been carried out in section 4.3 as it forms the basis of experiments carried out.

ASTM C384 is "Test method for impedance and absorption of acoustical materials by impedance tube method." This standard presents the use of an impedance tube for measuring parameters like impedance ratios as well as the normal incidence absorption coefficients.

ASTM C423 is "Test method for sound absorption and sound absorption Coefficients by the reverberation room method". This standard explains the testing of ceiling panels, carpets, furniture or absorbers. The test specimen mounted on of the walls in the reverberation room. The decay rate is used to measure absorption. The sound absorption average is for octave bands in between 200-2500 Hz.

ASTM E90 is "Test method for laboratory measurement of airborne sound transmission loss of building partitions and Elements". As per the standard building partitions such as roofs, doors, windows and other materials used in buildings may be tested for their capacity to transmit sound. In this method, two reverberation chambers, and a test specimen in between these two rooms are present. There shall be no other way of transmission of sound except through the test specimen via vibrations. The microphones are employed in these rooms to determine the space and time averaged sound pressure levels. These readings are used to determine the transmission loss of the test specimen.

Both the rooms can act as sound and receiver. The value of transmission loss can change upon interchanging the rooms, but the average of readings is the value of transmission loss. This resultant value is the actual transmission loss of the test specimen.

ASTM E1050 is "Test method for impedance and absorption of acoustical materials using a tube, two microphones and A digital frequency analysis system." An impedance tube along with two microphones, data acquisition and processing system and the speaker determine the absorption coefficients and acoustic impedance in the materials. A test sample similar to the size of the tube is placed in at one end of the tube and is backed by a hard wall. A white noise signal is generated from the speaker. The standing wave is separated into forward and backward traveling waves using two microphones located within a fixed distance from each other. The frequency range is dependent on the size of the tube and distance between the microphones. This method was evolved just to be faster while compared to the C384.

ASTM E2249 is "Standard test method for laboratory measurement of airborne transmission loss of Building partitions and elements using sound intensity". This test is same as test method E90 but except for major changes in the second room. The source room is still a diffusive reverberating room, but the receiver room is an anechoic chamber. The other important difference is that microphones gather data in the reverberation room, but a sound intensity probe collects information in the receiver room. The sound intensity is measured either by a discrete point method or a pattern scanning method. These intensity measurements are used to calculate the intensity transmission loss for test specimens.

ISO 354 is "Acoustics - Measurement of sound absorption in a reverberation room." It is a standard that is similar to ASTM C423 but includes specifications that are more detailed in comparison with its C423. In this method, the reverberation of the room is tested twice, once when there is no test specimen in the chamber and the next time when there is one. The number of decay measurements collected can be less in comparison to C423. The sound absorption coefficient is division sound absorption area and the area covered by test specimen; use of the two reverberation times gives the sound absorption coefficient.

ISO 10534-1 describes "Acoustics—Determination of sound absorption Coefficient and impedance or admittance—Part 1: Impedance tube Method". This method is another one that makes use of the impedance tube standing wave pattern to make the measurements of the acoustical parameters of the specimen under evaluation. A standing wave formed in between the source and the test specimen within a tube of particular dimensions. This standing wave is separated into the forward and backward traveling waves to make measurements. Two microphones and analysis system are used with an impedance tube to gather the data.

ISO 10534-2 describes "Acoustics—Determination of sound absorption Coefficient and impedance in impedance tubes—Part 2: Transfer-Function method". This method is similar regarding setup to that of ISO10534-1 except for the fact that the processing of the data uses complex acoustic transfer matrix method. The advantage of this approach is that it helps in faster processing of the data.

SAE J1400 is "Laboratory measurement of the airborne sound barrier performance of flat materials and assemblies." It is an alternative method developed by SAE to ASTM E90 and ASTM E2249. In this, there is a source room which is reverberation room and a receiver room that is an anechoic chamber. The transmission loss of a test specimen compares against a reference sample. The Correction factors are used to obtain the theoretical value of the reference sample based on the surface density of the materials. These correction factors calculated are meant to be approximations for any differences arising due to the setup of the test. As microphones utilize both the rooms space and time to collect averaged signals. These are used to calculate the sound pressure levels that in turn help in calculating the transmission loss. The frequency bandgap range of interest is 125 to 8000 Hz in the one-third octave band frequencies.

In this study five different foam samples were charecterized. The five foams were as follows BASF Basotect G (G), BASF Basotect G+ (G+), BASF Basotect UL (UL), Melamine Foam (M) and Divinycell Foam (Div). To understand the testing procedure and averaging technique for experiments refer to Section 4.3. Evaluation of transmission loss of four configurations with an aluminum plate and foam is conducted. Foam alone (FA) configuration, single aluminum plate in front of foam (SP-F), single aluminum

plate behind foam (SP-B), double aluminum plate (DA). The aluminum plate used is 0.025 inches thick and has a 3" square cross section. All foam samples are 1" thick. Basotect G and G+ are used most often in spacecraft launch systems while the UL is in aircraft applications. G and G+ are heavier and are said to have improved TL compared to the UL foam. The divinycell foam used is less foam and more plate-like behavior and is heavier compared to other foams. All the other foams are variants of melamine foam. The characterization of these foams has been performed using the parameter transmission loss and following the standard ASTM 2611. The results of this testing are in Fig. 9. The top left corner shows the testing results of just the five different foams. It is obvious from the results that divinycell foam has more plate-like behavior whereas the others behave in a similar fashion. The dip for G, G+, UL is at around 700 Hz. This dip indicates the first resonance mode of the test specimen. Whereas for the M foam, it is around 850 Hz. The top right corner shows the results from the back plate behind the foam configuration. Moreover, mostly the performance of Mel foam over aluminum back plate has the best performance. On the bottom left corner is the SP-F configuration this is relating to how we intend to make use of the foam and the UL foam dominates the region below the dip location. Melamine Foam has a better performance beyond the natural frequency of the plate. The bottom right corner shows the foam sandwiched in between two aluminum plates and performance compared to a double aluminum plate. It looks like the M foam is dominant over the entire region below dip. Whereas the G+ and UL share good performance in the above dip location. The UL foam has the best TL performance to its weight and hence it makes sense to use it in the air crafts as it is the lightest material. However, melamine foam seems to be the best performing foam overall based on TL. In general, we observe an improved transmission loss curve with addition of the foam in the high-frequency region and less improvement in the low-frequency region.

For the SP-F configuration an analysis of the TL with respect to mass density was carried out to outline a pattern for selection of best low frequency performing foam and based on the graphs form the Fig. we can conclude that the UL foam has the best performance in the range 200-800 Hz while compared with others in the SP-F configuration.

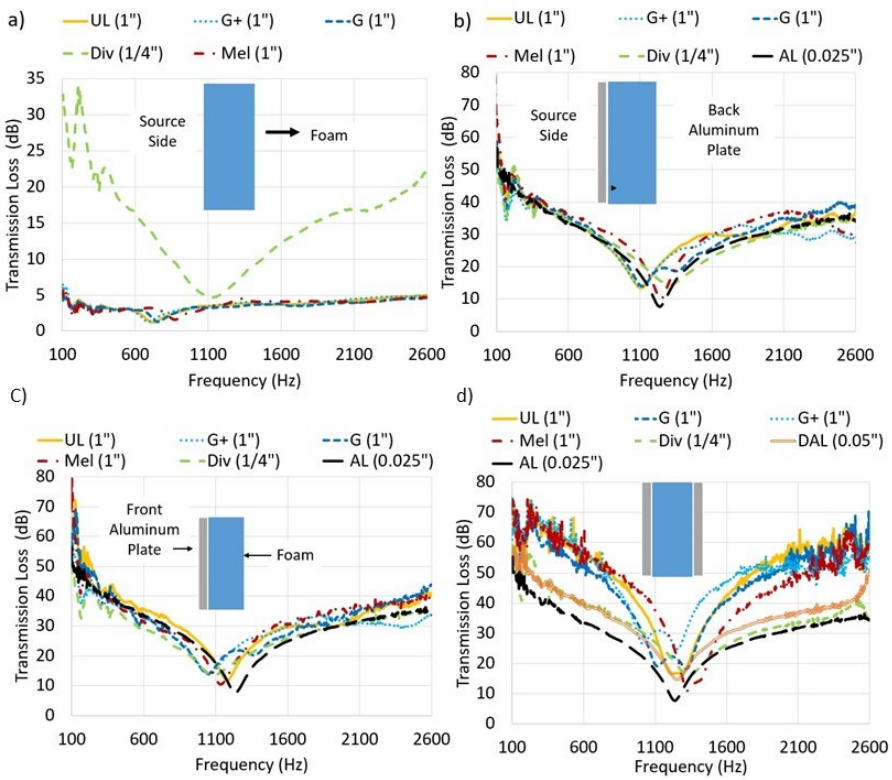

Figure 9: Transmission loss curves of foams in following configurations (a) Foam alone, (b) SP-B, (c) SP-F and (d) DP

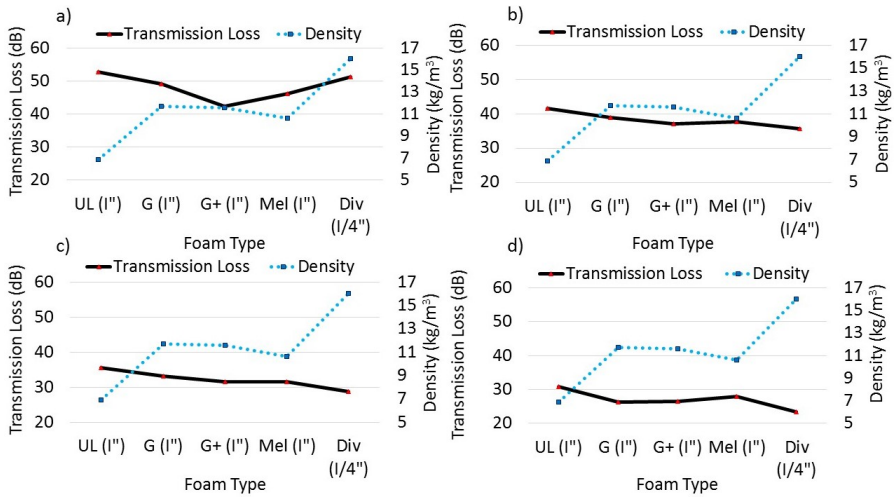

Figure 10: Single Plate Front (SP-F) configuration TL comparision with density at (a) 200, (b) 400, (c) 600 and (d) 800 Hz.

2.4. Summary

A brief description of the four different types of conventional acoustic materials currently being used were presented in the Section 2.1. Section 2.2 provides a description regrading the different types of absorbers and diffusers along with the mechanisms of absorption and diffusion in such acoustic materials. Some exotic acoustic materials were also covered in the same section. In the Section 2.3, the definitions of the acoustics properties and acoustic characterization techniques were discussed.

CHAPTER 3

Design of Metamaterials-Inspired Vibro-Impact Structures

The purpose of this chapter is to discuss the detailed design and conditions to improve effectiveness of MIVIS unit cells, the analysis techniques and simulation models employed in the process.

3.1. Introduction

The motivation for MIVIS conceptual models come from previous research conducted on acoustic metamaterials as well as energy harvesters. The mass loaded membrane type acoustic metamaterials are gaining popularity for their applications in LF acoustic noise mitigation applications. The advantage of such dynamic behavior goes into designing the MIVIS unit cell. The phenomenon of frequency 'up-conversion' in vibro-impact structures has also been used to construct efficient vibrational energy harvesters. Research has also been carried out on nonlinear energy sinks that can absorb low-frequency energy based on impacts upon structures and thereby mitigate low frequency by up-converting it into higher frequencies of the structure. These high frequencies come from the vibration mode shapes of the structure. Based on this model, tuned low-frequency mass loaded membrane type resonator attachments on a base structure for frequency up-conversion via the vibro-impact mechanism are studied. Low parasitic mass addition and broadband low-frequency transmission loss are some of the relevant outputs expected from the MIVIS. It might be interesting to incorporate broadband energy harvesting and sensing functionalists using piezoelectric layer. MIVIS for LF acoustic noise mitigation consists

of tuned vibro-impact attachments on a baseline structure (back plate). Mass loaded membrane type acoustic metamaterials that act as an LF acoustic absorber. Frequency up-conversion that is obtained from the impact on the back plate.

As shown in Fig. 11 the MIVIS builds by bringing synergy of ideas from previously conducted experimental research. The mass loaded membranes are adopted from the low-frequency narrow bandgap AM. These exhibit the resonance phenomena at a frequency that is less than the LF limit described previously. Pertaining to resonance phenomena they exhibit narrow-band improvement in transmission loss but take a hit on the stiffness of the structures. In another research, nonlinear energy harvesters were used in the form of vibro-impact upconversion to structure's mode shapes for mitigating LF seismic activity, 50% displacement reduction with just 3% mass addition is observed . Hence, these two ideas are combined to have a LF mass loaded membrane over a backing structure to initiate a contact between these to alleviate the incident LF acoustic waves.

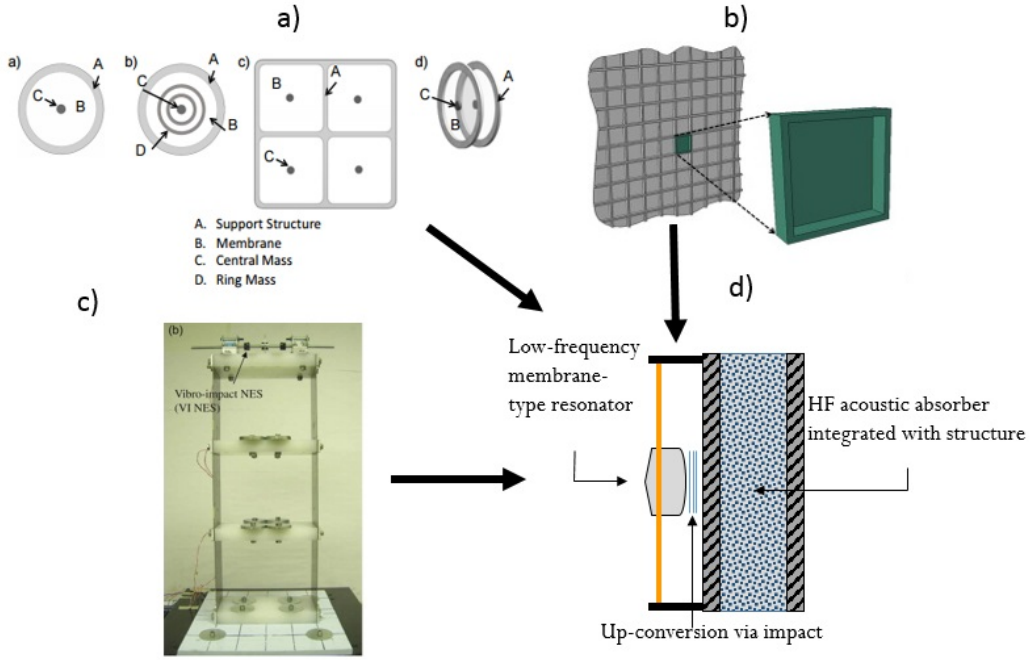

Figure 11: (a) Membrane-type acoustic metamaterials [11, 12], (b) Cellular metamaterial structures [13], (c) Vibro-impact energy sinks for seismic mitigation [14] and (d) MIVIS conceptual scheme.

Preliminary testing was conducted using 3D printed back plates as well as mass loaded membranes. Initially, some amount of warping of the back plates was observed due to uneven heat distribution but later on this was offset by using a smaller deposition rate at 80 mm/s and an efficient surface temperatures at 120 °C and 113 °C respectively. The back plates built were about a quarter inch thick and their testing for transmission loss obtained dip at the first mode shape of the plate. One major concern before the start of testing was the effect of the entrapped air in between the membrane and the back plate. For this reason, four different membrane designs were made that would be used for testing of MIVIS test articles initially. These four membrane designs are shown in the Fig. 12.

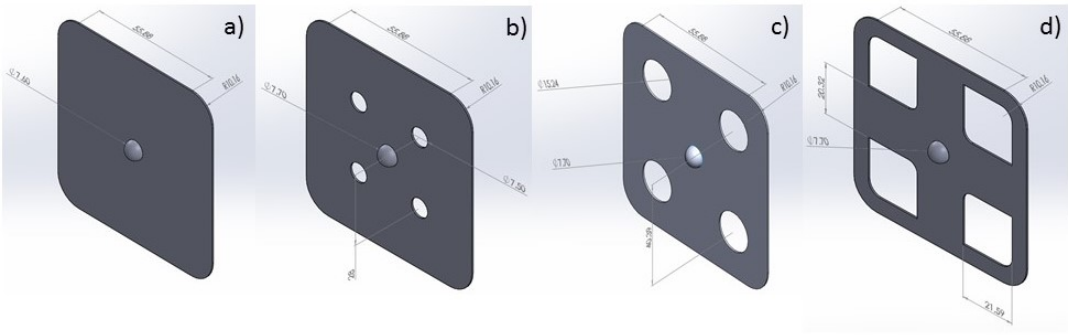

Figure 12: Various designs of mass loaded membranes designed to be 3D printed and tested as part of the MIVIS unit cell (a) simple membrane, (b) membrane with hole size of 7.5 mm, (c) membrane with hole size 15 mm and (d) quadrant-cut.

While the 3D print quality was good, the complex features such as the spherical ball in the center of the membrane is hard to print perfectly. This imperfection along with the quality of 3D printed materials to be more stiff led to the usage of customized off the shelf materials for testing which are discussed later.

As a preliminary step before the manufacturing and testing of the full MIVIS prototype unit cell, a 3D printed plastic MIVIS cell was made to explore transmission loss results from testing of such devices. A figure of the MIVIS unit cell and TL testing

results are shown in Fig. 13:

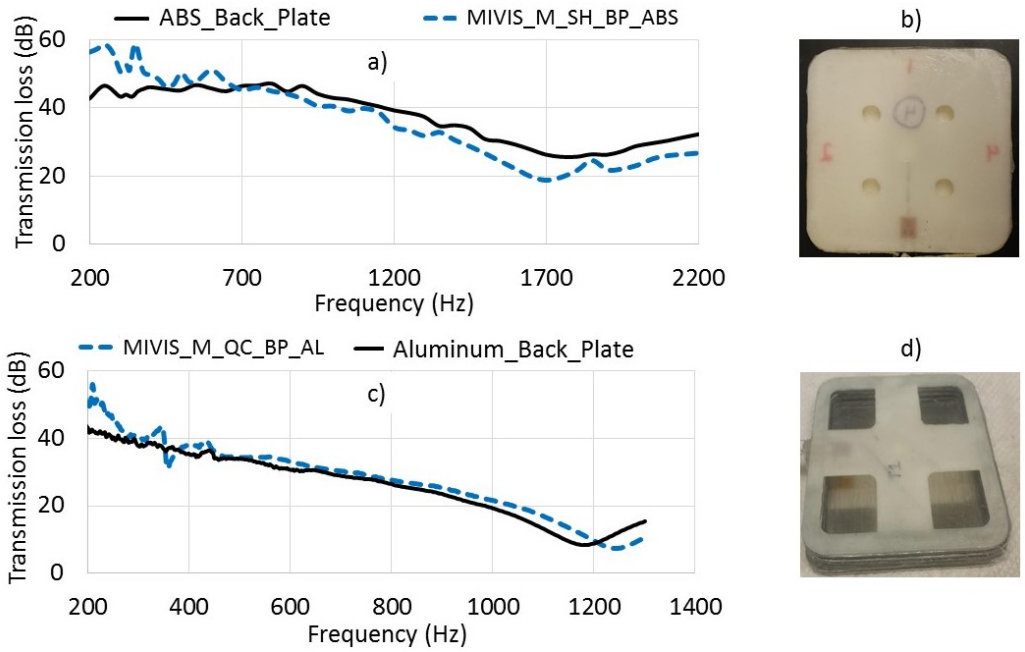

Figure 13: Transmission loss test results of preliminary 3D-printed MIVIS unit: (a) TL for MIVIS_M_SH_BP_ABS. (b) MIVIS_M_SH_BP_ABS test article. (c) TL for MIVIS_M_QC_BP_ABS. (d) MIVIS_M_QC_BP_ABS test article.

Two prototypes were tested to determine the charecteristic transmission loss of MIVIS unit cell. The first one was completely 3D printed. It was named MIVIS_M_SH_BP_ABS (first prototype) and the second one was a mix of 3D printed membrane and aluminum back plate MIVIS_M_QC _BP_AL (second prototype) they are as shown in Fig. 13(b) and (d) respectively. Here, M is a membrane, SH is a small hole of diameter 7.5 mm, QC is quadrant cut, BP is back plate, ABS is the plastic material and AL stands for the Aluminum plate. Although not fully representative of the planned MIVIS unit cell, this test is useful to determine the critical design elements. The gap between the impactor and back plate, as well as the entrapped air, plays a significant role in designing a successful vibro-impact resonator. As seen in Fig. 13, cutouts were made to some of the membranes to lessen the stiffness effect of trapped air between the membrane and the backing plate. The final MIVIS prototype will be used to test multiple membrane geometries with and without cutouts. Average of three trials was taken from multiple

runs to reduce the scatter that was occurring from boundary imperfections. A 10-15 dB increase in transmission loss in a continuous bandwidth of 20-50 Hz in the vicinity of membrane's resonance frequency is observed. TL peaks should correlate with modes of the MIVIS unit cell and it is of interest. Multiple peaks obtained from MIVIS with a quadrant cut membrane as seen in MIVIS_M_QC _BP_AL is due to complex modal behavior. Impactor gap and entrapped air interaction play a major role in transmission loss performance.

Fig. 14 shows the difference is acoustic spectrum data from pressure signals for the above 3D printed MIVIS test articles, when the impactor on MIVIS_M_QC _BP_AL is contacting (right in Fig. 14) and not contacting (left in Fig. 14) the backing plate. The acoustic spectra results are of importance from two standpoints: (1) We can tell if the impactor is making contact with the back plate and (2) we can now see the amplitude increase in the higher frequencies in the impact case versus the non-impact case.

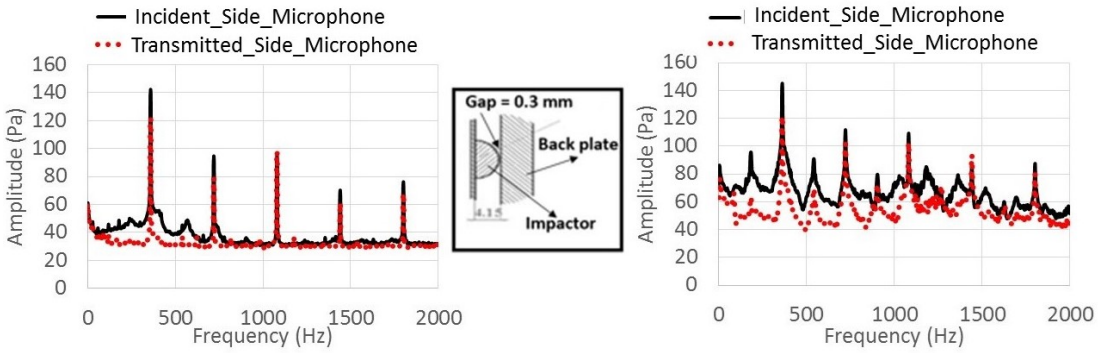

Figure 14: Spectrum plots of no impact vs impact of MIVIS unit cell

Based on the results from testing of prelim MIVIS unit cells, similar results were generated again with the addition of monotonic excitation. Also, the 3D printed design is optimized using the printer settings and the hole diameter in the membrane is increased to decrease the stiffness provided by the entrapped air. The first case was with the quadrant cut membrane placed over the frames and back plate is termed as MIVIS_M_QC_BP_AL. Here the symbol 'BP' at the end means back plate and 'M' means membrane. The gap maintained between the impactor and back plate in 2.1 mm.

Transmission loss is better in the range 178 to 1206 Hz than back plate alone except in one region; this has a maximum continuous bandwidth of 1028 Hz to record a improved TL. At 208 Hz the transmission loss is better by 13.4 dB. There are local peak and dip phenomena in the range of 314 to 430 Hz also for the monotonic excitation there is a deviation from the white noise TL at 348 Hz and is similar to that of back plate alone for the rest of the curve. The second case was with a bigger hole membrane (BH) with holes of diameter 15.0 mm and is termed as MIVIS_M_BH_BP_AL. TL in the range of 186 to 754 Hz is better than the back plate alone except in two regions. The bandwidth of the TL is better than back plate in the range of 668 Hz except for two places where it falls below that of the back plate. At 220 Hz the peak performance is better by 10.9 dB. There is local peak and dip Phenomena in the range around 310 to 442 Hz. Though this is a preliminary study, it does provide a good idea of the TL behavior of MIVIS test articles.

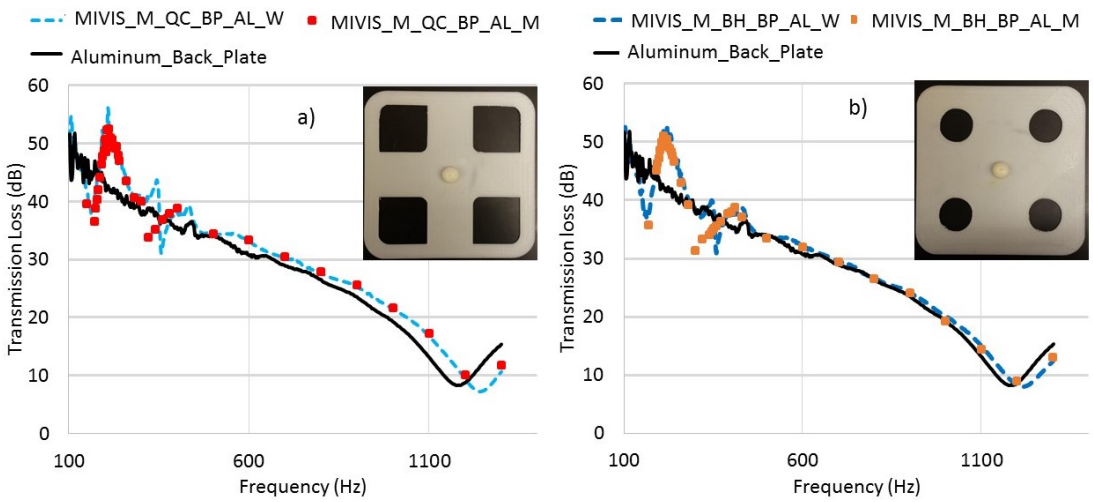

Figure 15: a) TL of MIVIS_M_QC_BP_AL unit cell with picture of membrane inset and b) same for MIVIS_M_BH_BP_AL unit cell.

3.3. Conceptual Design

The conceptual designing is a meticulous process to create a design that does a good job at making the prototype a reality. To understand the behavior of mass loaded membranes, which are going to act as locally resonant AM, it is necessary to have easily tunable design. Also, to introduce vibro-impact coupling between a LF mass-loaded membrane-type AM and a HF acoustic absorber to create an effective LF acoustic barrier conforming to application-specific constraints. Amongst many a significant contributor is the selection of material and the material damping that controls the effective deformation of the mass loaded membranes at resonance.

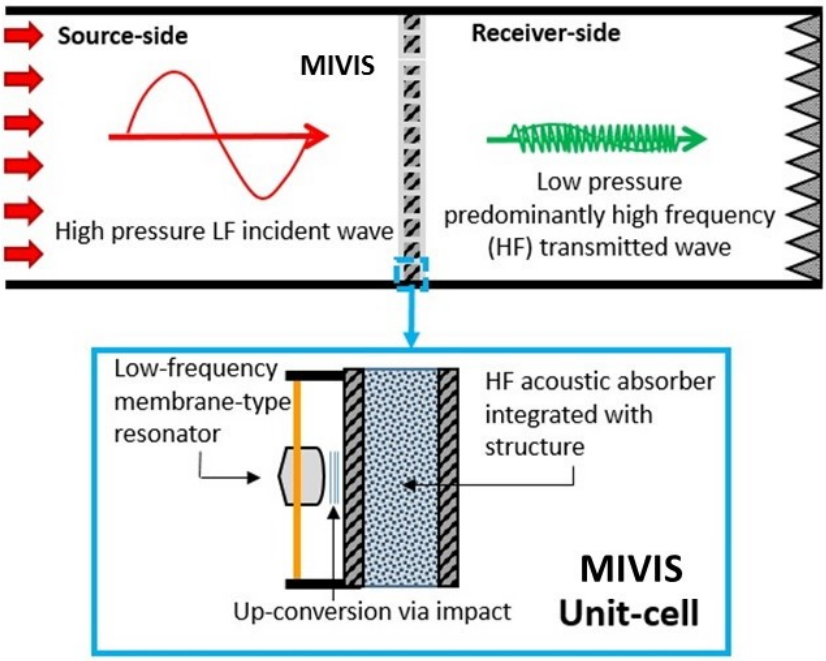

Figure 16: Schematic of a metamaterial-inspired vibro-impact structure.

Conceptual, preliminary designs made out of 3D printed components are initially tested and later better materials are investigated for application as MIVIS unit cell based on transmission loss performance. Mass addition to baseline structure is to be kept less than 10% to minimize parasitic mass addition. A 3D printer "MakerBot Replicator 2X" was employed to check the feasibility of a design and develop various test articles.

The material used was Acrylonitrile butadiene styrene (ABS). This rapid prototyping technique provides a fast way of optimizing the design and correct any malfunctioning features in short span of time with less added cost. Modulus, density and Poisson's ratio for the ABS material are 2 GPa, 1020 kg/m^3 and 0.39.

The conceptual design criterion was to minimize the mass addition to 10% of the original structure while retaining the primary stiffness of the structure. The conceptual MIVIS design has four key features: a) mass loaded membrane (MLM), b) frame, c) back plate and d) impactor. These four features are explicitly shown in Fig. 17. The MLM is made from a flexible membrane and is centrally loaded with a dome shaped rivet; some washers are available to increase or decrease the weight of the mass over the membrane. A locking washer is provided in the end to keep all the washers in place. The membrane has a hole of 1.59 mm in diameter and the radius of the rivet head is 7.86 mm. There are no holes in membrane to study the effect of reduced stiffness caused by the air that is entrapped in between the membrane and the back plate. The weight of the membrane is maintained at 10% of the weight of the back plate and frame combined. The frame is made by stacking together 'n' number of spacers with varying thicknesses to change the gap between the tip of the impactor and back plate as shown in Fig. 17(b) and (d). One washer is always kept under the rivet to give support and hence the height of the tip of impactor from the surface of the membrane is always maintained constant. The total thickness of the back plate is 2.21 mm. The weight of the membrane is approximately 3.5 g using ABS plastic that is 10% of the 34.7 g using the same material, which is the combined weight of the back plate with the frame.

Based on the MIVIS conceptual design we frame some of the objectives applicable to the design of the test article and they are:

1) To design a membrane that is thin enough to be flexible and pick up energy from the LF pressure waves leading to an impact, to have the resonance and antiresonance of membrane tuned to below 400 Hz after addition of the central mass.

2) To be able to select a back plate with the first resonant mode shape in between 400-2600 Hz and also posses a high coefficient of restitution between the impacting pair.

3) Having spacers that could be easily swapped to vary the gap (G) between the tip

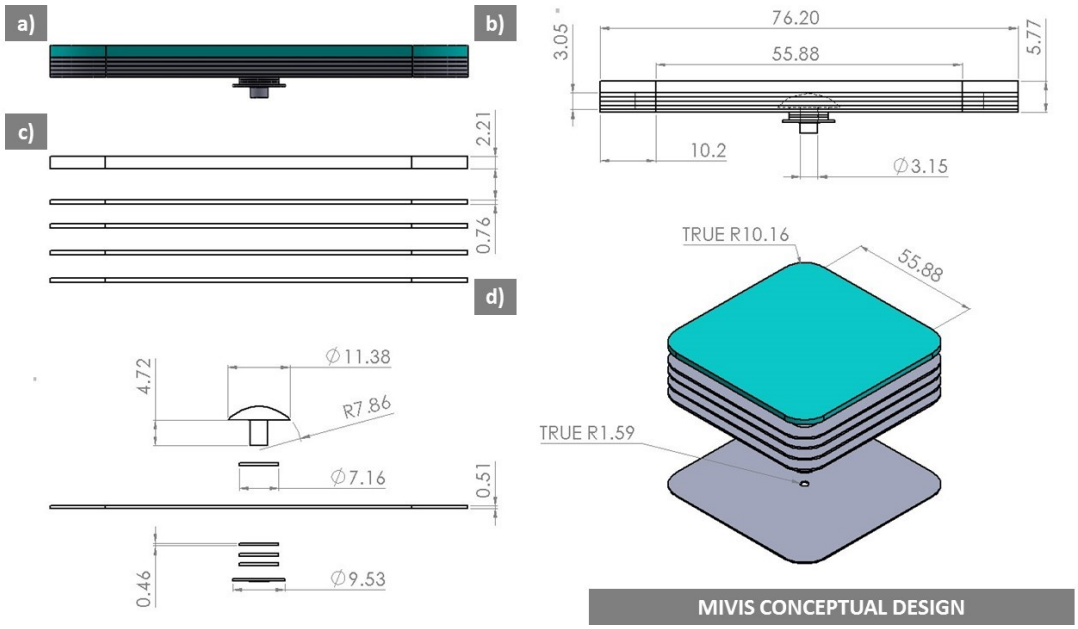

Figure 17: MIVIS conceptual design a) Solid side view, b) Drawing of the side view along with internal components, c) Exploded side view and d) Exploded isometric solid view. (All dimensions are in mm).

of the impactor and surface of the back plate. To have a very good surface finish on the swappable frames to remove uneven surfaces preventing leaking of entrapped air.

4) The impactor head must be made up of a hard material to be able to transfer impact without creating any disturbances that could be caused by stress due to the repetitive impact.

5) The washers used are small in size and hence must be made from a dense material.

6) The locking plate of the washer that will be applied to the shaft of the rivet must lock all the washers and maintain a proper tension between the washers.

3.4. Simulations

3.4.1 Development and Verification of Simulation Model

The first steps were taken towards the development of simulations and correlating these with testing results of simple flat plate test articles. This study was done to ensure agreement between simulation and testing results of simple symmetric structures. The model that was employed for transmission loss tube setup is shown in Fig. 18(a) and the boundary conditions (BC) are shown in Fig. 18(b). This model has been developed to reflect the testing conditions as closely as possible. The incident side tube and the transmitted side tube are the same sizes as the air column in the experimental setup i.e.; 36" each in length. The test article's dimensions are kept same as for the actual test articles standard properties are used. All degrees of freedom are locked on the edges. At the end of the transmission loss tube, a non-reflective boundary condition is used to avoid the generation of reflections in the transmitting tube. A frequency dependent perturbation analysis was simulated in the range of 50-2600 Hz.

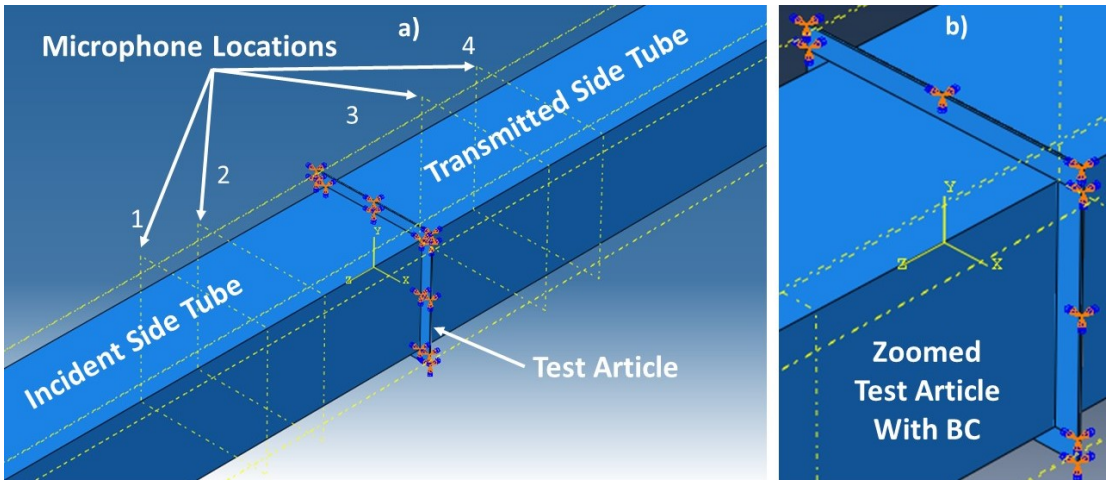

Figure 18: (a) A simulation model for transmission loss tube setup with the test article and (b) Zoomed view of the test article with boundary conditions (BC).

Initial simulation and testing effort is focused on the flat aluminum plate. The results of simulation and testing of a 0.65 mm plate are shown in Fig. 19(a). A good correlation

between the testing and simulation results is observed. The simulations predict the location of the transmission loss dip at 989 Hz for the aluminum plate. An estimated overall structural damping (ds) of 0.1 is required to match simulation and test results for both the aluminum plate. The damping value controls the depth of the TL dip seen in the graph. The ds parameter is an unknown quantity, and can only be tuned to match the experiments because it is quite not possible to calculate the resistance of any plate to the inertia caused by a cyclic pressure loading. The setting of boundary conditions plays a vital role in determining the output of the transmission loss. A detailed analysis of the effect of unit less structural damping is available from the experiments conducted in Section 4.3, where an effort was carried out to get a consistent clamping mechanism for fixing samples in the tube with the repetitively same boundary conditions. All the material properties for aluminum are given in Table 1.

A similar effort is made to 3D print a ABS plastic plate. The results of simulation and testing of the plastic sample are shown in Fig. 19(c). These results show a small difference in the location of TL dip compared to the aluminum plate. This difference might be arising from the nature of 3D printing that may produce variations in density and geometry away from the ideal properties. In the later stages contact simulations are developed to predict the response of monotonic excitation on the MIVIS unit cell and then optimize the MIVIS unit cell parameters to obtain the best up-converted results. All the material properties for ABS are given in Table 1.

The dip in the transmission loss curve is associated with the natural frequency of the plate. Standard books on the calculation of natural frequencies are available. Using the formulae from the reference [88], we get a good match for the calculated, simulated and measured value that is shown in Table 2. The formulae for the natural frequency of thin flat plates of uniform thickness with all edges clamped is:

$$w_n = B\sqrt{\frac{Et^2}{\rho a^4(1-\nu^2)}} \tag{5}$$

Where, E = Youngs modulus, t = thickness of the plate, a = length of square plate ρ = mass density, ν = Poisson's ratio, B = multiplication factor based on boundary

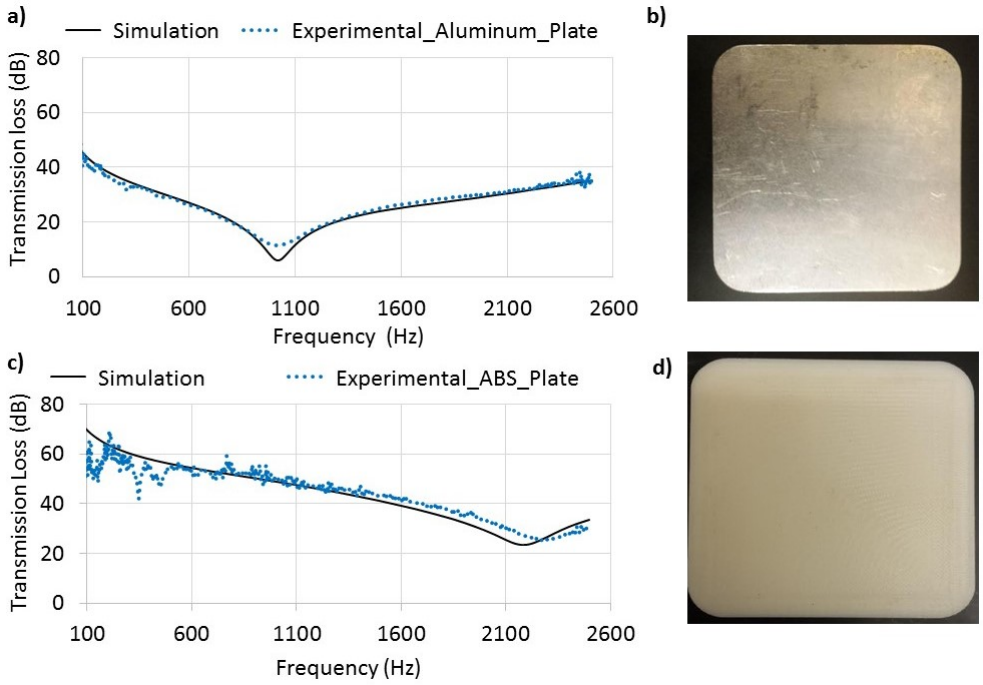

Figure 19: (a) Transmission loss data for simulation vs testing of a 0.65 mm Aluminum back plate, (b) 0.65 mm Aluminum backing plate, (c) Transmission loss data for simulation vs testing of a 0.25" 3D printed ABS plastic plate and (d) 0.25" ABS plastic plate.

condition related to outside edges clamped = 10.4.

Another study concerning the simulations was the effect of damping on the transmission loss curve. The value of the structural damping had become an important parameter in matching the flat plates simulation to experiment. The effective parameter is to be tuned from simulations with different damping values. This damping essentially acts as a resistance to the inertial forces of the structure. Various damping parameters were used to study the shape of the transmission loss curve at the resonance frequency. The more is the value for damping the less is the pressure created due to the reduced velocity of the structure that is connected to the transmitted air medium. The effect of damping on transmission loss are in the Fig. 20.

Table 1: Material properties

Material	Property	Value
Aluminum	Young's modulus	70 GPa
	Mass density	2700 Kg/m^3
	Poisson's ratio	0.3
ABS	Young's modulus	2 GPa
	Mass density	1020 Kg/m^3
	Poisson's ratio	0.35

Table 2: First mode shapes of plates of different sizes and material

Material	Thickness (mm)	Length (inch)	First Mode (Hz)
Aluminum	0.65	3	989
	0.65	2.75	1178
	0.65	2.5	1424
ABS	6.35	3	2182

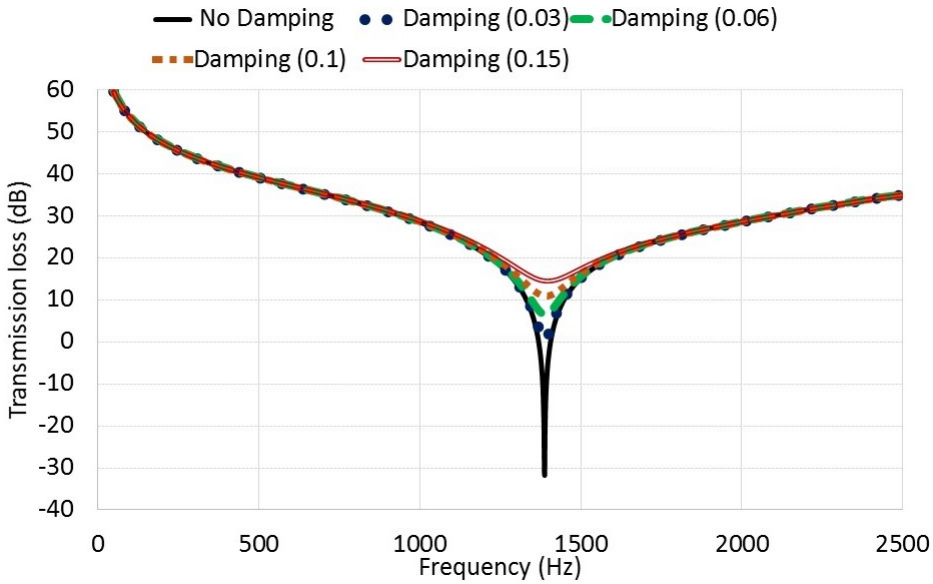

Figure 20: Variation of the Transmission Loss curves at the dip location for different values of structural damping

3.4.2 Effect of Entrapped Air in Simulations

Simulation of the MIVIS unit cell is carried out with a single mass loaded membrane and backing plate. The gap between the membrane and backing plate is simulated as an empty void with no entrapped air. The model is then improved to include the en-

trapped air between the membrane and backing plate. It is necessary to see that it was computationally limiting to develop the small spherical mass. A total mass equivalent to the hemispherical mass was allotted to the central node of the mesh. The results of multiple simulation runs as well as variation in membrane thickness and simulation damping are shown in Fig. 21. The thickness of the membrane is initially designed to be 0.6 mm. The material properties of the membrane are that of ABS plastic. The Aluminum back plate used has a thickness of 0.65 mm. Firstly no entrapped air is modeled, and from the plot, the dotted lines (MIVIS_D0p1_M0p6_No_Entrappedair) in the top indicate a high transmission loss and it is true as when there is no air medium, the waves are traveling only through the structure. Entrapped air is the term describing the air present in between the membrane and back plate. Later on, the entrapped air is modeled, and the three different damping ratios are tried for the membrane of thickness of 0.6 mm. It is obvious that as the structural damping progresses from 0 to 0.1 and then to 0.5, just amplitude of the peaks at resonance are affected. Above mentioned models are observed by following the dashed lines light blue, dark blue and compounded dotted light blue respectively (MIVIS_D0p0_M0p6_With_Entrappedair, MIVIS_D0p1_M0p6_With_Entrappedair,MIVIS_D0p5_M0p6_With_Entrappedair). For the three transmission loss curves as we start from left at 100 Hz and move up, we observe a first dip associated immediately with peak followed by two dips. The first dip on the transmission loss cure is related with the resonance of the membrane. Whereas, the first peak just after the first dip is associated with the anti-resonance frequency of the membrane. There are two more dips, and after these, there are two more features where due to phase change the peak and dip are the antiresonance and resonance of the membrane. The mode shapes associated with the first three dips for the model MIVIS_D0p1_M0p6_With_Entrappedair configuration are shown in Fig. 22. A total number of mode shapes for the MIVIS_D0p1_M0p6_With_Entrappedair configuration are 16 in the 50-2600 Hz frequency range. This first resonance mode occurs at 528 Hz for the given configuration. Here, only the membrane tends to move in and out of the plane leaving the back plate in the same position. The second dip occurs due to the motion dominated by both the membrane as well as the back plate occurring at 1123 Hz. The

third dip occurs at 1505 Hz and is due to the motion of the membrane and back plate.

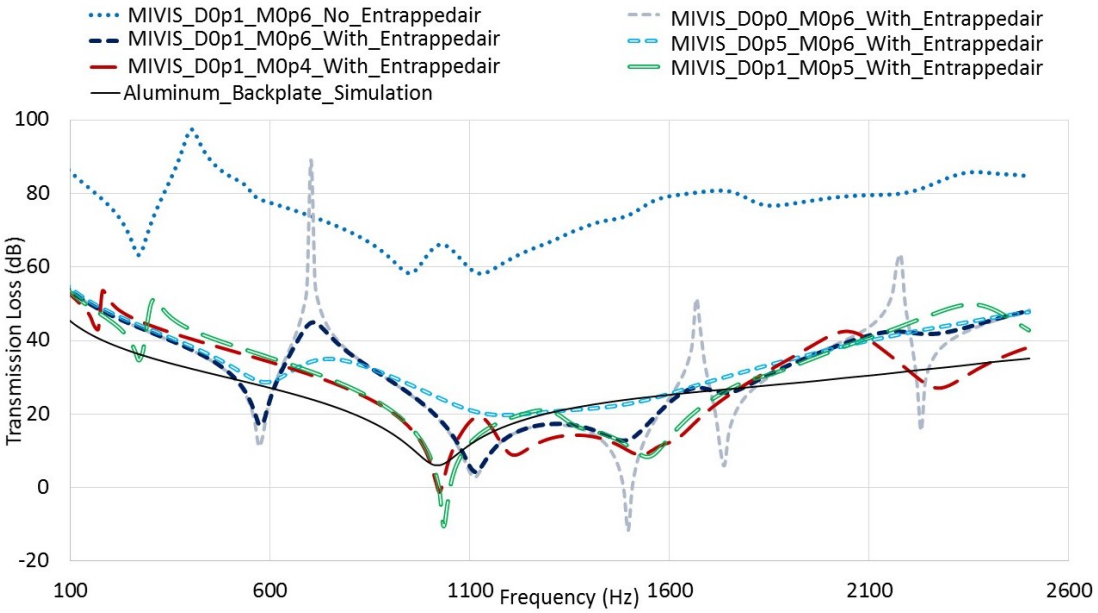

Figure 21: Simulated transmission loss characteristics of MIVIS including the effect of damping on membrane and without entrapped air.

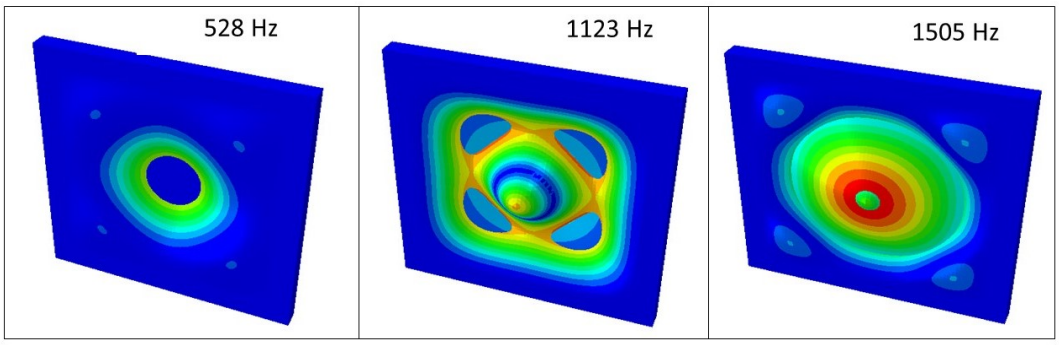

Figure 22: First three mode shapes responsible for the dips in the transmission loss curve of MIVIS.

The membrane and impactor of the MIVIS unit cell should be redesigned to resonate at frequencies below 400 Hz to pick up the LF noise from a specific source for up-conversion via vibro-impact. Modal analysis was carried out based on the transmission loss curves of the MIVIS structure. The purpose of this study is to investigate the trend

in variation of membrane thickness with the location of the dips. A phenomenon that occurs is the increase in the total number of mode shapes in between the range of 50-2600 Hz as the thickness decreases. Such a trend is observed from the data shown in Fig. 23. Here membranes of four different thicknesses starting from 0.6 mm and reduced by 0.1 mm every design are considered. Fig. 23 show that the modal frequencies can be decreased to the desired level by reducing the thickness of the ABS membrane below 0.5 mm. These thicknesses are widely available from manufacturers and are also thick enough to not permanently deform after continuous use to produce consistent results every time.

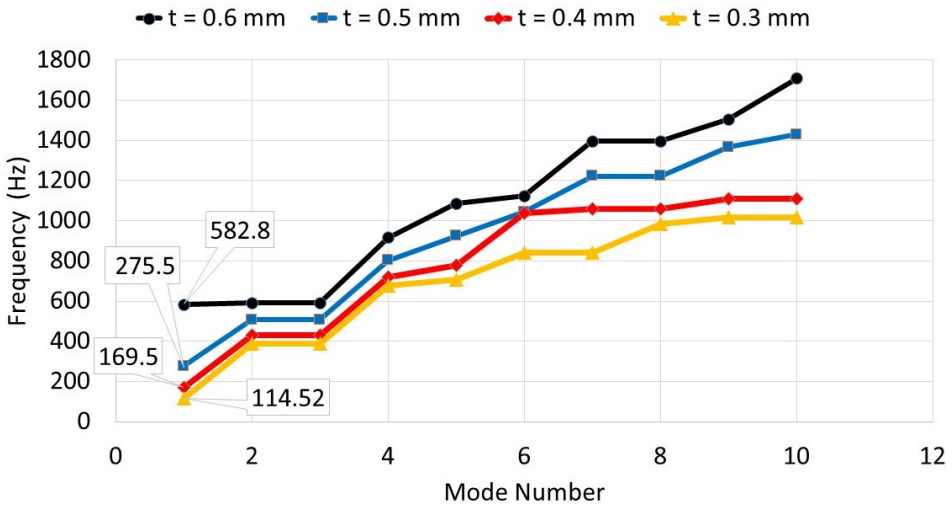

Figure 23: MIVIS simulated modal response - Variation in frequency (Hz) with changing membrane thickness (t in mm).

To reduce the order of modeling for entrapped air by approximating its stiffness and replacing it with discrete springs so that contact simulations are easier to implement. It was found that the best way to model the stiffness of the entrapped air column as springs was to use the adiabatic bulk modulus of the air in the formula for the effective stiffness of the entrapped air is given by:

$$k = \frac{KA}{L} \tag{6}$$

Where,

K = Adiabatic bulk modulus of air = 142000 Pa,

A = area of the cross section = 0.004 m^2 and

L = length of the entrapped air column = 4.15 mm.

Now, from this formula, the total stiffness is calculated, and for sixteen parallel springs to model the effective entrapped air stiffness the stiffness of each spring is approximately 8554.2 N/m. By approximating the stiffness of the air column, we were able to achieve a good relationship for transmission loss with spring and entrapped air. The results from these simulations as well as the modeling details are shown in the Fig. 24.

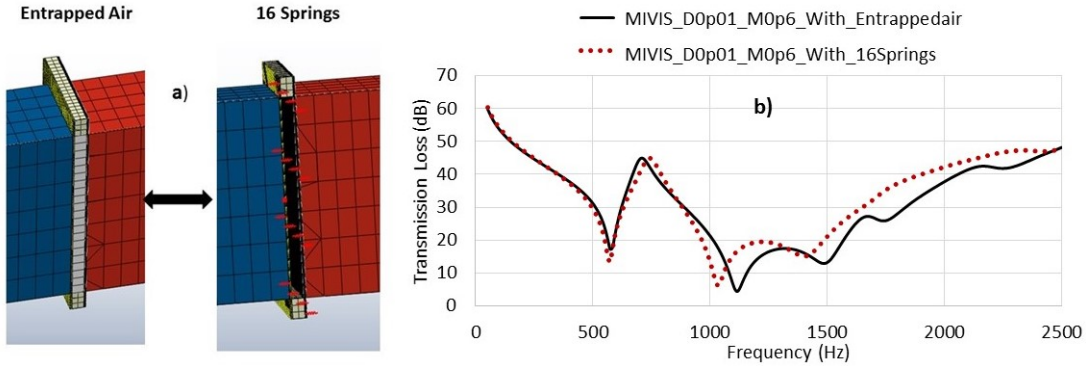

Figure 24: Comparison of the Transmission Loss for the entrapped air against 16 equally stiff springs.

3.4.3 MIVIS Simulation with Contact

Including contact phenomena in the simulation is a major step towards understanding the impact dynamics that would occur in the MIVIS. The spectral content of the pressure signals in the incident and the transmitted column is an important parameter to study. It will be interesting to examine this parameter as it is going to be different for both the contact and non-contact simulation. A steady state simulation will provide the database to build information that would lead to effective designing of the MIVIS unit cell. Maximizing the TL of low-frequency acoustic energy is an indicator of improvement in the performance. These are full fledged transient simulations that will record

the displacements of the membrane and back plate. The membrane and back plate displacements are used to study the correlation between the pressure signals and draw conclusions on their behavior. Firstly, comparing the difference between the contact and non-contact simulation to appreciate the importance of contact phenomena is done. For this, constructing two similar models with the added central hemispherical mass instead of the point loaded mass on the central node of the membrane is used in the MIVIS model that includes contact.

For creating the meshes in the simulations models, convergence studies were carried out. It was observed that a dense mesh would lead to erratic results and a coarse mesh did not accurately predict the correct values for frequencies of membranes and back plates. After analyzing different element types, Standard linear 3D stress hex elements were selected to perform both the perturbation and steady state simulations. The element sizes were assigned based on the convergence studies for each part. For the back plates the material along the thickness was divided into three elements and for the membrane this was four. For the air columns the standard linear acoustic hex elements were employed after doing convergence studies and accurately predicting the modes of these air columns.

Contact and non-contact simulation consist of the Aluminum back plate and ABS membrane with and without impactor respectively. Both of them have been modeled using 16 springs with the stiffness of each spring being 8554.2 N/m is a good approximation to replace the exact stiffness caused by the entrapped air. The material properties of the Aluminum back plate and ABS membrane used are same as in section 3.4.1. The gap between the tip of the impactor and back plate is 0.3 mm. Whereas, the gap between the central node of the membrane and backplate is 3.85 mm. Contact initiation is obtained at 564 Hz, which is also the first mode of the membrane. The computational time required to get data from transient dynamic simulation with contact is higher to obtain steady state pressures. If we increase the structural damping in the non-contact simulation, the steady state reaches quickly but will also affect the efficiency of up-conversion. Four microphone locations were used to record the pressure signals and the back plate, and membrane displacements are registered using the points at their central node. The

description of the impedance tube setup along with the contact and non-contact model are shown in Fig. 25. The microphone locations are based on the distance from the reference plane, which is the plane of the surface facing transmitted side tube of the back plate. Microphone locations are kept same to the experimental setup, and the values for the distance from reference plane can be found in Section 4.3.

Figure 25: a) MIVIS simulation model with contact b) MIVIS without contact c) Four microphone locations relative to the specimen.

The FFT of the microphone pressure signals at locations 3 and 4 show that impact has created higher frequency content while reducing lower frequency content peaks as desired. The locations 3 and 4 are present in the transmitted side of the test specimen. We can see in the Fig. 26(a) that the excitation frequency 568 Hz transmitted at an amplitude of 49 Pa in the case of transient non-contact simulation. Whereas, in the Fig. 26(b) it can be seen that the excitation frequency reduces to 13 Pa and there is a generation of high-frequency pressure waves in between 1000 Hz to 2000 Hz and the pressure levels are in the range of 2-8 Pa.

.

For the contact and non-contact simulation, the node at the center of the back plate was used to determine the back plate displacement in both cases. Fig. 27 shows the displacement history of the membrane and back plate without and with impact. As expected the membrane has a smaller displacement with impact compared to the non-impact case, where the displacements will attenuate due to the absorption of the excitation frequency and this phenomenon is prevented in contact leading. The deformations

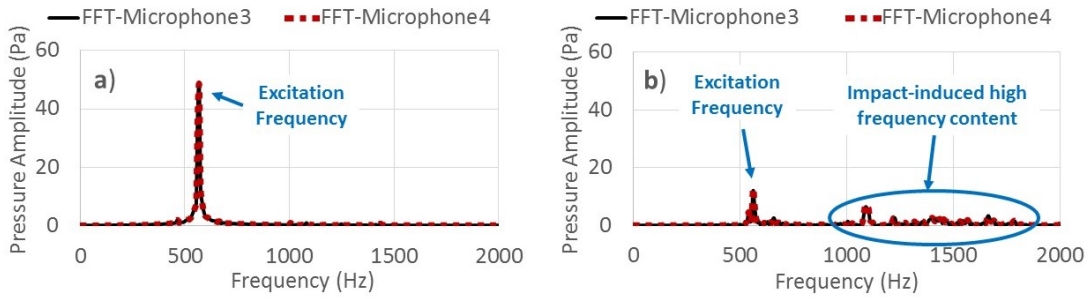

Figure 26: FFT of the pressure signals at microphone locations 3 and 4 to represent pressure amplitude from MIVIS simulation a) without contact and b) with contact.

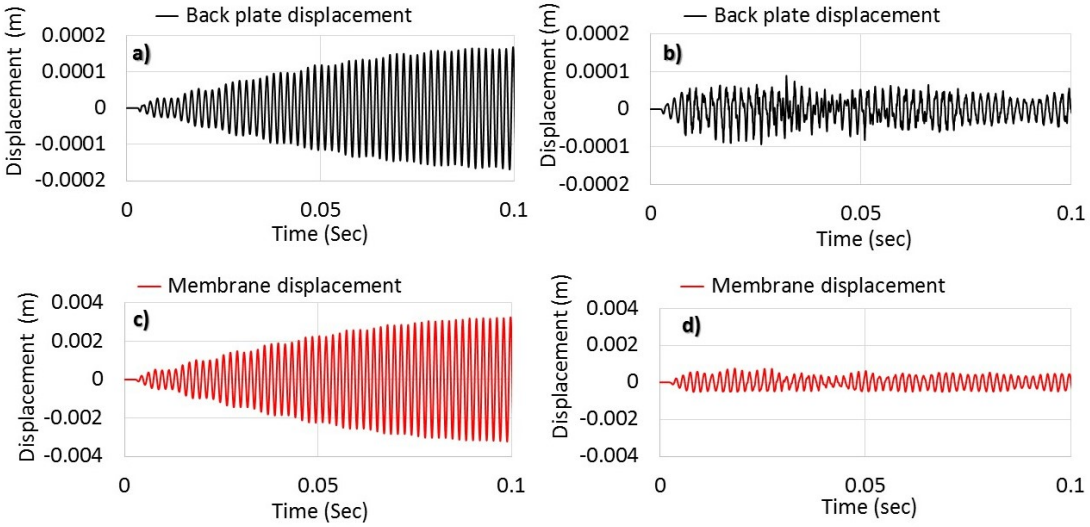

Figure 27: Back plate displacement of the MIVIS unit cell a) without contact, b) with contact c) Membrane displacement of the MIVIS unit cell without contact and d) same as earlier with contact.

within the hemispherical mass are negligible

To optimize the configuration of the MIVIS unit cell and to effectively up-convert most of the lower frequency acoustic energy into the high-frequency content. Increasing or decreasing the resting distance between the impactor and back plate may provide an increase in the up-converted energy by allowing a larger membrane displacement and more impact velocity. Further simulations are done by varying design parameters that are adopted as indicators for the design refinement process.

After being able to successfully demonstrate the contact phenomena for MIVIS unit cell making use of the simulations for the next study was based on solving the question of: what is the best gap configurations between the impactor and the back plate so that least low-frequency acoustic energy and the highest high-frequency energy is transmitted? This alternately means how to reduce the low-frequency content and increase the high-frequency content to have an efficient vibro-impact phenomena? Three different gaps i.e.; 0.1, 0.3 and 0.5 mm were simulated to determine the most efficient up-conversion for MIVIS vis-a-vis gap. The results from this study were correlated to make conclusions. The microphone locations 1 and 2 provide similar data for incident and reflected waves but at different locations, and microphone 3 and 4 are same because of the absence of reflections in simulation models. In the Fig. 28 plots for the pressure signal and its FFT at microphone locations 1 and 3 are provided to point out the behavior of the incident and transmitted wave. Also, the back plate displacement plots are with its FFT results.

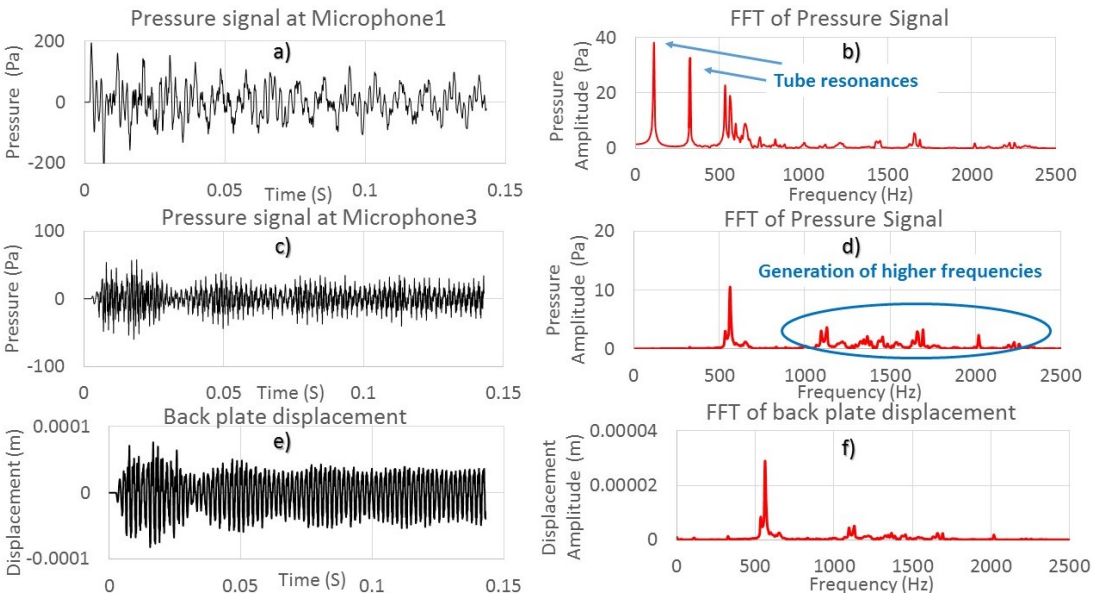

Figure 28: (a) Pressure signal at microphone location 1 for MIVIS unit cell with gap 0.1 mm, (b) and its FFT, (c) Pressure signal at microphone location 3 for MIVIS unit cell with gap 0.1 mm, (d) and its FFT, (e) Back plate displacement of the MIVIS unit cell with a gap of 0.1 mm, (f) and its FFT.

The plot of the power spectrum for these locations is a new technique that is intro-

duced in this thesis report for analysis of pressure signals. The area under each power spectrum quantifies the acoustic energy present in the wave. The calculation of the power spectrum is based upon squaring the amplitude of pressure at each frequency as given by the mathematical calculations based on energy spectral density. The area under the power spectrum distribution curve is equal to the total signal power given by parseval's theorem. The power spectrum provides us with an information of the signal regarding energy available in the system. From Fig. 29, it is clear that there is new high-frequency content generated on the transmitted side and also there is a reduction in the excitation frequency that is at 568 Hz in the transmitted side. A more detailed explanation on the generation of the tube resonances is explained later. From the Table 3, we can say that the total power is reduced by 33,340 units as the acoustic waves pass through the MIVIS unit cell. This means only 7.5 % of total acoustic energy is transmitted. Now if we look at the incident side almost 96 % of the energy on the incident side is in 0-1000 Hz range and the rest of the energy is in the high-frequency range above 1000 Hz. If we look at the transmitted power the percentage of total energy in 0-1000 Hz is 44.6 % and in 1000-2000 Hz is 31.6 %, and rest of the energy is scattered in the frequencies above 2000 Hz. Hence the raw values of power indicate that there is some up-conversion of high-frequency waves from the contact phenomena that comes from the low-frequency power. The units for the power are watt, but it is to be multiplied by a factor to obtain the exact value.

Table 3: Power (P) under the power spectrum on the FFT of the incident and transmitted side pressure signal

Location	P (Total)	P (0-1000 Hz)	P (1000-2000 Hz)
Incident side	36024	34777	966.1
Transmitted side	2683.9	1197.6	850.5

Conclusions about the role of a gap for improving the effectiveness of the impact for maximum energy up-conversion is obtained from data provided by the simulations. Fig. 30(a) shows the pressure amplitude at the microphone location 3 of the transmitted wave

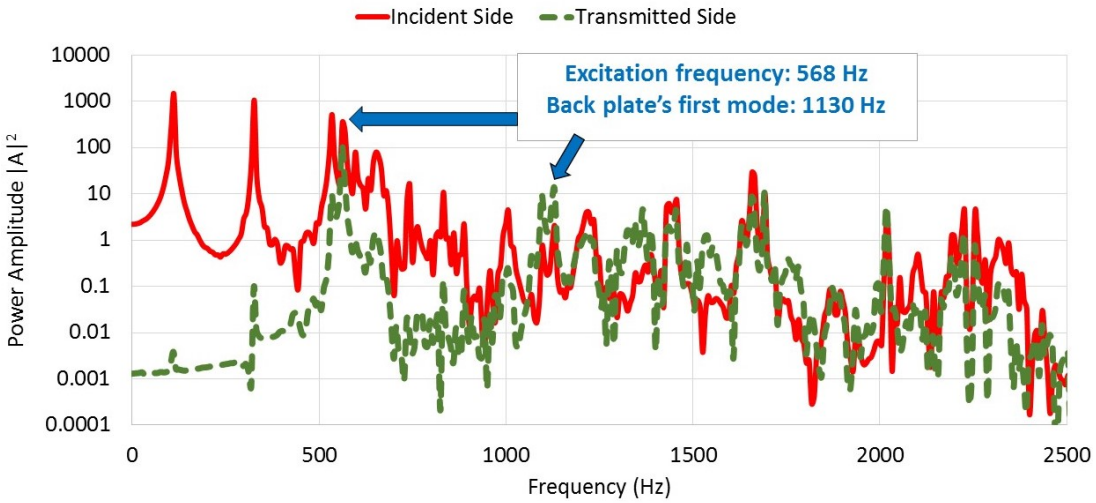

Figure 29: Power spectrum of the incident and transmitted side. Energy reduction and frequency up-conversion is observed with MIVIS unit cell with gap of 0.1 mm.

at the excitation frequency which is 568 Hz. It is evident that this amplitude is lowest for the 0.3 mm gap. It means that the targeted low-frequency incident on the MIVIS unit cell is up-converted the most in the case of the gap being 0.3 mm. NC is the no contact case where the contact is not simulated, but mass is a point load on the membrane, which shows the maximum transmission amplitude of the low-frequency excitation in the transmitting side. Hence, in general, we conclude that the contact phenomena is better at mitigating the low-frequency excitation. Similarly, in Fig. 30(b) and (c) we see that the displacement amplitudes of the membrane and backplate are the least at a gap configured at 0.3 mm. The Fig. 30(d) shows the area under the power spectrum from 1000-2000 Hz as the natural frequency of the back plate lies within this range. We notice how the area under the power spectrum that denotes the acoustic energy present in the system between this frequency range is highest for the 0.3 mm gap case. This phenomenon is because of the new high-frequency content generated from the impact on the back plate and as the impact is more efficient for the 0.3 mm gap case. For the MIVIS unit cell among the simulated cases, the best up-conversion occurs for the 0.3 mm case.

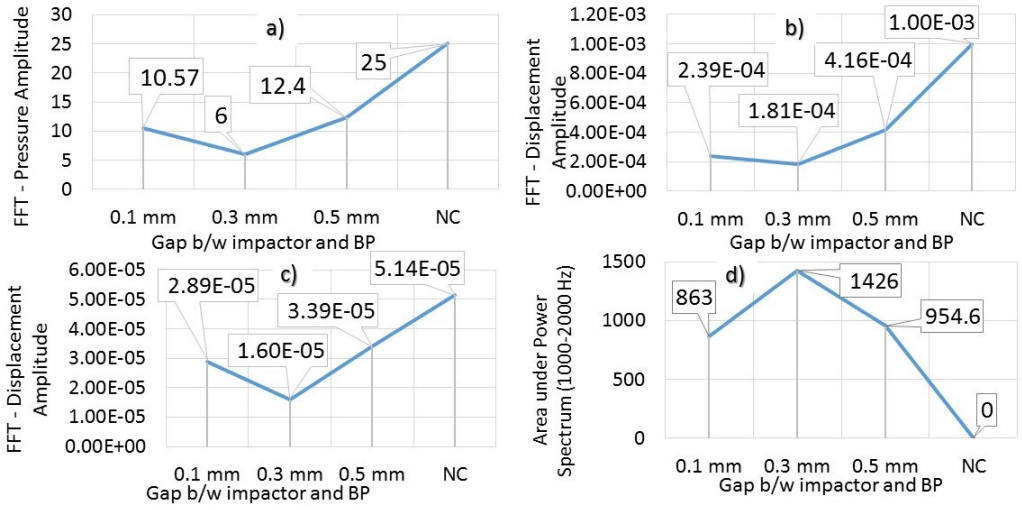

Figure 30: For various MIVIS unit cells at 564 Hz excitation a) Pressure amplitudes from the FFT of the transmitted pressure signal, b) Displacement amplitudes from the FFT of the membrane, c) Displacement amplitudes from the FFT of the back plate, d) Area under the power spectrum of each transmitted wave from 1000-2000 Hz.

One observation in all the simulations conducted for MIVIS for contact had unknown low frequencies popping up on the spectrum. On a closer inspection of these frequencies, they were found to have a pattern. First, there is a dominant peak, and the other two peaks are about approximately three and five times the frequency at which the first peak is observed in the FFT of the incident side pressure signal. The existence of these signals can be explained by using the phenomena of a closed air column on both sides that produces resonant standing waves. In the Fig. 31(a) the tube used was of length 24", and the resonance frequency for the tube of this length is 143 Hz but we see a peak at 162 Hz and the other peaks are at 485 Hz and 830 Hz and these are approximately triple and five times the 162 Hz. The difference between the 143 Hz and 162 Hz must occur because one of the tube ends has a membrane and is not a perfectly closed air column. A similar trend is observed with the 36" tube and 42" tube as seen in Fig. 31(b) and (c).

Based on the data collected from these simulations, we wanted to observe contact at very low frequency and hence we designed a mass loaded membrane by increasing the

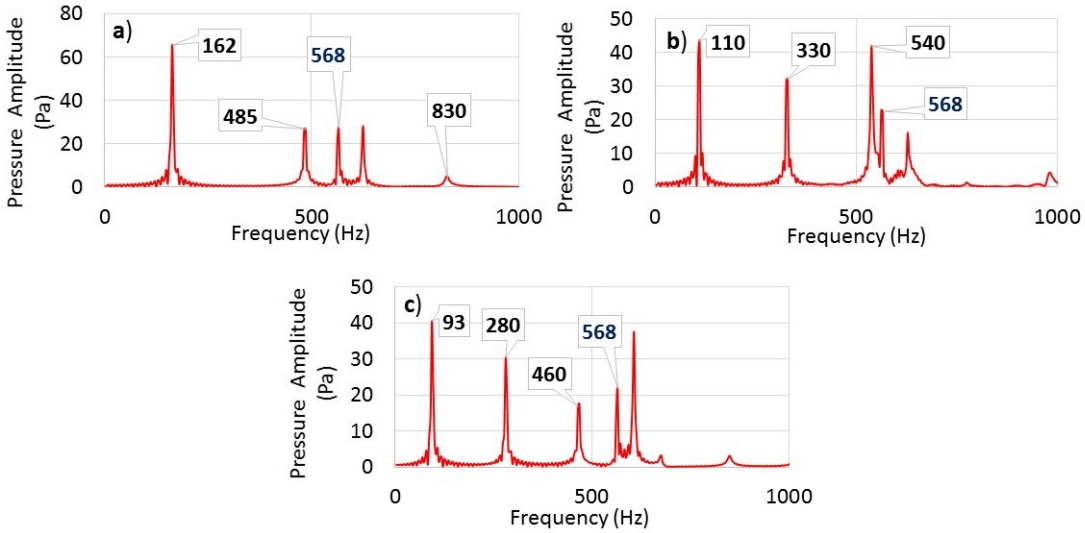

Figure 31: FFT of the pressure signal for a a) 24" long incident tube, b) 36" long incident tube, c) 42" long incident tube.

central mass and reducing the thickness. The resonance frequency of this MIVIS unit cell structure was at 100 Hz. One of the major breakthroughs in the research was the simulations result shown in Fig. 32. It shows the results of simulated up-conversion of incident low frequency to transmitted high frequency, from the optimization of MIVIS structure that was arrived at after running a different set of numerical simulations. The membrane was designed to resonate at a natural frequency of 100 Hz, and the backing plate was made out of aluminum due to the boundary conditions of the aluminum plate the natural frequency of this backing structure was 1200 Hz. It is very clearly evident from the power spectrum plots of the incident and transmitted side microphone that the incident 100 Hz excitation in the acoustic field after interaction with the MIVIS unit cell consists of the natural frequency of the backing structure in the transmitted signal, in this case, natural frequency of aluminum plate being 1200 Hz. The transmitted side microphone signal has the dominant frequency as 1200 Hz and this means that the transmitted acoustic field is free from the dominant incident low-frequency noise. This optimized MIVIS unit cell simulation reinforces the proof of concept.

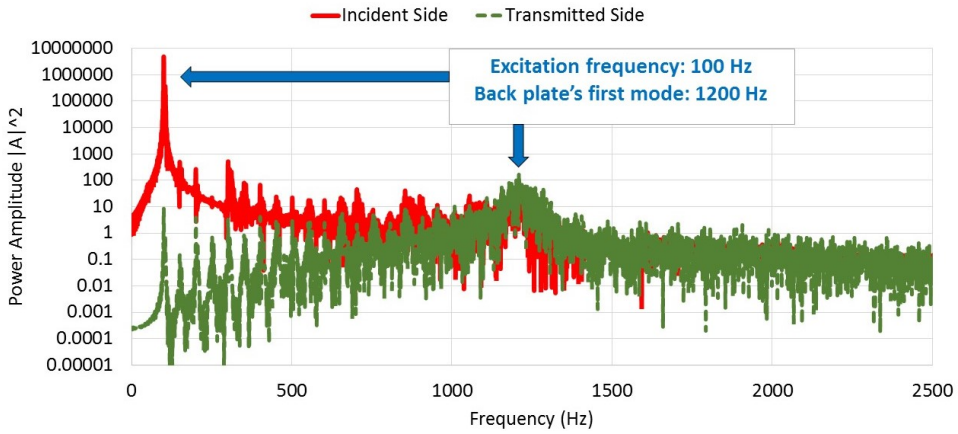

Figure 32: Power spectrum of the incident and transmitted side, energy reduction corresponding to excitation frequency and up-conversion to first mode of back plate is observed.

3.5. Summary

In this chapter, it started by developing an understanding of research that was focused on narrow band acoustic metamaterials and mitigation of low-frequency seismic waves. Next, the study moved on to prelim studies using 3D printed test articles and testing them in TL tube. Conceptual design is discussed to develop ideas for designing the test article with functional materials. A comprehensive analysis was carried out with various types of non-contact, contact simulation. The proof-of-concept for the design using simulations was achieved. Some interesting features are observed via simulations by doing parametric studies. Overall this study gives valuable feedback on the behavior of the MIVIS unit cell.

CHAPTER 4

Experiments

The purpose of this chapter is to introduce the reader to the experimental techniques used to evaluate the MIVIS unit cell followed by the discussion of results.

4.1. Introduction

After generating the proof of concept from the extensive simulation work, it is required to make a full-fledged experimental effort to produce the evidence for same. The challenges faced in the experimental setup would be significant leading to the usage of transmission loss tube setup for acquiring dynamic impact data. The experimental data might lead us to results that deviate from the models; this can be due to assumptions made in the model or some sources of errors in the experimental setup.

The experimental procedure consisted of different steps such as, selection of materials for each part of the MIVIS unit cell, testing these materials against each other to select the best to suit technical requirements and other steps that are discussed at length in this chapter. Selection of membranes was based on already available off the shelf materials. Tuning of these membranes to required frequencies that generate mode shapes by placing the necessary weights at the center can be done. Brass and copper washers were selected to increase or decrease weight that is centrally placed on mass-loaded membranes (MLM). These washers were inserted over the shaft of a dome-headed rivet for ease of addition and removal; this assembly was held in place by using a lock nut. Controlling the gap between the tip of the impactor and back plate should be simple. Therefore, swappable

modular frames of varying thicknesses are proposed to change the gap. All these steps are necessary to design a MIVIS unit cell that will generate results to fulfill the hypothesis for this work.

This chapter contains a detailed investigation of testing and selection of different types of materials to be used as part of the MIVIS unit cell. The transmission loss experimental setup is explained in detail with its limitations. In the discussion of results, some of the techniques are evolved for using a transmission loss tube for dynamic testing of impact phenomenon.

4.2. Test-Article Design and Fabrication

To demonstrate proof-of-concept for the MIVIS approach and also examine the effect of parameters such as air gap, membrane type, mass addition among others, a series of test articles were fabricated and tested. Test items for the MIVIS are from commercially available materials. Modular metal spacers to allow easy adjustment of the gap between impactor and backing structure has to be chemically etched to improve the surface finish. The exploded view of MIVIS prototype with part of the transmission loss tube is shown in Fig. 33, chemically etched metal spacers are placed in between the membrane and the backing structure. The mass of the impactor is changed by addition or removal of washers from the rivet assembly. The membrane itself is swapped to change thickness and material, and together, the fundamental resonance frequency of the MIVIS unit cell.

The choices for the backing structure is to represent typical aerospace structures, and therefore a CFRP back plate - a combination of carbon fiber face sheet with Divinycell foam core composite, Aluminum, and Steel was selected. Seven different back plate configurations were available for testing. First four were CFRP plates i.e.; Divinycell foam sandwiched between two of the two layered carbon fiber sheets. These four sandwiched back plates were 0.087", 0.156", 0.200" and 0.284" thick, weight of these were 7.3 g, 7.6 g, 7.8g and 8.3 g respectively. Along with these, we had a 0.025" steel back plate and a 0.025" aluminum back plate. There was another two layered carbon fiber composite for

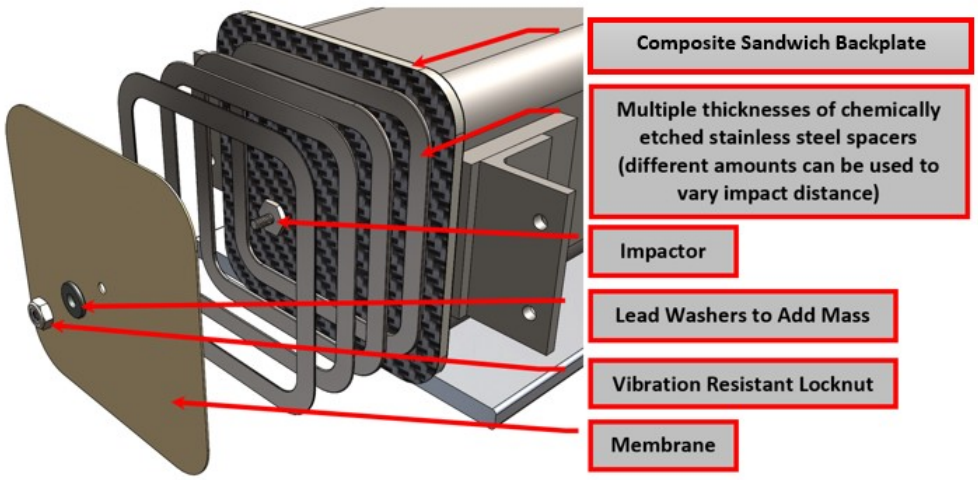

Figure 33: Exploded view of the MIVIS unit cell test article assembly with part of the transmission loss tube. Picture Courtesy: C2Si.

testing as a possible back plate with weight being 2.2 g. The cross section of all these test articles was a square of side 3" with a fillet radius of 0.4". From the Fig. 34 we can make a selection for the best back plate based on the transmission loss responses of all the back plates under testing. Nomenclature in the legend is described as "Part name_Material_Thickness," here part name is back plate (BP) and material is CFRP with thickness 0.087" this will be written as BP_CFRP_0p087. All the CFRP back plates were manufactured at C2Si and provided for testing. The metal plates were cut in the lab at Oklahoma state university.

The first dip locations for the three sandwiched back plates of 0.156", 0.2" and 0.284" are beyond 2600 Hz. This value is out of the test ranges for the transmission loss tube, and hence these three cannot be used as back plates. The double layered carbon fiber has very less weight and is a flexible material and hence out of consideration. The remaining Steel, Aluminum, and 0.087" thick CFRP are selected. Since, Steel is heavy and avoided in aircraft structures, Aluminum and the CFRP back plates are selected for testing. Because our hypothesis includes impact phenomena, this means that a back plate with a higher value of the coefficient of restitution will generate the best impact.

Initially, selection of five different types of membranes for testing was made. They

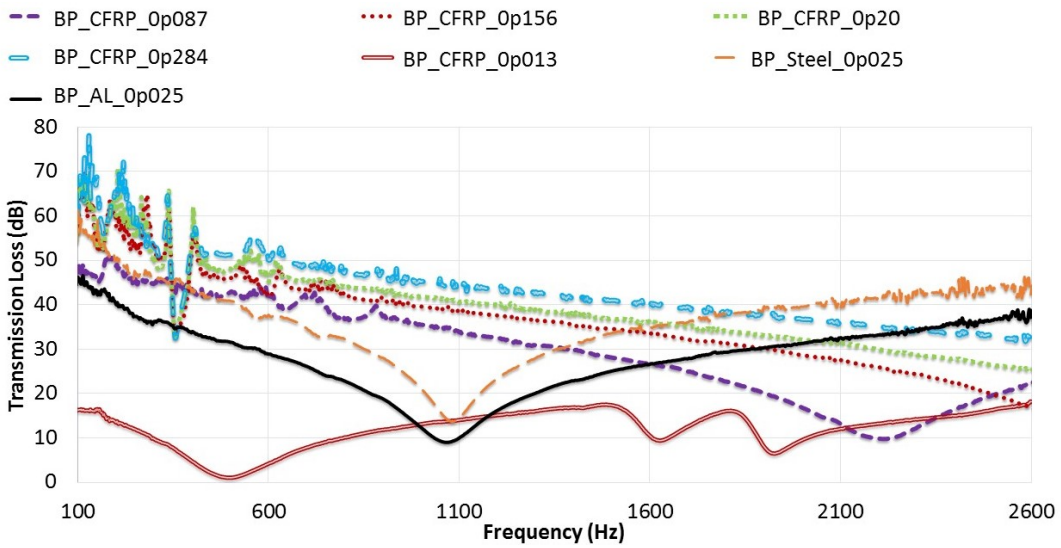

Figure 34: Transmission loss curves of the back plates of various thicknesses and materials

were ABS plastic membranes of five different thickness. They were 0.05", 0.02", 0.01", 0.005" and 0.003"; their weights were 7.5 g, 9.1 g, 1.7 g, 0.8 g and 0.5 g respectively. It was found that 0.005" and 0.003" membranes did not generate consistent results due to variations and were rejected. Two-ply carbon fiber composite membrane of weight 2.2 g was also tested but had 500 Hz high-frequency first mode. This would require a considerable mass addition to bring down the first mode to fit our low-frequency objective making it ineffective against the mass constraint. The testing of these membranes were performed by sticking them over one of the 0.03" thick spacers. In Fig. 35, the transmission loss curves for the three different membranes have been reported. Each experiment has been carried out three times and has been averaged to remove any inconsistencies. Black solid, blue compound solid, red compound dashed lines represent experimental results for the 0.01", 0.02" and 0.05" membranes placed in a transmission loss configuration exposed to white noise. As the thickness increases the first dip is observed at a higher frequency. For the 0.01" membrane it is at 200 Hz, for 0.02" it is at 330 Hz and for 0.05" it is at 780 Hz. Adding a mass at the center decreases the value of frequency of the first mode. Simulations show a good match with the experimental transmission loss. Here black dotted line represents simulations for 0.01" membrane the peaks are sharp in the simulation because small damping of 0.02 was used. The blue square dots represent

the simulation for the 0.02" membrane and the simulations seem to match it well. Also, the red dashed lines represent simulation for the 0.05" membrane and have a considerably good match with the experiment. Hence, these three membranes were accepted to have a good performance in our testing setup because of consistent generation of mode shapes at the same frequency.

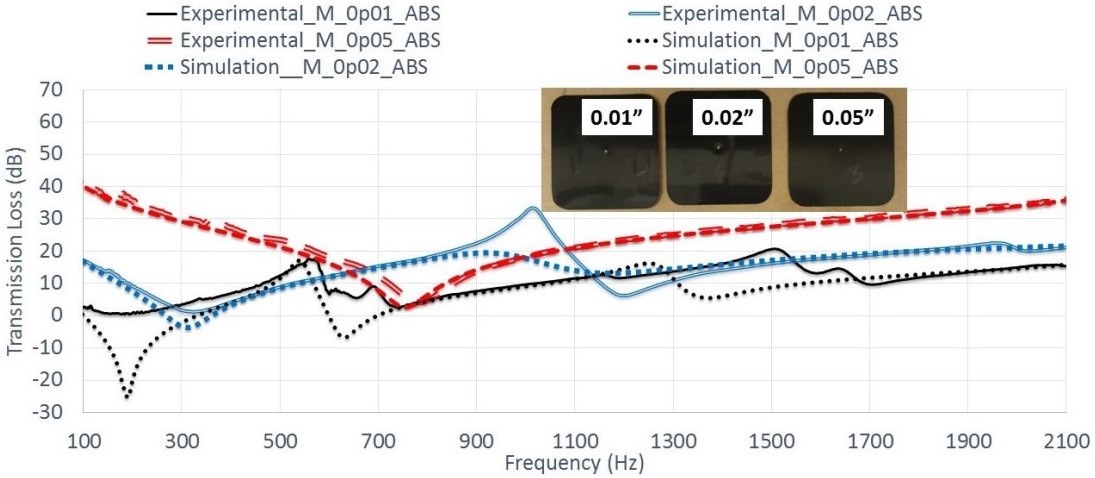

Figure 35: Experimental and Simulated transmission loss curves of membranes of various thicknesses

The material for selected membranes was acrylonitrile butadiene styrene (ABS) plastic, and the manufacturer specified Young's modulus, density and Poisson's ratio for the ABS were 2x10^9 Pa, 1020 Kg/m^3 and 0.39 respectively. For the back plates, Young's modulus, density, and Poisson's ratio of the carbon fiber were 5.5x10^{10} Pa, 1688.5 Kg/m^3 and 0.25 respectively and those for the Divinycell foam were 7.2x10^7 Pa, 60.8 Kg/m^3 and 0.4 respectively. The material properties for aluminum plate used are the same as the ones used in Section 3.4.

After selection of the membranes and back plates, it was necessary to select materials for impactors that would up-convert the kinetic energy from the membrane and transfer it to back plate via impact. Also, it was important to be able to add and remove the weight of the central impactor to tune the membrane to a particular frequency. Rivets of both aluminum and steel each weighing 0.25 g and 0.6 g were available. To add and remove weight washers of different materials were used. The brass flat washer was about

0.13 g, and the flat aluminum washer was 0.09 g. To lock these washers and rivet in place, we had a push nut weighing 0.19 g. Finally, a configuration of 1.37 g of central mass with the selected membranes is put forth for further testing. With the addition of the spacers in between the MLM and back plate would complete the fabrication of test article for MIVIS unit cell.

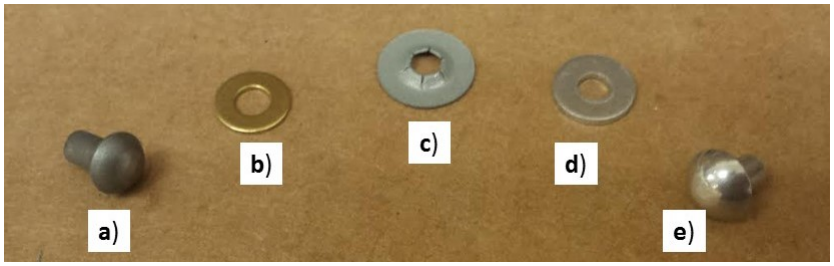

Figure 36: a) Aluminum dome head rivet, b) Brass flat washer, c) Locknut, d) Aluminum flat washer and e) Plain steel dome head rivet.

Finally, the material required to put the MIVIS unit cell together for experimental evaluation is spacers. 16 spacers with four different thicknesses were made available. These spaces were accurately cut and chemically etched to produce a high-quality surface finish by C2Si. The number of spacers in various configurations was changed to control the gap between the tip of the impactor and back plate. The set of four spacers each with thickness 0.03", 0.01", 0.005" and 0.002" were used. We were able to create three different impactor and back plate gaps for test configurations.

The membrane of thickness 0.02" (0.5 mm) is used for the experiments involving MIVIS based on the first mode shape frequency at 170 Hz and antiresonance frequency at 328 Hz. The 0.05" membrane after adding 1.37 g was not selected because the resonance frequency was 490 Hz and antiresonance frequency at 1100 Hz. For 0.05” membrane resonance is above the low-frequency cutoff defined set at 400 Hz. The 0.01" membrane after loading mass has resonance frequency at 100 Hz and antiresonance frequency at 136 Hz. It becomes a constraint to measure low frequencies on the lower boundary of testing range for transmission loss tube. Therefore, the 0.01" thick membrane was not considered as an effective membrane to employ in the given test setup. Hence, the 0.02" thick mass loaded membrane was selected with frequencies in the desired range of

Figure 37: Spacers of thickness a) 0.76 mm, b) 0.25 mm, c) 0.13 mm and d) 0.05 mm. (Manufactured at C2Si)

interest.

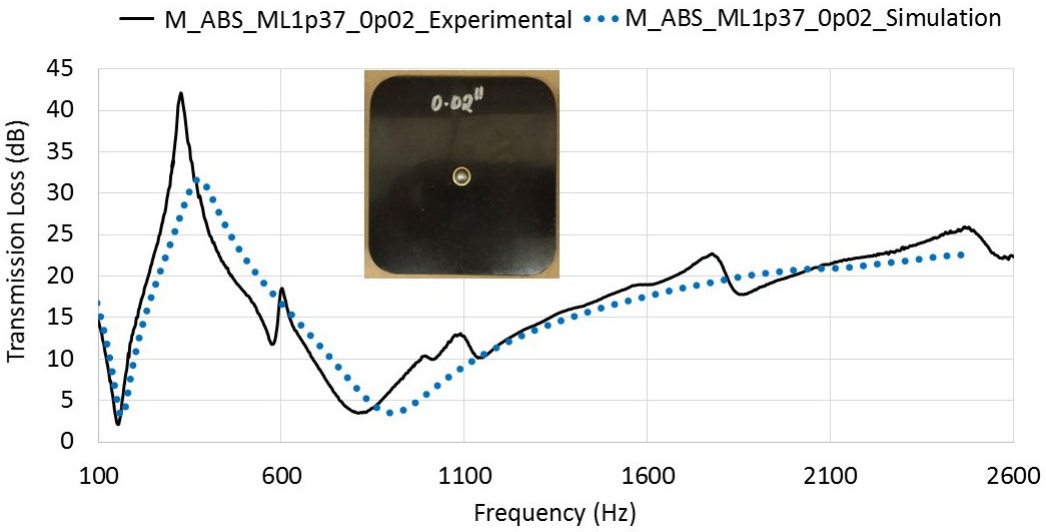

Figure 38: Transmission loss plot of the mass loaded membrane selected for MIVIS unit cell

Considering low-frequency range of interest, the ABS plastic membrane of 0.5 mm (0.02") thickness has been chosen along with a centrally affixed steel rivet and washer

assembly with a total mass of to 1.37 g. Using four different stainless steel spacers of 0.76 mm, 0.25 mm, 0.13 mm and 0.05 mm, three different gap settings between the impactor and backing plate were created. The test matrix for various cases is given in Table 4. The nomenclature for MIVIS test cases is defined for example as: 'MIVIS_M0p02_BP_CF_G_0p01mm,' where, M stands for membrane and 0p02" is the thickness of the membrane (0.02" or 0.5 mm); BP refers to the back plate. Followed by (CF) for CFRP composite and (AL) for Aluminum as the choice for the back plate, and G stands for the gap between the impactor tip and the backing plate followed by its value (0p01mm). Based on the selection of three gap configurations and two membranes total six MIVIS test configurations are created as shown in Table 4.

Table 4: MIVIS and baseline parameters for experimental cases.

Case No	**MIVIS unit cell**	**Membrane (0.5 mm)**	**Al Back plate (0.65 mm)**	**CF Back plate (2.2 mm)**	**Gap (0.1 mm)**	**Gap (1.0 mm)**	**Gap (1.7 mm)**
1	MIVIS_M0p02_BP_CF_G_0p1mm	Y	N	Y	Y	N	N
2	MIVIS_M0p02_BP_CF_G_1p0mm	Y	N	Y	N	Y	N
3	MIVIS_M0p02_BP_CF_G_1p7mm	Y	N	Y	N	N	Y
4	MIVIS_M0p02_BP_AL_G_0p1mm	Y	Y	N	Y	N	N
5	MIVIS_M0p02_BP_AL_G_1p0mm	Y	Y	N	N	Y	N
6	MIVIS_M0p02_BP_AL_G_1p7mm	Y	Y	N	N	N	Y
7	Baseline_BP_CF (NF = 2200 Hz)	N	N	Y	N	N	N
8	Baseline_BP_AL (NF = 1070 Hz)	N	Y	N	N	N	N

Fig. 39 shows a typical MIVIS unit cell assembly that is put together for testing in the acoustic transmission loss tube. The internal open area of the tube has a 2.5" square cross section dimension with the thickness of the tube walls being 0.25" and an external fillet radius is 0.4". The MIVIS unit cell has a 3" square cross section having a 0.25" fillet radius fits snugly inside the tube and is clamped in place to seal any gaps completely. To ensure consistent boundary conditions clamping force was applied using spring tensioned cables for all the specimens.

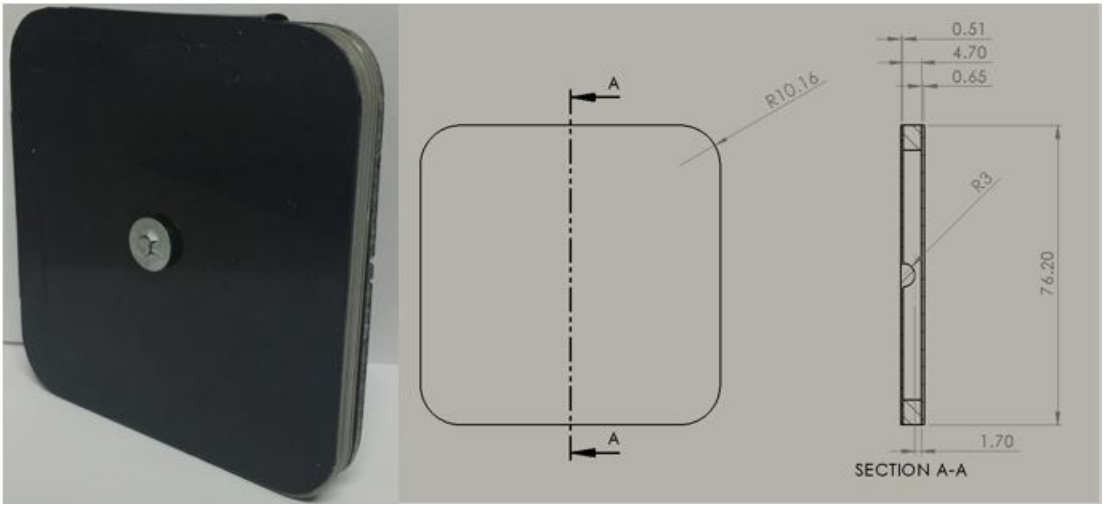

Figure 39: Assembled MIVIS unit cell test article (left) and its drawing with cross sectional view

4.3. Experimental Setup and Methods

The process of testing is part of an extensive research effort to evaluate different structures and materials for various applications in aerospace structures, unmanned aerial vehicles (UAV), to provide a reduction in low-frequency acoustic noise. The test setup of normal incidence impedance tube is generally used to evaluate the STL for different structural material samples.

Impedance tube is a configuration that is used to measure the properties of acoustic materials as shown in Fig. 40. It consists of two tubes of the same internal area that are placed on the either side of the test sample. The upper and lower frequency ranges that can be measured inside this tube depends on upon the dimensions of the tube. If transmission loss is to measure over a broadband frequency range, it is taken forward by having different sizes of impedance tubes. The cross section of this tube can be either circular, rectangular or square and shall have a constant cross-sectional dimensions from end to end. One end of the tube is excited with a source of loudspeaker that generates waves traveling inside the tube. Some microphones are placed on the top surface of this tube to measure the pressure at these locations. These are in a way such that the

diaphragms are flush with inside surface of the tube. A data acquisition system used to collect the data from these microphones, and a computer along with custom applications to process the acquired data.

Tube venting is a concept, where temporary pressure variations that are generated either during the installation or removal of the test specimen are prevented from affecting the quality of testing. This venting phenomenon leads to the deflection of the diaphragm on the microphones and to counter this a pressure relief opening of some type is provided to reduce the damage that can occur to the diaphragm. Mounting the test specimen can be done by clamping the specimen to the tube. Care must be taken to mount multiple samples in a consistent manner, and to reproduce the same boundary conditions every time. A small opening around the edge might have an impact on the transmission loss calculations. Any small gaps are sealed with petroleum jelly, modeling clay or putty. It is desirable to have a specimen that possesses a relatively flat surface for testing to avoid diffusion effects.

Testing is carried out in the transmission loss (TL) tube as shown in Fig. 40. This tube is built to test specimens according to ASTM standard designation: E2611 - 09 [89]. It makes use of two tubes along with a speaker, four microphones and a data acquisition system to determine various acoustic properties. In this method acoustic transfer matrix is used for determining various characteristic properties of materials such as:

- transmission coefficient
- normal incidence transmission loss
- absorption loss
- reflection coefficient
- absorption coefficient
- propagation wave number in material
- characteristic impedance in material

The transmission loss tube setup is made up of different types of apparatus as shown in Figure 40. The equipment has been built based on the specifications defined in ASTM standard designation: E2611-09 ("Standard Test Method for Measurement of Normal Incidence Sound Transmission of Acoustical Materials Based on the Transfer

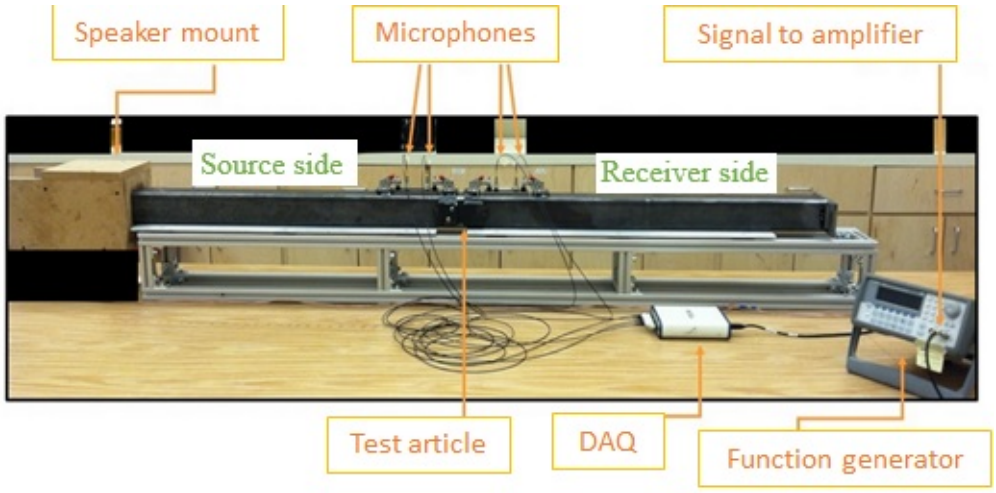

Figure 40: Experimental setup of normal incidence transmission loss tube [15].

Matrix Method"). It has a 72 inches long tube made out of steel with a square cross section and 2.5" x 2.5" open internal dimensions and 3" x 3" external dimensions. The excitation of the air column is by making use of kicker KSC4 speaker that is driven by a function generator made by keysight. This signal is amplified by a Carver A-500x power amplifier that is placed in between speaker and function generator. Four 1/4" microphones are used to measure the sound pressure signals at a specific location inside the transmission loss tube. The data from the microphones are being used to measure the physical properties of the samples of interest. The signals from microphones processed through a National Instruments USB-4431 data acquisition (DAQ) module and the data is recorded and processed on a desktop computer to determine various characteristic properties of the samples.

The TL tube can be employed to determine the characteristic properties of structures with a 3" x 3" square cross-section. Our primary interest lies in measuring the transmission loss, frequency content of the incident signal as well as transmitted signal. Determining the other acoustic properties will be beneficial for analyzing important phenomena and will help in developing greater insight into the behavior of test articles. Analyzing the transmitted signal is of peculiar importance in this research work.

To make measurements and characterize the acoustic properties of the structure, it

is placed in between the incident side and the transmitted side tube. Different types of excitation can be applied using the speaker, such as white noise or monotonic acoustic plane waves. After a continuous incidence of such waves on the specimen or structure, a standing wave is formed that can be decomposed into forward and backward traveling waves by measuring sound pressure signals at four different locations, two on either side of the test specimen.

The working frequency range for the test setup is found to be between 80-2500 Hz.

$$f_l < f < f_u \tag{7}$$

Where:

f = operating frequency, Hz,

f_l = lower frequency of the tube, Hz and

f_u = upper frequency of the tube, Hz.

The low-frequency limit f_l is dependent on the spacing between the microphones and the accuracy of the analysis system. The microphone spacing shall be greater than one percent of a wavelength corresponding to the lower frequency of interest. However, a large spacing between the microphones enhances the accuracy of the measurements. Whereas, the upper-frequency limit f_u is dependent on the diameter of the tube but mainly is based on the theory of plane waves. To maintain a plane wave propagation in a tube, the maximum frequency can be calculated as given by

$$f_u < \frac{Kc}{d} \tag{8}$$

Where:

f_u = upper frequency of the tube, Hz

c = speed of sound, m/s and

d = section dimension of the tube, m

$K = 0.5$, for rectangular tubes.

The testing of structures needs to be carried out within the frequency range to avoid cross-modes that occur at higher frequencies. The minimum gap that must be maintained

between the source of the sound and nearest microphone must be a minimum of 3 times the tube diameter to subside the non-plane waves being generated by the source of excitation. The source of excitation is expected to provide uniform power response over the frequency range of interest. Microphone diameter is recommended to be less than 20% of the wavelength of the highest frequency of interest. Microphones must be sealed; this might interfere with proper operation of the microphone vent, in turn, causing a significant amount of change to the low frequency. The tube shall not have dust or rough surfaces and must be non-porous to maintain a low sound attenuation. The tube walls should be rigid and massive so that most of the sound is transmitted through the test specimen and not walls of the tube.

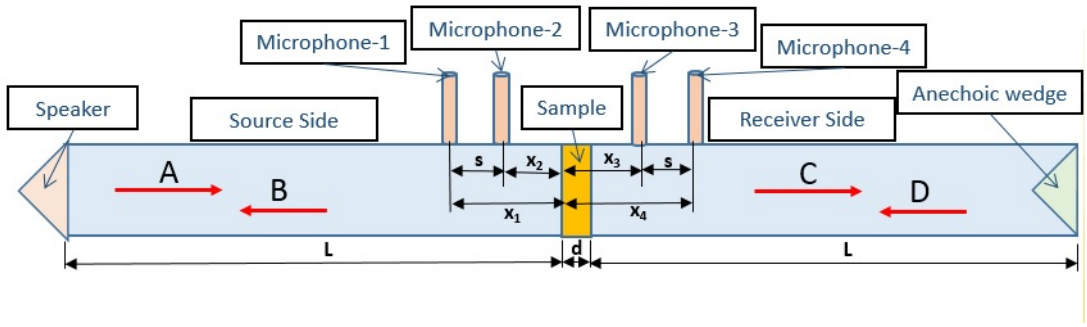

Figure 41: Schematic diagram of normal incidence transmission loss tube.

The reference plane is defined as the plane of the specimen on the incident side of the upstream tube. Here, the sound impinges on the reference surface in the perpendicular direction. Plane waves generated in the tube are composed of forward and backward traveling waves due to the formation of a standing wave pattern. Sound pressure calculated at four locations, and their relative phase and amplitudes data can be calculated from this experiment. Fig. 41 shows a schematic of the normal incidence transmission loss tube. The incident and reflected waves are generated inside the tube. To attenuate the reflected wave inside the receiver side, an 18" long wedge-shaped foam is placed at the end of the tube; this also known as an anechoic wedge. This wedge is made from a sound absorbing material such as fiberglass or foam. The termination of the tube may be changed so as to accommodate for the open or closed termination which is employed

in testing of test articles that are not symmetric. There are different parameters defined as shown in Fig. 41. They are:

A = incident wave amplitude,

B = source-side reflected wave amplitude, and

C = transmitted wave amplitude,

D = receiver-side reflected wave amplitude,

L = length of the impedance tube,

d = thickness of the sample,

s = distance between the microphones,

x_1 = distance of the first microphone from the surface of the specimen,

x_2 = distance of the second microphone from the surface of the specimen,

x_3 = distance of the third microphone from the surface of the specimen,

x_4 = distance of the fourth microphone from the surface of the specimen,

P_1 = pressure at microphone location 1,

P_2 = pressure at microphone location 2,

P_3 = pressure at microphone location 3,

P_4 = pressure at microphone location 4.

Let us define the formulae that can be used to determine these parameters:

$$P_1 = Ae^{-jkx_1} + Be^{jkx_1} \tag{9}$$

$$P_2 = Ae^{-jkx_2} + Be^{jkx_2} \tag{10}$$

$$P_3 = Ae^{-jkx_3} + Be^{jkx_3} \tag{11}$$

$$P_4 = Ae^{-jkx_4} + Be^{jkx_4} \tag{12}$$

Here, k is the wave number and is defined as the ratio of angular frequency and speed

of sound. The coefficients of the pressure signal can be evaluated from the equations given as follows

$$A = \frac{j(P_1 e^{jkx_2} - P_2 e^{jkx_1})}{2sink(x_1 - x_2)} \tag{13}$$

$$B = \frac{j(P_2 e^{jkx_1} - P_1 e^{jkx_2})}{2sink(x_1 - x_2)} \tag{14}$$

$$C = \frac{j(P_3 e^{jkx_4} - P_4 e^{jkx_3})}{2sink(x_3 - x_4)} \tag{15}$$

$$D = \frac{j(P_4 e^{jkx_3} - P_3 e^{jkx_4})}{2sink(x_3 - x_4)} \tag{16}$$

Now, the sound transmission loss is defined as logarithm of the ratio of amplitudes of transmitted and incident wave given by:

$$TL = 20log\left|\frac{C}{A}\right| \tag{17}$$

The advantages of impedance tube is that of being less expensive, less time-consuming to test small samples, rapid technique and does not require experienced professionals

Before the start of all the experiments the tube was standardized by upgrading the clamping mechanism for test articles. The measurement of the transmission loss is a quantity that is dependent on the boundary conditions of the sample inside the tube. There is a difference in the effective load on the structure when a test specimen is placed every time in between two tubes without clamping. Hence a clamping method was introduced by employing a tensioning spring that connects to two tubes. The spring extends to a particular stop value, and this mechanism ensures that same amount of loading on the boundaries of the test specimen in every test. Also to prove this point we ran a test with and without tensioning rig to find that there was an increase in the natural frequency of the test specimen under the tensioning rig. This is because of the

stiffness increases caused by an improved overlap between the boundaries of the tubes and test specimen. In our case, the increase in the natural frequency relating to the new clamping mechanism changed from 1128 Hz to 1184 Hz. These results are shown in the Fig. 42(b).

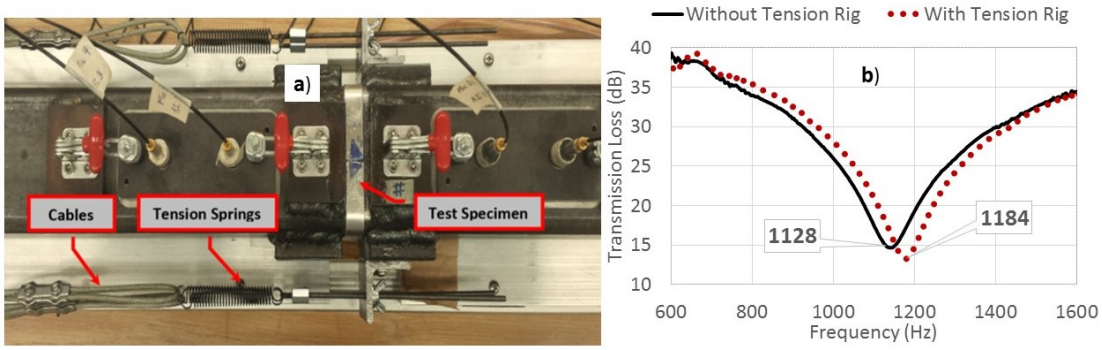

Figure 42: (a) Cables and tensioning springs in top view, (b) Transmission loss curves obtained with and without tensioning rig.

A steel plate of 3" cross-section and 0.65 mm thickness was used as a control sample. Also the Fig. 43 indicates the three trials of this control sample along with the average of these three trials. There is very less deviation between all the trials except at the boundaries of testing limits. Transmission loss for all the experiments done have been calculated by doing an average of three trials conducted.

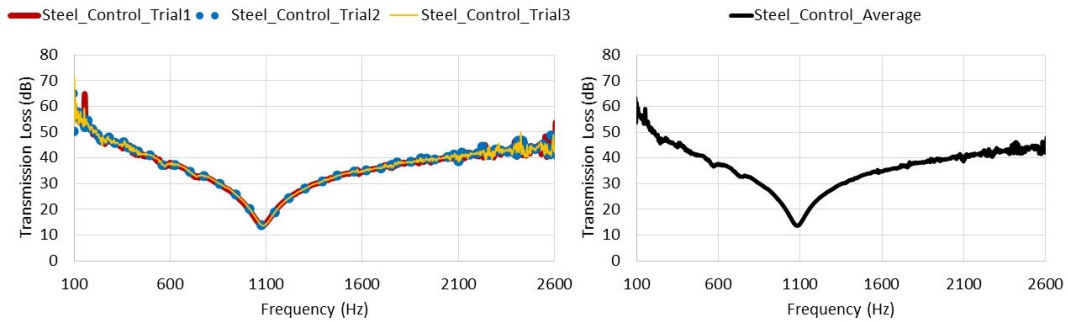

Figure 43: On the left is the transmission loss curves for three individual trials of Steel control sample and on right is the average of these three trials.

4.4. Discussion of Results

After an extensive testing phase, the data obtained from the experimental investigation was evaluated and correlated using simulations. The first three cases of the MIVIS unit cell experimental configurations from Table 4 are MIVIS_M0p02_BP_CF_G_0p1mm, MIVIS_M0p02_BP_CF_G_1p0mm and MIVIS_M0p02_BP_CF_G_1p7mm. These three configurations were tested but not simulated as the upconversion phenomena observed in the MIVIS configurations with aluminum back plate had better indicators of upconversion. From the experiments, if we look at the MIVIS_M0p02_BP_CF_G_0p1mm configuration, it is clearly visible that there is upconversion of low-frequency incident acoustic excitation to the high frequency transmitted acoustic response. Plotting the FFT of the pressure signals on the incident and the transmitted side gives us a clear indicator of this phenomena as shown in Fig. 44.

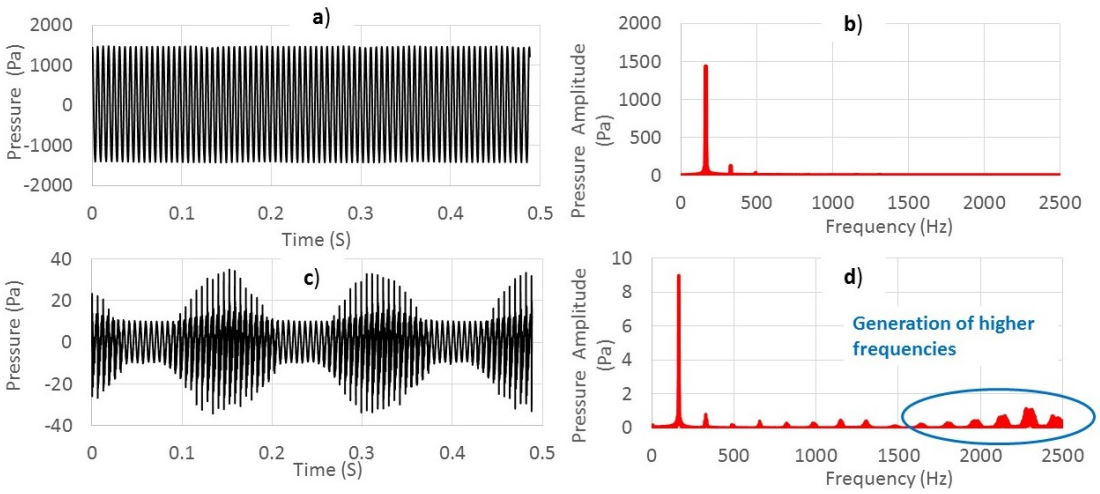

Figure 44: For the MIVIS_M0p02_BP_CF_G_0p1mm configuration: a) Incident side pressure signal, b) FFT of incident side pressure signal, c) Transmitted side pressure signal and d) FFT of transmitted side pressure signal.

Transmission loss of first case (MIVIS_M0p02_BP_CF_G_0p1mm) of MIVIS unit cell with a gap of 0.1 mm was tested under white noise and monotonic excitation, starting from 100 Hz and varying the frequency increment from 20 to 1 Hz based on resonant and antiresonant frequencies. The monotonic TL gives a good correlation with white noise.

The deviation was higher in the vicinity of the critical frequency of 164 Hz. Transmission loss curve indicates a dip at the natural frequency of the membrane as well as at other two higher frequencies that fall within the testing range. There is an antiresonance peak between every dip and that is where there is a maximum improvement in the TL compared to back plate of about 5 dB at first peak and 15dB at second peak. The improvement in the TL is in the bandwidth of 50 Hz. Overall improvement in the transmission loss can be observed as shown in Fig. 45.

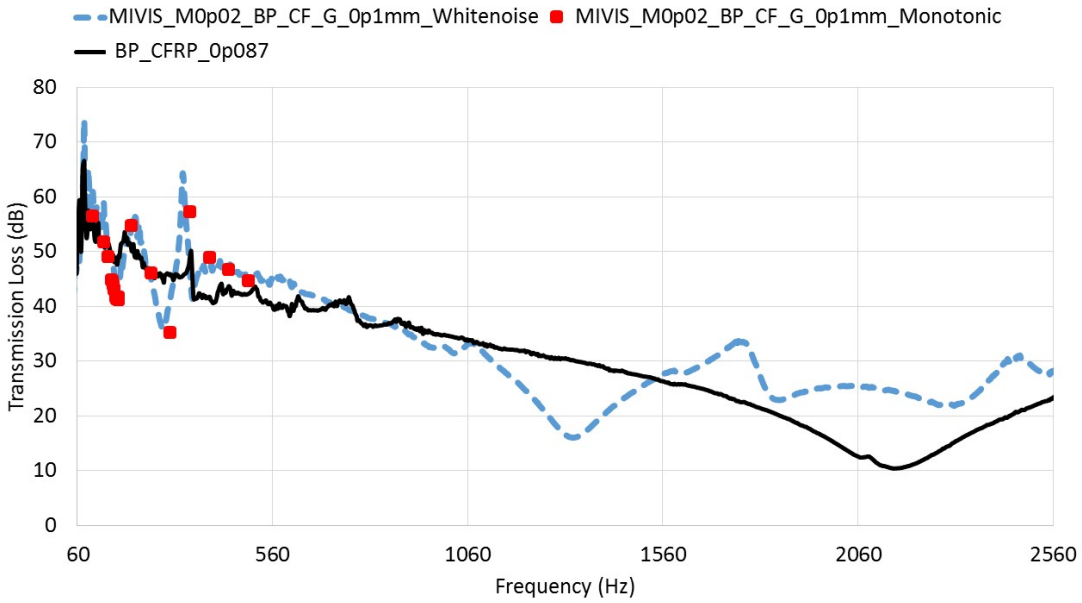

Figure 45: Transmission loss from experiments for the case 1 unit cell and baseline CFRP back plate.

For the second case (MIVIS_M0p02_BP_CF_G_1p0mm) of MIVIS unit cell with a gap of 1.0 mm was tested under white noise and monotonic excitation for its transmission loss characteristics. The increments size and the starting frequency is consistent with the testing of the first case. The impact is occurring on FFT at 212 Hz and 328 Hz. The monotonic red dots line up with the white noise except for a few frequencies just above 328 Hz. Transmission loss curve indicates a dip at the 196 Hz, 288 Hz, and 356 Hz. There is an antiresonance peak between every dip and that is where there is a maximum improvement in the TL of about 5 dB at first peak and 10dB at second peak. The

improvement in the TL is in 30 Hz bandwidth. This case does not perform better than the first case, there is some deviation in the low-frequency region which must have been caused by the overheating of the speakers as it was tested after an evaluation for correct amplitude settings of low-frequency monotonic excitation. The transmission loss can be observed by looking at the narrow band in Fig. 46.

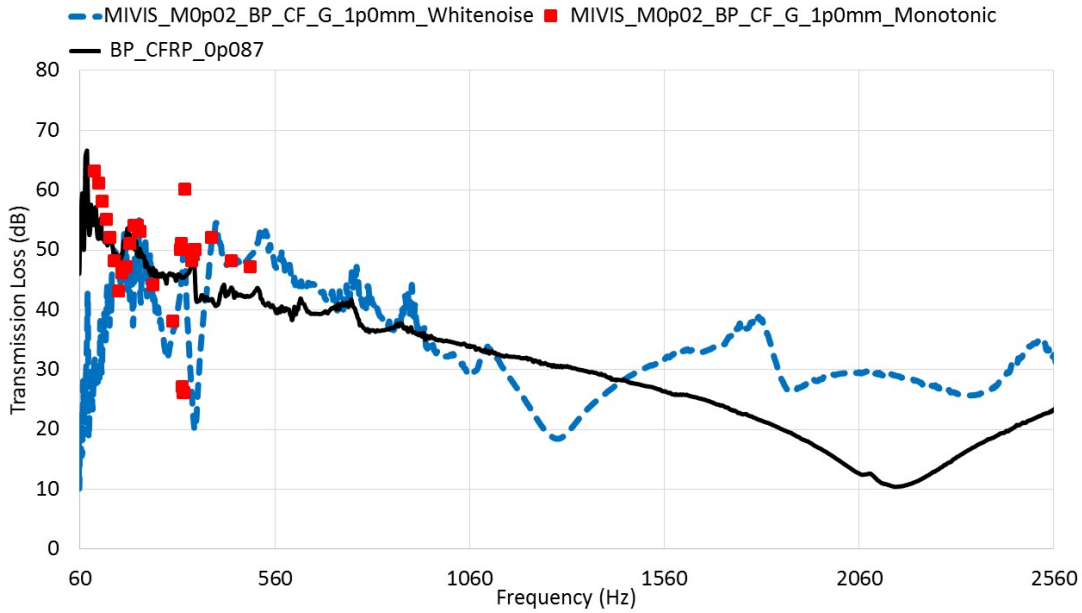

Figure 46: Transmission loss from experiments for the case 2 unit cell and baseline CFRP back plate.

Transmission loss of third case (MIVIS_M0p02_BP_CF_G_1p7mm) of MIVIS unit cell with a gap of 1.7 mm is excited under white noise and monotonic with the same test conditions as the previous tests. The impact registered on FFT at 328 Hz. The monotonic red dots line up with the white noise except for a few frequencies just above 328 Hz. Transmission loss curve indicates a dip at the 170 Hz, 272 Hz, and 356 Hz. There is a peak associated with every dip and that is where there is a maximum improvement in the TL of about 5 dB at first peak and 20 dB at second peak. The improvement in the TL is in 40 Hz bandwidth. Transmission loss behavior can be observed by looking at the narrow band in Fig. 46.

Amongst the six different MIVIS cases tested, the MIVIS test articles showed initial

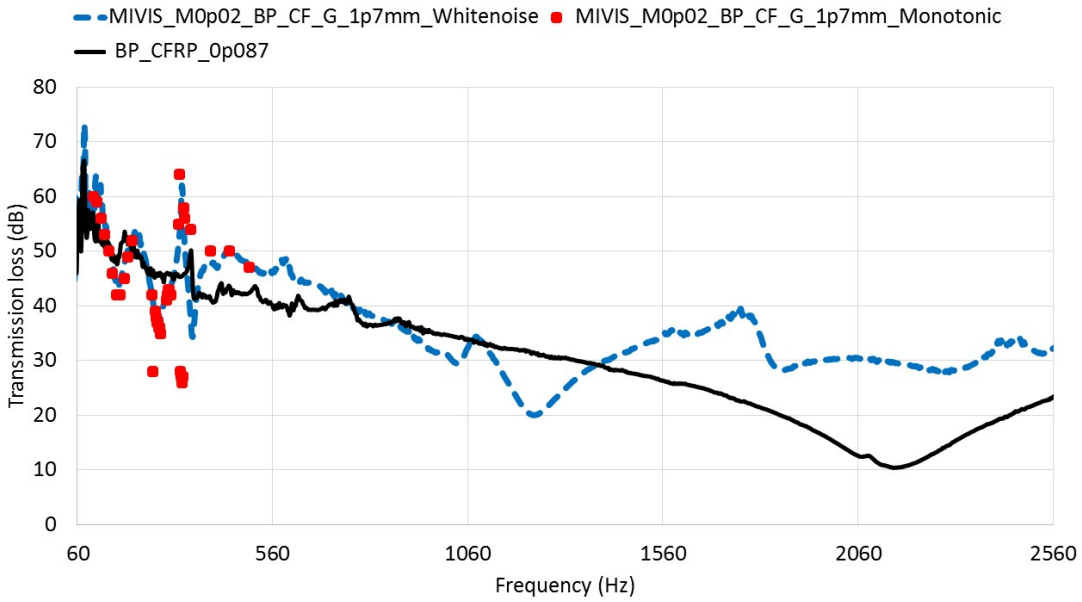

Figure 47: Transmission loss from experiments for the case 3 unit cell and baseline CFRP back plate.

results to claim up-conversion. Hence an extensive effort to perform simulations was carried out for this case. For the case 4 (MIVIS_M0p02_BP_AL_G_0p1mm) as defined in Table 4, it was found to provide improved transmission loss performance when compared to Aluminum back plate as shown in Fig. 48. Five different plots are available in this figure for evaluating transmission loss performance. Dotted blue lines are for MIVIS simulation and dashed blue line is for MIVIS unit cell experiment; blue lines represent MIVIS, and the solid black line represents Aluminum back plate experiment alone. A lighter shade of black dotted lines represents back plate simulation. Red markers are for values associated with monotonic transmission loss for the MIVIS unit cell.

Experimental and simulation results for the 0.65 mm aluminum back plate and the MIVIS with a 0.2 mm thick membrane having a centrally loaded mass of 1.37 grams, maintained at a gap of 0.1 mm between the tip of impactor and back plate are shown in Fig. 48. The cross-sectional view of symmetric mode shapes from simulations which correlate with the resonance frequencies in the transmission loss curve for MIVIS unit cell is shown in Fig. 49. It is concluded from Fig. 48 the maximum increase in trans-

mission loss is about 25 dB at around 324Hz. Significant TL improvement exists at least over a continuous bandwidth of 120 Hz. There is a match between the simulated and the experimental results. From the simulations, it is concluded that the mode shapes occurring at 250 Hz and 1746 Hz dominated by the properties of the membrane and those at 976 Hz and 1384 Hz by the properties of the back plate. There are slight deviations that are observed in the simulation results at the mode shapes from the MIVIS unit cell experiment. The reason for this is that every mode shape has a different damping value and if one of the peaks is matched with the experiment by adjusting the value of damping, the other peaks are affected as they have some other value at that mode shape. A damping to the back plate equal to 0.1 and same is allotted to the membrane in this simulation. Hence we can see that due to an underdamped value assigned for back plate its oscillations are compromised at the first dip location in a simulation.

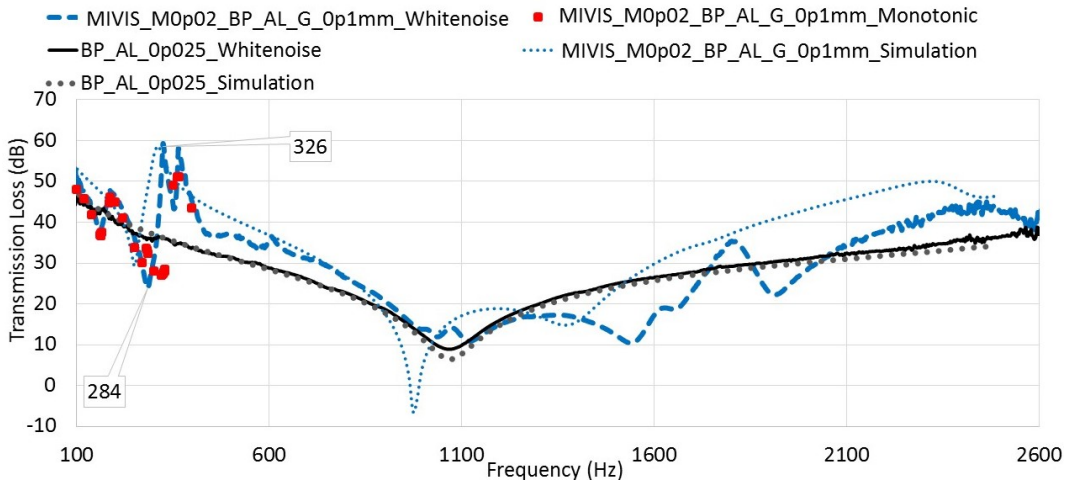

Figure 48: Transmission loss from simulations as well as experiments for the case 4 unit cell and baseline aluminum back plate.

The red square dots represents the TL at monotonic frequencies on all the plots for TL characterization of MIVIS unit cell. Monotonic excitation means that an acoustic wave is incident at a particular amplitude with a given excitation frequency and then the ratio of transmitted to incident wave amplitude is measured, and TL is computed from these calculations. We can observe that most of the monotonic TL points lie over the white noise TL, but at around the peak TL around 326 Hz there is a trend reversal for

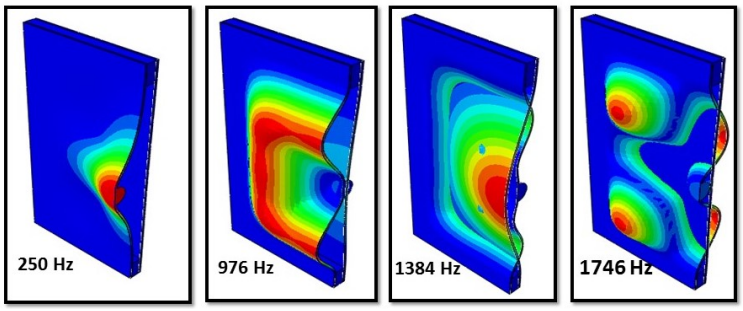

Figure 49: Symmetric mode shapes of the case 4 unit cell corresponding to the frequencies on the TL curve.

monotonic excitations. This reversal also happens to be the point at which the contact phenomena is observed to be optimum. The displacement of the membranes center is maximum at such a frequency, but at the same time, the surface averaged displacement is a small value at the same frequency. The reason for the monotonic TL to decrease at this point is associated with the phase reversal between the membrane and the back plate at the antiresonance frequency. Due to this phase reversal, the contact that is generated can be hard as the two bodies are moving towards one another. Also, the reason that adds up to the reduction is that as the contact phenomena take place, the back plate takes the energy from the impact and starts vibrating at its natural frequency. If the paths of the membrane and back plate are to interfere then, the contact is going to take place. Moreover, due to this phase reversal and then the continuous contact with the back plate, the transmitted acoustic energy contains both the excitation and back plates natural frequency leading to more excitation energy being transferred and in turn decreasing the monotonic TL.

The case 5 (MIVIS_M0p02_BP_AL_G_1p0mm) of MIVIS unit cell as defined in Table 4, was found to provide excellent transmission loss performance as shown in Fig. 50. Experimental and simulation results for the 0.65 mm aluminum back plate for the MIVIS with a 0.5 mm thick membrane having an impactor mass of 1.37 grams, maintained at a gap of 1.0 mm between the tip of impactor and back plate are in Fig. 50. The cross-sectional view of symmetric mode shapes from simulations which correlate with the resonance frequency features in the transmission loss curve of MIVIS unit cell

are in Fig. 51. It is from Fig. 50 the maximum increase in transmission loss is about 36 dB at around 324Hz. Significant TL improvement exists at least over a continuous bandwidth of 180 Hz. In the Fig. 50 there is a good match for the experimental and simulated case for the TL of MIVIS unit cell. There is some mismatch after the peak this is due to an extreme value of damping used in the simulation. The damping given to the back plate is 0.3, and so the back plate is heavily damped, and the membrane has no damping and hence a very sharp peak is observed at anti-resonance. Also, it is important to note that this case has an improved TL of 36 dB as compared to back plate, which is best observed in the experiments. The continuous bandgap of TL improvement is cut short by 20 Hz. The explanation for the mode shapes and monotonic applies to this case as well as to the case 6; it is discussed next and it has the best results from all cases tested.

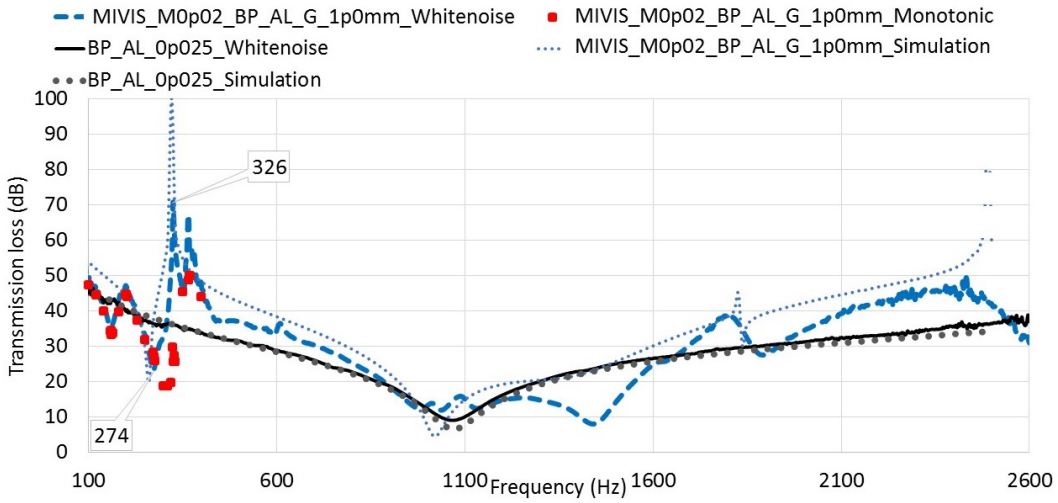

Figure 50: Transmission loss from simulations as well as experiments for the case 5 unit cell and baseline aluminum back plate.

Amongst the six different MIVIS cases tested, case 6 (MIVIS_M0p02_BP_AL_G_1p7mm) as defined in Table 4, was found to provide best transmission loss performance as shown in Fig. 52. Five different plots have been plotted in this figure for comparing transmission loss for this case. Dotted blue lines are for MIVIS simulation and dashed blue line is for MIVIS experiment; blue lines represent MIVIS and the solid black line

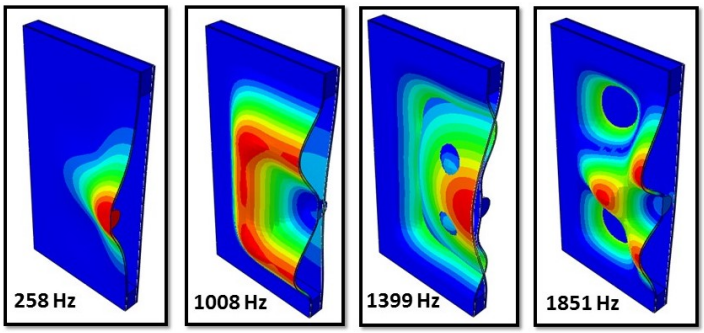

Figure 51: Symmetric mode shapes of the case 5 unit cell corresponding to the frequencies on the TL curve.

represents aluminum back plate experiment alone. Lighter shared of black dotted lines represent backplate simulation. Red markers are used for values of monotonic transmission loss for the MIVIS unit cell. Experimental and simulation results for the 0.65 mm aluminum back plate and for the MIVIS with a 0.5 mm thick membrane having an impactor mass of 1.37 grams, maintained at a gap of 1.7 mm between the tip of impactor and back plate are shown in Fig. 52. The cross-sectional view of symmetric mode shapes from simulations which correlate with the resonance dip features in the transmission loss curve of MIVIS unit cell are shown in Fig. 53. It can be seen from Figure 52 the maximum increase in transmission loss is about 35 dB at around 325 Hz. Significant TL improvement exists at least over a continuous bandwidth of 200 Hz. There is a very reasonable match between the simulations as well as the experiments.

Fig. 54(b) and (d), show a maximum continuous bandwidth of transmission loss increase and the variation of the peak transmission loss increase with respect to the gap between the impactor and the back plate for all the cases of MIVIS that were tested. The peak increase in TL is defined as the increase in TL for MIVIS over the baseline back structure when TL for MIVIS is highest and maximum continuous bandwidth is defined as the frequency range over which the MIVIS TL is at least 10 dB above the back structure's TL. Dashed blue color represents the MIVIS with an Aluminum back plate and is denoted by "MIVIS_AL_Back_Plate," whereas red color represents MIVIS with CFRP back plate and is denoted as "MIVIS_CRPF_Back_Plate." The results

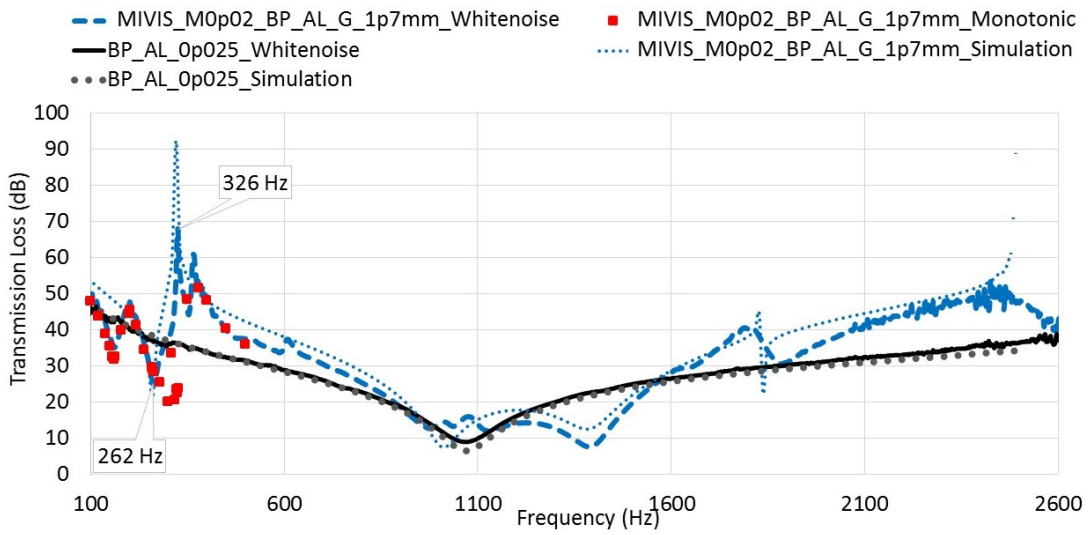

Figure 52: Transmission loss from simulations as well as experiments for the case 6 unit cell and baseline aluminum back plate.

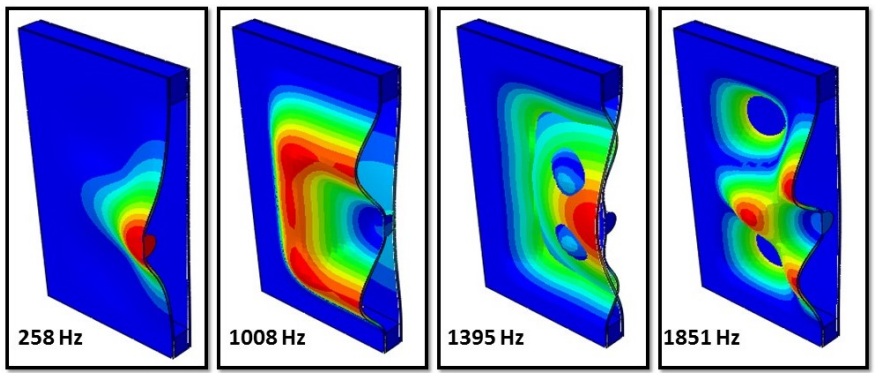

Figure 53: Symmetric mode shapes of the case 6 unit cell corresponding to the frequencies on the TL curve.

indicate that there may exist optimum values for the gap setting which maximize either performance parameters but these values for the gap need not be the same. A case by case optimization of the MIVIS design would be required to suit specific application and performance scenarios. This phenomenon is similar to the one seen in the Section 3.4.3, where we found an effective gap at which the performance was optimum and hence this fits the theory predicted at the simulation stage.

The MIVIS_M0p02_BP_AL_G_0p01mm unit cell was monotonically excited using

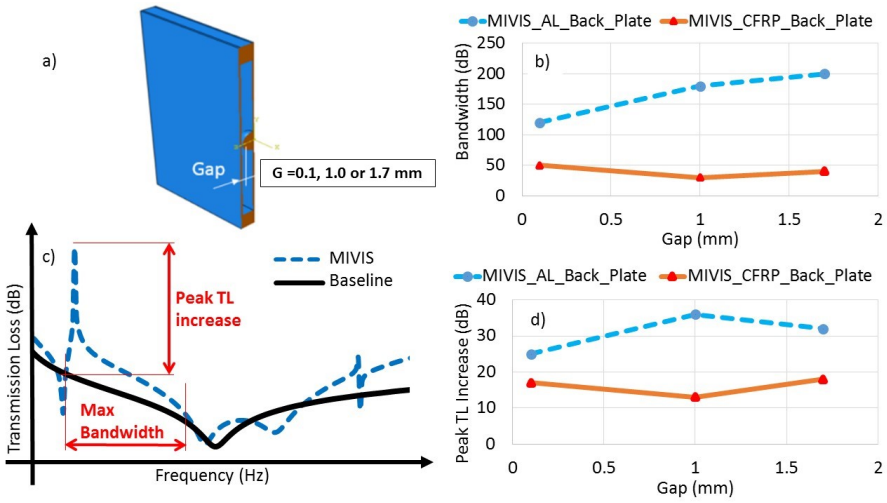

Figure 54: (a) Cross-sectional view of MIVIS showing the gap parameter, (b) Maximum bandwidth versus gap for all six MIVIS cases, (c) Graphic showing the peak TL increase and maximum bandwidth parameters and (d) Peak TL increase.

a speaker source at its anti-resonance frequency at a high amplitude of the input. The membrane made a continuous impact with the back plate, and the steady state was reached, this pressure signal was recorded. The frequency of excitation was 328 Hz with 40 mVrms input amplitude with the full gain of the amplifier. This pressure signal can be seen in the Fig. 55. Now, a simulation model was developed to mimic the same mechanism. Some unknown parameters are needed to be tuned to get the same mechanism from the simulation. Mainly the pressure estimation had a major impact on the amplitude of the transmitted pressure signal. In the simulation, a total of 50 Pa was used as the amplitude for the monotonic excitation at the same frequency and after running the transient steady state simulation and performing some iterations, the pressure signal was obtained that matched exactly with the shape obtained from the experiment. It can be observed that the distance between the bigger peaks is 0.003 s and this translates into a frequency of 328 Hz that is the antiresonance frequency of the structure. Next, the distance between the smaller peaks is estimated to be 0.001 s and this translates to the natural frequency of the back plate that is around 1100 Hz. Hence the transmitted signal is majorly a combination of the excitation and the back plate resonance. This is similar to our hypothesis.

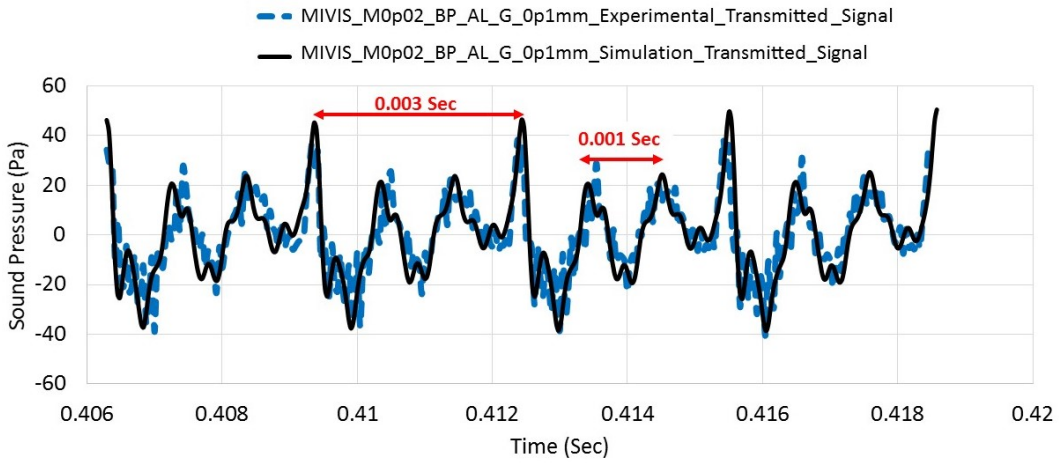

Figure 55: Experimental and simulated transmitted pressure signals at monotonic excitation (antiresonance frequency) for MIVIS unit cell with gap 0.1 mm and aluminum back plate.

The proof of concept for up-conversion of low-frequency acoustic waves into high-frequency acoustic waves can be clearly seen in the spectrogram of the transmitted signals for MIVIS unit cell as shown in Fig. 56(a). The acoustic input excitation frequency is at 324 Hz, as the time progresses three different power levels are considered. For the low power level, it is important to observe that the low-frequency excitation is completely missing on the transmitted side. Whereas the same signal is visible clearly in just with the aluminum backing plate as shown in Fig. 56(b). Upon increasing the power, the up-converted frequencies due to impact match closely with the natural frequency of the backing plate. Hence the transmitted side consists of the excitation frequency along with the up-converted modes of the backing plate. Whereas no such phenomena are observed in just the Aluminum backing plate structures that can be seen in Fig. 56(b).

In the Fig. 57, we are comparing the spectrograms for the incident and transmitted signal of the MIVIS unit cell with a gap G = 1.7 mm recorded continuously after reaching steady state for 43 Sec. These spectrograms are mainly divided into intermittent contact and contact zones. It is evident from both the transmitted spectrogram that there is up-conversion into high-frequency waves corresponding to the back plate's natural frequency. The two stages of contact are obtained by increasing the amplitude of the incident signal

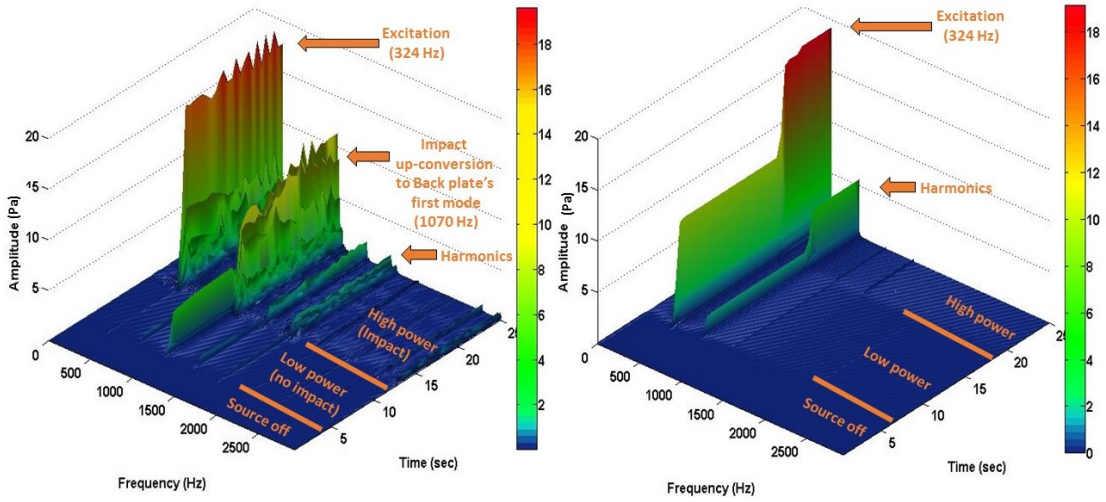

Figure 56: (a) Spectrogram of the MIVIS unit cell and (b) Spectrogram of the Aluminum backing structure.

to the upper limit of the equipment. As the contact takes place and there is an increase in the incident pressure amplitude, we see that there is a sharp decrease in the excitation frequency amplitude on the transmitted side of the MIVIS unit cell. Also, there is an increase in the up-converted back plate's mode generated pressure waves. Using the result from this experimental case, it can be conveniently said that as the incident LF energy increases there is an improvement in the mechanism of up-conversion.

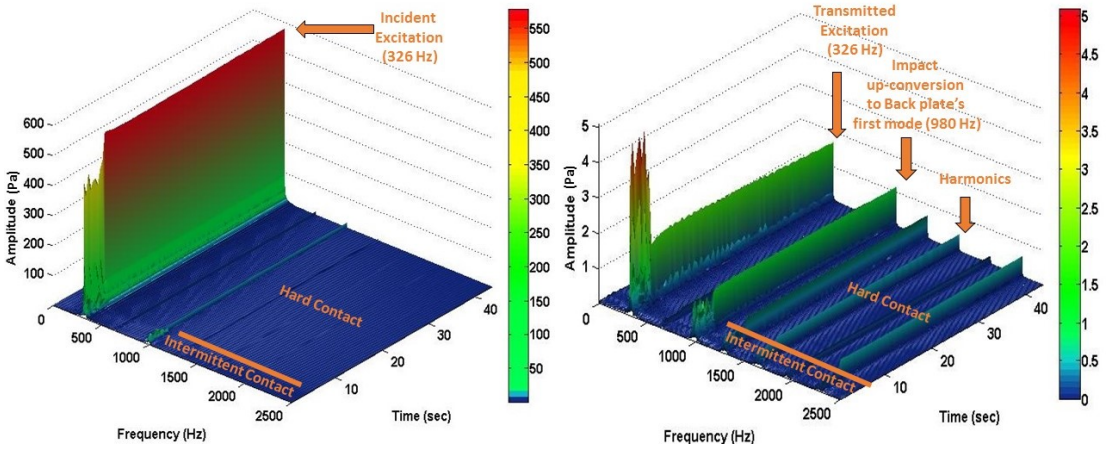

Figure 57: (a) Spectrogram of the incident pressure signal for MIVIS unit cell with G = 1.7 mm and (b) Spectrogram of the transmitted pressure signal for same.

In the Fig. 58(a), we can see the Spectrogram for the transmitted signal of the MIVIS unit cell with a gap G = 1.0 mm for 25 Sec and in Fig. 58(b) for MIVIS unit cell with gap G = 0.1 mm for 43 Sec. These spectrograms are mainly divided into no contact and contact zones. It is clear from both the spectrograms that there is up-conversion into high-frequency waves corresponding to the back plate's natural frequency. It is to be noted that both of these specimens have different excitation pressure amplitudes, hence the amplitudes of the output LF pressure cannot be compared. However, it is of importance to note that the ratio of the amplitude of the back plate's natural frequency to the excitation frequency is less at the small gap. In fact, this ratio is 0.2 for a gap of G = 0.1 mm, it is 0.6 for a gap of G = 1.0 mm and 0.25 for a gap of 1.7 mm. Therefore it is easy to conclude that there is an optimum gap present at which the up-conversion mechanism is best, and for our case, it occurs for the gap G =1.0 mm.

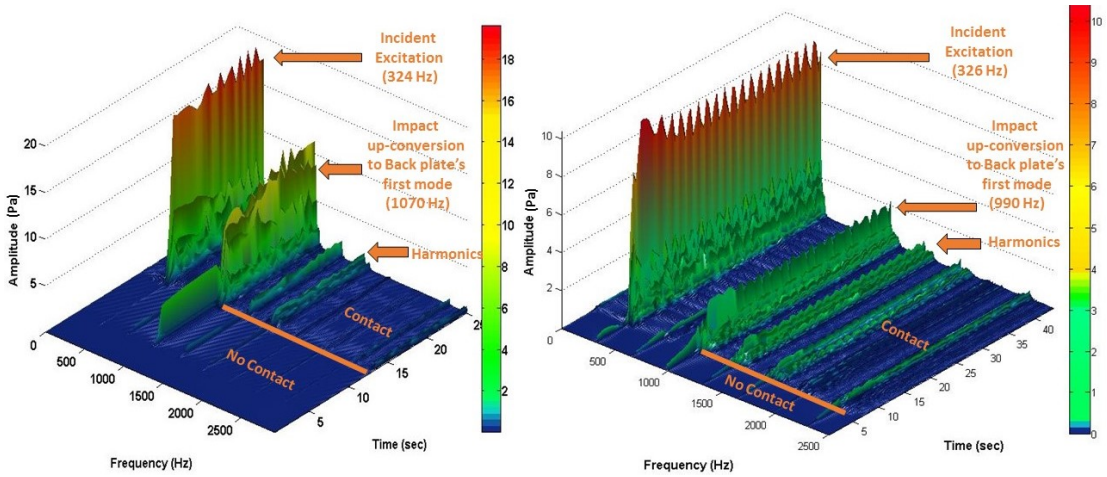

Figure 58: (a) Spectrogram of the MIVIS unit cell with G = 1.0 mm and (b) Spectrogram of the MIVIS unit cell with G = 0.1 mm.

A comparison of the low-frequency transmission loss performance measured from experiments for MIVIS unit cell and state of the art (SOA) foam materials of 1" thickness used in aerospace applications is shown in Figure 10. The ultralight (UL) foam is a high-quality super light foam made for specifically to be employed in aircraft structures. The G+ foam is a heavier version of the melamine foam that are employed in spacecraft structures. The meaning of each curve is explained in the Fig. 59 itself. As can be

seen in Fig. 59(a), the MIVIS displays as much as 35 dB of transmission increase over the foams with a maximum continuous bandwidth of significantly increased transmission loss exceeding 200 Hz in the 300-500 Hz range. In Fig. 59(b) as much as 32 dB of peak TL increase and 300 Hz of the continuous bandwidth of increased transmission loss in 300-600 Hz range is noticeable. The MIVIS, while retaining original functionality of the backing structure and being relatively lightweight and compact can significantly improve low-frequency transmission loss performance.

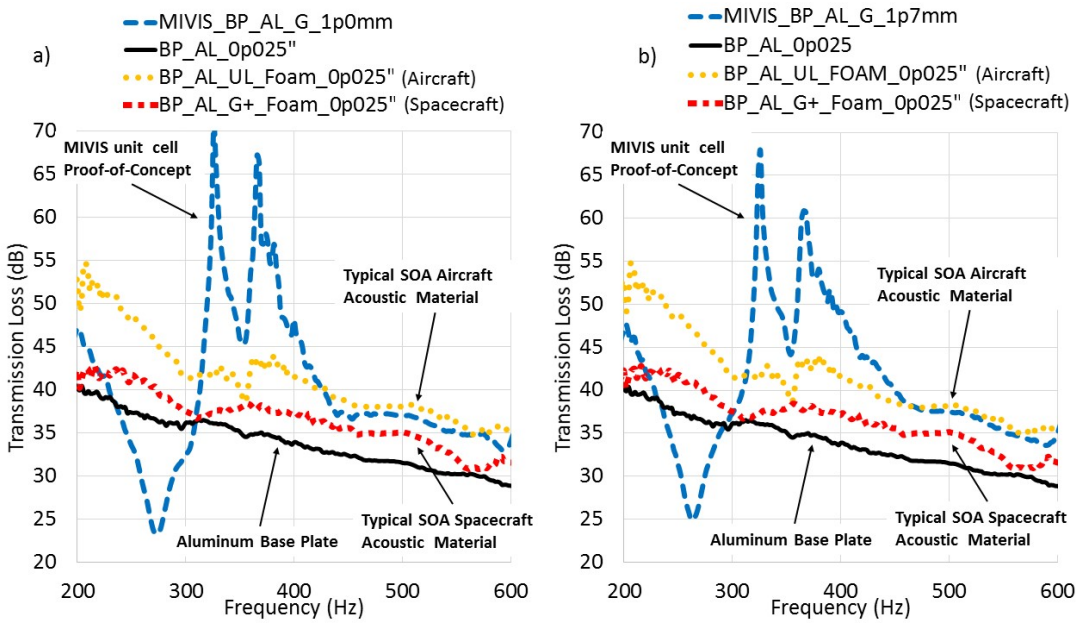

Figure 59: Low-Frequency transmission loss of MIVIS unit cell performance compared to the SOA aerospace application materials, a) MIVIS unit cell with gap 1.0 mm and aluminum back plate and b) MIVIS unit cell with gap 1.7 mm and aluminum back plate.

4.5. Summary

Chapter 4 starts with the selection process utilized in the construction of MIVIS unit cell. The steps involve the selection of back plate, membranes, frames, impactors and washers. This was in itself a technically challenging task and involved engineering decisions based on the experimental results. Once the selection the material was made the testing of these materials provides results that were correlated with simulations. Results that are developed from the data reinforces the hypothesis.

CHAPTER 5

Conclusions and Recommendations

The purpose of this chapter is to make the closing statements on the MIVIS and their implications in the field of acoustic noise mitigation techniques.

5.1. Conclusions

The low-frequency transmission loss (TL) characteristics of metamaterial-inspired vibro impact structures (MIVIS) having vibro-impact attachments were investigated. MIVIS employs structurally-integral tuned mas-loaded membrane-type resonators that could pick up energy from incident low-frequency sound waves and utilize the mechanism of frequency up-conversion via impacts, transfer the energy to higher modes in a backing sandwich structure. MIVIS and baseline backing structures were evaluated using a standard transmission loss tube setup. MIVIS displays as much as 36 dB of transmission increase over state-of-the-art foams or the backing structure alone with a maximum continuous bandwidth of significantly increased transmission loss exceeding 200 Hz in the 300-500 Hz range. Good agreement between simulations and experiments were observed including correlation of MIVIS modal response with the TL dips. Also, the pressure signals generated due to the impact was predicted accurately by the simulation. This means that further designs can be investigated without actually performing experiments to study effects caused by various parameters.

The effect of design parameters such as the gap between impactor tip and backing structure on TL performance was examined. It was observed that the best transmission

loss was obtained for the aluminum back plate at a gap of 1.0 mm. All the mode shapes responsible for the features in the TL curves have been identified and their dependence on material properties verified.

Vibro-impact up conversion of low-frequency excitation to the first mode of the backing structure in the transmitted signal was experimentally observed using spectrograms. For an excitation of 324 Hz the impact lead to the up-conversion to Back plate's first mode at 1070 Hz. For the hard contact a decrease in the amplitude of the transmitted pressure signal was observed. The up-converted pressure signals from the back plates resonance reduces for the gap setting of 0.1 mm to 20% with respect to the excitation frequency in comparison with the 60% for a gap setting of 1.0 mm.

The transmitted pressure signal for the MIVIS with aluminum back plate and a gap of 0.1 mm contained a combination of the incident and back plates corresponding wave with time difference at 0.003 Sec and 0.001 Sec corresponding to the excitation frequency and natural frequency of the back plate respectively.

Further optimization of materials, geometries, and configurations for MIVIS could provide a feasible lightweight, compact and structurally integrated solution for low-frequency acoustic noise mitigation for which there are scarcely any practical solutions at present.

5.2. Recommendations

A rapid growth of in the field of acoustic metamaterials (AM) has attracted vibrant research and technological applications. This potential has been identified by the funding agencies and industry to further their growth. Some recommendations are identified based on the ideas that were generated as a part of this thesis.

1) Scope of MIVIS:

The MIVIS unit cell can be further studied for enhancing broadband TL using tuned multiple MIVIS unit cells to match source characteristics having multiple dominant peaks. By quantitative evaluation of the difference between the contact phenomena

occurring at both the resonance and the anti-resonance frequency for the MIVIS unit cell.

2) Analytical Model for Spring-Mass:

Development of a semi-analytical lumped parameter model incorporating vibro-impact based on the restitution equation will give insight into the contact phenomena. The transmission loss characteristics can be converted into spring mass systems and a successful theory for transition would lead to faster evaluation of the mass loaded membrane as well as the MIVIS unit cell. The semi-analytical model combined with the spring mass system will lead to prediction of MIVIS characteristics without any need of experiment or simulation.

3) Improved Demonstrations and Benchmarking MIVIS:

Follow-on experimental studies that can incorporate foam backing structures to enhance attenuation of the up-converted high frequency (HF) content will lead to further reduction in energy of the transmitted waves.

References

[1] H. H. Hubbard. Aeroacoustics of flight vehicles: Theory and practice. Volume 1: Noise sources. *NASA Langley Research Center*, Vol1: Noise Sources, Aug 01, 1991.

[2] W. O. Hughes, A. M. McNelis, and M. E. McNelis. Acoustic test characterization of melamine foam for usage in nasa's payload fairing acoustic attenuation systems. *28th Aerospace Testing Seminar*, 2014.

[3] M. G. Jones, W. R. Watson, and J. G. June. Optimization of microphone locations for acoustic liner impedance eduction. *8th AIAA/CEAS Aeroacoustics Conference*, 2002.

[4] H. H. Huang, C. T. Sun, and G. L. Huang. On the negative effective mass density in acoustic metamaterials. *International Journal of Engineering Science*, 47(4):610 – 617, 2009.

[5] M. Yang, G. Ma, Z. Yang, and P. Sheng. Coupled membranes with doubly negative mass density and bulk modulus. *Physics Review Letters*, 110:134–301, Mar 2013.

[6] J. Mei, G. Ma, M. Yang, Z. Yang, W. Wen, and P. Sheng. Dark acoustic metamaterials as super absorbers for low-frequency sound. *Nature Communications*, Mar 2012.

[7] G. Ma, M. Yang, Z. Yang, and P. Sheng. Low-frequency narrow-band acoustic filter with large orifice. *Applied Physics Letters*, 103(1), 2013.

[8] M. Yang, C. Meng, C. Fu, Y. Li, Z. Yang, and P. Sheng. Subwavelength total acoustic absorption with degenerate resonators. *Applied Physics Letters*, 107(10), 2015.

[9] R. Sugimoto, R. J. Astley, and P. B. Murray. Low frequency liners for turbofan engines. *20th International Congress on Acoustics*, 2010.

[10] T. J. Cox and P. D'Antonio. *Acoustic absorbers and diffusers - theory, design, and application*. CRC Press, 2009.

[11] C. J. Naify, C. Chang, G. McKnight, and S. Nutt. Transmission loss and dynamic response of membrane-type locally resonant acoustic metamaterials. *Journal of Applied Physics*, 108(11), 2010.

[12] C. J. Naify, C. Chang, G. McKnight, F. Scheulen, and S. Nutt. Membrane-type metamaterials: Transmission loss of multi-celled arrays. *Journal of Applied Physics*, 109(10), 2011.

[13] S. Varanasi, J. S. Bolton, T. H. Siegmund, and R. J. Cipra. The low frequency performance of metamaterial barriers based on cellular structures. *Applied Acoustics*, 74(4):485 – 495, 2013.

[14] F. Nucera, F. Lo Iacono, D.M. McFarland, L.A. Bergman, and A.F. Vakakis. Application of broadband nonlinear targeted energy transfers for seismic mitigation of a shear frame: Experimental results. *Journal of Sound and Vibration*, 313(1–2):57 – 76, 2008.

[15] J. R. Callicoat, R. J. Gaeta, and J. D. Jacob. Composite materials providing improved acoustic transmission loss for uavs. *20th AIAA/CEAS Aeroacoustics Conference*, 2014.

[16] J. M. Manimala. *Dynamic behavior of acoustic metamaterials and metaconfigured structures with local oscillators*. DISSERTATIONS. Purdue University, 2014.

[17] J. B. Pendry, A. J. Holden, W. J. Stewart, and I. Youngs. Extremely low frequency plasmons in metallic mesostructures. *Physics Review Letters*, 76:4773–4776, Jun 1996.

[18] V. G. Veselago. The electrodynamics of substances with simultaneously negative values of electric permittivity (ε) and magnetic permeability (μ). *Soviet Physics Uspekhi*, 10(4):509, 1968.

[19] J. B. Pendry, A. J. Holden, D. J. Robbins, and W. J. Stewart. Magnetism from conductors and enhanced nonlinear phenomena. *IEEE Transactions on Microwave Theory and Techniques*, 47(11):2075–2084, Nov 1999.

[20] J. Li and C. T. Chan. Double-negative acoustic metamaterial. *Physics Review Letters*, 70:055602, Nov 2004.

[21] N. Fang and et al. Ultrasonic metamaterials with negative modulus. *Nature Materials*, 5:452–456, June 2006.

[22] Y. Ding, Z. Liu, C. Qiu, and J. Shi. Metamaterial with simultaneously negative bulk modulus and mass density. *Physics Review Letters.*, 99:093904, Aug 2007.

[23] Y. Cheng, J. Y. Xu, and X. J. Liu. One-dimensional structured ultrasonic metamaterials with simultaneously negative dynamic density and modulus. *Physics Review B*, 77:045134, Jan 2008.

[24] C. T. Chan, Jensen Li, and K. H. Fung. On extending the concept of double negativity to acoustic waves. *Journal of Zhejiang University Science A*, 7(1):24–28, 2006.

[25] J. B. Pendry. Negative refraction makes a perfect lens. *Physics Review Letters.*, 85:3966–3969, Oct 2000.

[26] S. Zhang, L. Yin, and N. Fang. Focusing ultrasound with an acoustic metamaterial network. *Physics Review Letters.*, 102:194301, May 2009.

[27] C. M. Park, J. J. Park, S. H. Lee, Y. M. Seo, C. K. Kim, and S. H. Lee. Amplification of acoustic evanescent waves using metamaterial slabs. *Physics Review Letters.*, 107:194301, Nov 2011.

[28] J. J. Park, C. M. Park, K. J. B. Lee, and S. H. Lee. Acoustic superlens using membrane-based metamaterials. *Applied Physics Letters*, 106(5), 2015.

[29] N. Fang, H. Lee, C. Sun, and X. Zhang. Subdiffraction-limited optical imaging with a silver superlens. *Science*, 308(5721):534–537, 2005.

[30] J. Li, L. Fok, X. Yin, G. Bartal, and X. Zhang. Experimental demonstration of an acoustic magnifying hyperlens. *Nature Materials*, 8(1476-1122):931–934, 2009.

[31] D. Schurig, J. J. Mock, B. J. Justice, S. A. Cummer, J. B. Pendry, A. F. Starr, and D. R. Smith. Metamaterial electromagnetic cloak at microwave frequencies. *Science*, 314(5801):977–980, 2006.

[32] R. Liu, C. Ji, J. J. Mock, J. Y. Chin, T. J. Cui, and D. R. Smith. Broadband ground-plane cloak. *Science*, 323(5912):366–369, 2009.

[33] V. A. Podolskiy and E. E. Narimanov. Near-sighted superlens. *Optics Letters*, 30(1):75–77, Jan 2005.

[34] X. Zhang and Z. Liu. Superlenses to overcome the diffraction limit. *Nature Materials*, 7(6):435–441, 2008.

[35] C. Shen, Y. Xie, N. Sui, W. Wang, S. A. Cummer, and Y. Jing. Broadband acoustic hyperbolic metamaterial. *Physics Review Letters.*, 115:254301, Dec 2015.

[36] M. Oudich, Y. Li, B. M. Assouar, and Z. Hou. A sonic band gap based on the locally resonant phononic plates with stubs. *New Journal of Physics*, 12(8):083049, 2010.

[37] M. Oudich, M. Senesi, M. B. Assouar, Massimo Ruzenne, J. Sun, B. Vincent, Z. Hou, and T. T. Wu. Experimental evidence of locally resonant sonic band gap in two-dimensional phononic stubbed plates. *Physics Review B*, 84:165136, Oct 2011.

[38] M. Rupin, F. Lemoult, G. Lerosey, and P. Roux. Experimental demonstration of ordered and disordered multiresonant metamaterials for lamb waves. *Physics Review Letters*, 112:234301, Jun 2014.

[39] R. Zhu, X. N. Liu, G. L. Huang, H. H. Huang, and C. T. Sun. Microstructural design and experimental validation of elastic metamaterial plates with anisotropic mass density. *Physics Review B*, 86:144307, Oct 2012.

[40] M. Farhat, S. Guenneau, and S. Enoch. Ultrabroadband elastic cloaking in thin plates. *Physics Review Letters.*, 103:024301, Jul 2009.

[41] N. Stenger, M. Wilhelm, and M. Wegener. Experiments on elastic cloaking in thin plates. *Physics Review Letters.*, 108:014301, Jan 2012.

[42] A. Colombi, P. Roux, S. Guenneau, and M. Rupin. Directional cloaking of flexural waves in a plate with a locally resonant metamaterial. *The Journal of the Acoustical Society of America*, 137(4):1783–1789, 2015.

[43] R. Zhu, X. N. Liu, G. K. Hu, C. T. Sun, and G. L. Huang. Negative refraction of elastic waves at the deep-subwavelength scale in a single-phase metamaterial. *Nature Communications*, 5, 2014.

[44] M. Dubois, E. Bossy, S. Enoch, S. Guenneau, G. Lerosey, and P. Sebbah. Time-driven superoscillations with negative refraction. *Physics Review Letters.*, 114:013902, Jan 2015.

[45] Y. Lai, Y. Wu, P. Sheng, and Z. Q. Zhang. Hybrid elastic solids. *Nature Materials*, 10(8):620–624, 2011.

[46] Y. Wu, Y. Lai, and Z. Q. Zhang. Elastic metamaterials with simultaneously negative effective shear modulus and mass density. *Physics Review Letters.*, 107:105506, Sep 2011.

[47] S. Brûlé, E. H. Javelaud, S. Enoch, and S. Guenneau. Experiments on seismic metamaterials: Molding surface waves. *Physics Review Letters.*, 112:133901, Mar 2014.

[48] H. H. Huang and C. T. Sun. Wave attenuation mechanism in an acoustic metamaterial with negative effective mass density. *New Journal of Physics*, 11(1):013003, 2009.

[49] S. H. Lee, C. M. Park, Y. M. Seo, Z. G. Wang, and C. K. Kim. Acoustic metamaterial with negative density. *Physics Letters A*, 373(48):4464 – 4469, 2009.

[50] S. Yao, X. Zhou, and G. Hu. Investigation of the negative-mass behaviors occurring below a cut-off frequency. *New Journal of Physics*, 12(10):103025, 2010.

[51] H. H. Huang and C. T. Sun. Continuum modeling of a composite material with internal resonators. *Mechanics of Materials*, 46:1 – 10, 2012.

[52] R. U. Ahmed and S. Banerjee. Wave propagation in metamaterial using multiscale resonators by creating local anisotropy. *International Journal of Modern Engineering*, 13:51–59, 2013.

[53] G. W. Milton and J. R. Willis. On modifications of newton's second law and linear continuum elastodynamics. *Proceedings of the Royal Society of London A: Mathematical, Physical and Engineering Sciences*, 463(2079):855–880, 2007.

[54] S. Yao, X. Zhou, and G. Hu. Experimental study on negative effective mass in a 1D mass–spring system. *New Journal of Physics*, 10(4):043020, 2008.

[55] T. Bückmann, N. Stenger, M. Kadic, J. Kaschke, A. Frölich, T. Kennerknecht, C. Eberl, M. Thiel, and M. Wegener. Tailored 3d mechanical metamaterials made by dip-in direct-laser-writing optical lithography. *Advanced Materials*, 24(20):2710–2714, 2012.

[56] X. Zheng, H. Lee, T. H. Weisgraber, M. Shusteff, J. DeOtte, E. B. Duoss, J. D. Kuntz, M. M. Biener, Q. Ge, J. A. Jackson, S. O. Kucheyev, N. X. Fang, and C. M. Spadaccini. Ultralight, ultrastiff mechanical metamaterials. *Science*, 344(6190):1373–1377, 2014.

[57] G. W. Milton. *The Theory of Composites*. Cambridge University Press, 2002.

[58] T. Bückmann, M. Thiel, M. Kadic, R. Schittny, and M. Wegener. An elasto-mechanical unfeelability cloak made of pentamode metamaterials. *Nature Publishing Group*, 5, 2014.

[59] M. Kadic, T. Bückmann, N. Stenger, M. Thiel, and M. Wegener. On the practicability of pentamode mechanical metamaterials. *Applied Physics Letters*, 100(19), 2012.

[60] J. S. Bolton, N. M. Shiau, and Y. J. Kang. Sound transmission through multi-panel structures lined with elastic porus materials. *Journal of Sound and Vibration*, 191(3):317 – 347, 1996.

[61] S. A. Lane, S. Griffin, and R. E. Richard. Fairing noise mitigation using passive vibroacoustic attenuation devices. *Journal of Spacecraft and Rockets*, 43:31–44, Jan 2006.

[62] D. Y. Maa. Theory and design of microperforated panel sound-absorbing constructions. *Scientia Sinica*, 18:55–71, 1975.

[63] K. Idrisi, M. E. Johnson, A. Toso, and J. P. Carneal. Increase in transmission loss of a double panel system by addition of mass inclusions to a poro-elastic layer: A comparison between theory and experiment. *Journal of Sound and Vibration*, 323(1–2):51 – 66, 2009.

[64] M. R. F. Kidner, C. R. Fuller, and B. Gardner. Increase in transmission loss of single panels by addition of mass inclusions to a poro-elastic layer: Experimental investigation. *Journal of Sound and Vibration*, 294(3):466 – 472, 2006.

[65] R. A. Prydz, L. S. Wirt, H. L. Kuntz, and L. D. Pope. Transmission loss of a multi-layer panel with internal tuned helmholtz resonators. *The Journal of the Acoustical Society of America*, 87(4):1597–1602, 1990.

[66] Z. Liu, X. Zhang, Y. Mao, Y. Y. Zhu, Z. Yang, C. T. Chan, and P. Sheng. Locally resonant sonic materials. *Science*, 289(5485):1734–1736, 2000.

[67] M. Hirsekorn, P. P. Delsanto, N. K. Batra, and P. Matic. Modelling and simulation of acoustic wave propagation in locally resonant sonic materials. *Ultrasonics*, 42(1–9):231 – 235, 2004. Proceedings of Ultrasonics International 2003.

[68] C. J. Naify, C. Chang, G. McKnight, and S. Nutt. Transmission loss of membrane-type acoustic metamaterials with coaxial ring masses. *Journal of Applied Physics*, 110(12), 2011.

[69] C. J. Naify, C. Chang, G. McKnight, and S. R. Nutt. Scaling of membrane-type locally resonant acoustic metamaterial arrays. *The Journal of the Acoustical Society of America*, 132(4):2784–2792, 2012.

[70] Z. Yang, H. M. Dai, N. H. Chan, G. C. Ma, and P. Sheng. Acoustic metamaterial panels for sound attenuation in the 50–1000 hz regime. *Applied Physics Letters*, 96(4), 2010.

[71] Y. Chen, G. Huang, X. Zhou, G. Hu, and C. T. Sun. Analytical coupled vibroacoustic modeling of membrane-type acoustic metamaterials: Membrane model. *The Journal of the Acoustical Society of America*, 136(3):969–979, 2014.

[72] Y. Zhang, J. Wen, Y. Xiao, X. Wen, and J. Wang. Theoretical investigation of the sound attenuation of membrane-type acoustic metamaterials. *Physics Letters A*, 376(17):1489 – 1494, 2012.

[73] O. Kopmaz and S. Telli. Free vibrations of rectangular plate carrying distributed mass. *Journal of Sound and Vibration*, 251(1):39 – 57, 2002.

[74] C. J. Naify, C. Huang, M. Sneddon, and S. Nutt. Transmission loss of honeycomb sandwich structures with attached gas layers. *Applied Acoustics*, 72(2–3):71 – 77, 2011.

[75] Z. Yang, J. Mei, M. Yang, N. H. Chan, and P. Sheng. Membrane-type acoustic metamaterial with negative dynamic mass. *Physics Review Letters*, 101:204301, Nov 2008.

[76] M. H. Ming-Hui Lu, L. Feng, and Y. F. Chen. Phononic crystals and acoustic metamaterials. *Materials Today*, 12(12):34–42, 2009.

[77] Y. Zhang, J. Wen, H. Zhao, D. Yu, L. Cai, and X. Wen. Sound insulation property of membrane-type acoustic metamaterials carrying different masses at adjacent cells. *Journal of Applied Physics*, 114(6), 2013.

[78] R. Bellet, B. Cochelin, P. Herzog, and P.O. Mattei. Experimental study of targeted energy transfer from an acoustic system to a nonlinear membrane absorber. *Journal of Sound and Vibration*, 329(14):2768 – 2791, 2010.

[79] M. Schroeder. *Number Theory in Science and Communication*. Springer, 2009.

[80] Rossing Editor. *Springer Handbook of Acoustics*. Springer, 2007.

[81] S. E. Makris, C. L. Dym, and J. M. Smith. Transmission loss optimization in acoustic sandwich panels. *The Journal of the Acoustical Society of America*, 79(6):1833–1843, 1986.

[82] J. M. P. António, A. Tadeu, and L. Godinho. Analytical evaluation of the acoustic insulation provided by double infinite walls. *Journal of Sound and Vibration*, 263(1):113 – 129, 2003.

[83] W. C. Tang, H. Zheng, and C. F. Ng. Low frequency sound transmission through close-fitting finite sandwich panels. *Applied Acoustics*, 55(1):13 – 30, 1998.

[84] M. Bruneau and C. Potel. *Materials and Acoustics Handbook*. Wiley, 2009.

[85] P. H. Parkin, H. R. Humphreys, and J. R. Cowell. *Acoustics, Noise and Buildings*. Faber and Faber, 1979.

[86] P. D'Antonio and J. H. Konnert. The reflection phase grating diffusor: Design theory and application. *Journal of Audio Engineering Society*, 32(4):228–238, 1984.

[87] T. J. Cox, James A. S. Angus, and P. D'Antonio. Ternary and quadriphase sequence diffusers. *The Journal of the Acoustical Society of America*, 119(1), 2006.

[88] C. M. Harris and A. G. Piersol. *Harris' Shock and Vibration Handbook*. McGraw-Hill, 2005.

[89] ASTM International. ASTM:E2611 - 09 Standard test method for measurement of normal incidence sound transmission of acoustical materials based on the transfer matrix method. *ASTM Standards*, Vol: 04.06, 2014.

VITA

ANUJ REKHY

Candidate for the Degree of

Master of Science

Thesis: Low-Frequency Acoustic Noise Mitigation Characteristics of Metamaterials-Inspired Vibro-Impact Structures

Major Field: Mechanical & Aerospace Engineering

Completed the requirements for the Master of Science in Mechanical & Aerospace Engineering at Oklahoma State University, Stillwater, Oklahoma in Dec, 2016.

Completed the requirements for the Bachelor of Science in Mechanical Engineering at the Jawaharlal Nehru Technological University, Hyderabad, India in May, 2012.

Experience:

Research Assistant — Jan 2015 - Present

Solid & Structural Dynamics Lab, OSU-Stillwater

Teaching Assistant — August 2014 - May 2016

MAE, OSU-Stillwater

Production Engineer — July 2012 - July 2014

Engine Plant, Piaggio Vehicles Private Limited.